UNIVERSITY OF CALIFORNIA, SAN DIEGO

Controller Certification:
The Generalized Stability Margin Inference for a Large Number of MIMO Controllers

A dissertation submitted in partial satisfaction of the
requirements for the degree Doctor of Philosophy

in

Engineering Sciences (Aerospace Engineering)

by

Jisang Park

Committee in charge:

Professor Robert R. Bitmead, Chairperson
Professor Raymond de Callafon
Professor J. William Helton
Professor Kenneth Kreutz-Delgado
Professor Miroslav Krstić

2008

The dissertation of Jisang Park is approved, and it is acceptable in quality and form for publication on microfilm:

Chairperson

University of California, San Diego

2008

To my wife Eunhwa and my two month old son Kangho
who let me feel God's love

TABLE OF CONTENTS

LIST OF FIGURES

LIST OF TABLES

ACKNOWLEDGEMENT

For this thesis, there has been direct and indirect, hearty and unforgettable, support from many people. Through this space, I would like to express my thanks for all that they have done for me.

My study and research at UCSD would not be able to be done without Bob's support and advise. He always enjoyed to teach me and guide me. My words here cannot be enough to express my appreciation. Also, I would like to give my thank to Jan Bitmead for her warm concern and smile and her abundant dinner tables for me and Eunhwa. I owed much to them.

Many professors in UCSD helped me preparing this thesis. Specially, I show my appreciation to the thesis committee members: Professors Raymond de Callafon, J. William Helton, Kenneth Kreutz-Delgado, and Miroslav Krstić. They readily gave me time for reading my thesis and giving advice on it.

I would like to thank Dr. Abbas Emami-Naeini and Dr. Robert Kosut at SC Solutions Inc. for their support and invaluable discussions on this research.

Finally, I express my special love and thanks to my wife Eunhwa, new born son Kangho and our parents who have sacrificed many things for me.

Chapter 2 includes the reprints of the following papers:

Jisang Park, Robert R. Bitmead - *Controller Certification*, Automatica, Vol. 44 No. 1, Jan. 2008. pp. 167 – 176

Jisang Park, Robert R. Bitmead - *Controller Certification*, 44th IEEE Conference on Decision and Control, and European Control Conference in Seville, Spain, Dec., 2005. pp. 6442–6447

Jisang Park, Robert R. Bitmead - *Vinnicombe's Winding Number Condition is not Transitive: Impacts for Adaptive Control*, IFAC Workshop on Adaptation and Learning in Control and Signal Processing in Yokohama, Japan, Aug., 2004. pp. 783–787

Chapter 3 includes the reprints of the following papers:

Jisang Park, Robert R. Bitmead - *Simultaneous Scaling for MIMO Controller Certification*, Automatica, submitted, Oct. 2007.

Jisang Park, Robert R. Bitmead - *Simultaneous Scaling for MIMO Controller Certification*, 46th IEEE Conference on Decision and Control in New Orleans, LA, USA, Dec, 2007. pp. 4409–4414

The dissertation author was the primary author and the co-author listed in these publications directed and supervised the research.

VITA

1997	B.S. (Aeronautical and Mechanical Engineering) Hankuk Aviation University, GyeongGi-Do, Korea
1999	M.S. (Aerospace Engineering) Hankuk Aviation University, GyeongGi-Do, Korea
1999–2001	Intern Researcher, Korea Institute of Science and Technology Seoul, Korea
2005	Intern Researcher, S C Solutions Inc. Sunnyvale, CA, USA
2002–2008	Research Assistant, University of California, San Diego, USA
2006	C. Phil. (Aerospace Engineering) University of California, San Diego, USA
2008	Ph.D. (Aerospace Engineering) University of California, San Diego, USA

PUBLICATIONS

Journal Papers

1. Jisang Park, Robert R. Bitmead
   Controller Certification
   Automatica, Vol.44 No.1, Jan. 2008, pp. 167-176.

2. Jisang Park, Robert R. Bitmead
   Simultaneous Scaling for MIMO Controller Certification
   Automatica, Submitted, Oct. 2007.

3. Yong Mo Lim, Jisang Park, Byoungkyu Kim, Jong-Oh Park, Su Hyun Kim,
   Experimental Study on the Movement of Pneumatic Actuating Mechanism for Self-Propelling Endoscope, Journal of the Korean Society of
   Precision Engineering, Vol. 18, No. 10, pp 194–199, Oct. 2001.

4. Jai-Hyuk Hwang, Jisang Park
   Analysis on Dynamics of Aircraft Landing Gear under Nonstationary Random Excitation Using Nonlinear Model, Journal of the Korean Society for
   Aeronautical and Space Sciences, Vol. 27, No. 4, pp.75–83, Jun. 1999.

Conference Papers

1. Jisang Park, Robert R. Bitmead
   Simultaneous Scaling for MIMO Controller Certification, 46th IEEE Conference on Decision and Control in New Orleans, LA, USA, pp. 4409–4414, Dec, 2007.

2. Jisang Park, Robert R. Bitmead
   Controller Certification, 44th IEEE Conference on Decision and Control,
   and European Control Conference in Seville, Spain, pp. 6442–6447, Dec., 2005.

3. Jisang Park, Robert R. Bitmead
   Vinnicombe's Winding Number Condition is not Transitive: Impacts for Adaptive Control, IFAC Workshop on Adaptation and Learning in Control and Signal
   Processing in Yokohama, Japan, pp. 783–787, Aug., 2004.

4. Yong Mo Lim, Jinhee Lee, Jisang Park, Byoungkyu Kim, Jong-Oh Park,
   Su Hyun Kim, *A Self-Propelling Endoscopic System*, Proceedings of the 2001 IEEE/RSJ International Conference on Intelligent Robotics and Systems,
   pp.1117 – 1122.

5. Yong Mo Lim, Jisang Park, Byoungkyu Kim, Jong-Oh Park, Su Hyun Kim,
   Yeh-Sun Hong, *Pneumatic Impulsive Actuating Mechanism for Microcapsule-Type Endoscope*, Proceedings of the 32nd International Symposium on Robotics,
   pp.1865 – 1868, Seoul, Korea, April, 2001.

6. B.-J. Yi, H.Y. Ra, J.H. Lee, Y.S. Hong, J.S. Park, S.-R. Oh, I.H. Suh, W.K. Kim
   Design of a Parallel-Type Gripper Powered by Pneumatic Actuators
   Proceedings of the 2000 IEEE/RSJ International conference
   on Intelligent Robotics and Systems, pp.689–695.

7. Jisang Park, Byounkyu Kim, Kyoungdea Kim, Jong-Oh Park, Yeh-Sun Hong, Su Hyun Kim, *Locomotive Mechanism with Cam for a Robotic Colonoscope*, Proceedings of The 2001 Korean Society of Mechanical Engineers, Vol. B pp.271 –276.

Patents

1. US 6,824,508 B2: Byungkyu Kim, Jisang Park, Kyoungdea Kim, Yehsun Hong, Soohyun Kim, Jongoh Park, *Micro Robot*, Nov. 30, 2004

2. US 6,702,734 B2: Byungkyu Kim, Youngmo Kim, Jinhee Lee, Jisang Park, Soohyun Kim, Jongoh Park, *Self-propelled endoscopic micro robot and system for intestinal endoscopy*, Mar. 9, 2004

FIELDS OF STUDY

Major Field: Engineering (Aerospace Engineering)

Studies in Control and Estimation.
Professors Robert R. Bitmead, Raymond de Callafon,
Miroslav Krsitć, William M. McEneaney, Robert E. Skelton

Studies in Mathematics.
Professors Patrick Fitzsimmons, Philip E. Gill, Linda Rothschild,

ABSTRACT OF THE DISSERTATION

Controller Certification: The Generalized Stability Margin Inference for a Large Number of MIMO Controllers

by

Jisang Park

Doctor of Philosophy in Engineering Sciences (Aerospace Engineering)
University of California, San Diego, 2008
Professor Robert R. Bitmead, Chairperson

In this dissertation, we investigate MIMO stability margin inference of a large number of controllers using pre-established stability margins of a small number of ν-gap-wise adjacent controllers. The generalized stability margin and the ν-gap metric are inherently able to handle MIMO system analysis without the necessity of repeating multiple channel-by-channel SISO analyses. This research consists of three parts: (i) development of a decision support tool for inference of the stability margin, (ii) computational considerations for yielding the maximal stability margin with the minimal ν-gap metric in a less conservative manner, and (iii) experiment design for estimating the generalized stability margin with an assured error bound.

A modern problem from aerospace control involves the certification of a large set of potential controllers with either a single plant or a fleet of potential plant systems, with both plants and controllers being MIMO and, for the moment, linear. Experiments on a limited number of controller/plant pairs should establish the stability and a certain level of margin of the complete set. We consider this certification problem for a set of controllers and provide algorithms for selecting an efficient subset for testing. This is done for a finite set of candidate controllers and, at least for SISO plants, for an infinite set. In doing this, the ν-gap metric will be the main tool. We provide a theorem restricting a radius of a ball in the parameter space so that the controller can guarantee

a prescribed level of stability and performance if parameters of the controllers are contained in the ball. Computational examples are given, including one of certification of an aircraft engine controller. The overarching aim is to introduce truly MIMO margin calculations and to understand their efficacy in certifying stability over a set of controllers and in replacing legacy single-loop gain and phase margin calculations.

We consider methods for the computation of; maximal MIMO stability margins $b_{\hat{P},C}$, minimal ν-gap metrics δ_ν, and the maximal difference between these two values, through the use of scaling and weighting functions. We propose simultaneous scaling selections that attempt to maximize the generalized stability margin and minimize the ν-gap. The minimization of the ν-gap by scaling involves a non-convex optimization. We modify the XY-centering algorithm to handle this non-convexity. This is done for applications in controller certification.

Estimating the generalized stability margin with an accurate error bound has significant impact on controller certification. We analyze an error bound of the generalized stability margin as the infinity norm of the MIMO empirical transfer function estimate (ETFE). Input signal design to reduce the error on the estimate is also studied. We suggest running the system for a certain amount of time prior to recording of each output data set. The assured upper bound of estimation error can be tuned by the amount of the pre-experiment.

1

Introduction

In this dissertation, we study the inference of generalized stability margins for a large number of controllers. The stability guarantee of candidate controllers is given by pre-established stability margins of a small number of ν-gap-wise adjacent controllers. The generalized stability margin and the ν-gap metric are inherently able to handle MIMO stability analysis without the necessity of repeating multiple channel-by-channel SISO analyses. This research consists of three parts: (i) development of a decision support tool for inference of the stability margin, (ii) computational considerations for obtaining the maximal stability margin with the minimal ν-gap metric in a less conservative manner, and (iii) experiment design for estimating the generalized stability margin with an assured error bound.

1.1 Motivation

This problem was formulated in the aerospace industry, where a single engine is required to operate at a large number of possible constraint points depending on task. Often the demand for highly efficient operation pushes engine conditions to the their physical limits. For instance, the best thermal efficiency of an engine is attained at the temperature of near melting point of parts. Temperature overshoot can cause catastrophic turbine degradation. Fan and compressor efficiency is best at near stall, surge, and flutter margins. Once the fan or compressor is operated beyond these margins, the engine would suffer from unstable operation for a while, which is unacceptable to

an aircraft that requires high performance maneuvering. Therefore, a high performance jet engine must respect many possible constraints. Typically, Dynamic Inversion and/or Model Predictive Control are applied to generate linearized engine controllers to maintain stability and control at one of a large number of possible operating constraints (Davies, Holt & Griffin 2006, Holt 2006). Particularly in jet engine control for a Short Takeoff and Vertical Landing (STOVL) aircraft, constraints are connected with the engine hardware limits such as actuator amplitude/rate limits, operating temperature limits, cooling flow pressure ratio limits, and compressor stall margin. The upper limits will not be active at the same time as lower limits on the one variable. The engines are necessarily highly coupled MIMO systems. The same engine operates in low altitude, low velocity, high power demand for short takeoff and in supersonic flight, leading to dramatically different constraint sets operating. For example, if there were 20 constraints and up to four were active at any one instance, there are 6196 possible combinations of constraints, and hence roughly this many different controllers. In practice, the plant-controller testing will need to be fully MIMO and to permit the computation of generalized stability margin as a function of frequency. This, as we will show, will require H_∞-norm estimation, which is a data-intensive and therefore costly experimental test, for each controller. This motivates our desire to minimize the number of necessary test points by developing an inferential technique. In recent days, by the Group for Aeronautical Research and Technology in Europe (GARTEUR), active research on certification of flight control law has been done (Fielding, Varga, Bennani & Selier 2002). In (Fielding, Varga, Bennani & Selier 2002), different kinds of tools for clearance of flight control laws were investigated including the ν-gap analysis, μ-synthesis, bifurcation method, and optimization-based the worst case search method. In this dissertation, we will use the ν-gap metric for the stability inference tool for a high performance jet engine controllers. The ν-gap metric was introduced by Vinnicombe (Vinnicombe 1993) as the notion of closeness between systems in the feedback control sense. The generalized stability margin of a plant and controller pair denotes a neighborhood of perturbations about the normalized coprime factors of the plant stabilized by controller such that the perturbed closed-loop system will remain stable (McFarlane & Glover 1989). A higher value of the generalized stability margin is equivalent to the ability of the feedback loop to retain stability margin against the larger

deviations in controllers. For a single-input-single-output (SISO) system, the gain margin (GM) with the phase margin (PM), the magnitude margin, and delay margin can be used as a measure for the stability robustness. Vinnicombe's ν-gap metric with the generalized stability margin can be understood as an extension of SISO stability robustness to the realm of multi-input-multi-output control systems. Glover et al. (Glover, Vinnicombe & Papageorgiou 2000) provide the interpretation of the generalized stability margin with allowable gain and phase changes of independent input and output channel without loosing stability. A fundamental relationship between stability margin, $b_{P,C}$, and distance between candidate controllers, $\delta_\nu(C_i, C_j)$, is given by,

$$\arcsin b_{P,C_j} \geq \arcsin b_{P,C_i} - \arcsin \delta_\nu(C_i, C_j). \tag{1.1}$$

Definitions of terms in (1.1) will be given in Chapter 2. This inequality is a dual expression of (Vinnicombe 1993) where the ν-gap is used to measure plant variability and/or uncertainty. Whereas, we use the ν-gap metric to explain the legitimate amount of controller variations. In (1.1), the larger stability margin of the C_j can be inferred by the larger b_{P,C_i} with the smaller distance between two controllers. In Chapter 2, we will develop a decision support tool for certification of a large set of MIMO controllers using the inference inequality (1.1). Our aim is to replace multiple legacy channel-by-channel certifications by a single full MIMO procedure.

In Chapter 3, we will discuss a method for computing a non-conservative margin and ν-gap through LMI formulations. Crucial ingredients of controller certification are computations of the generalized stability margin and the ν-gap between any two controllers. Theses computations involve finding H_∞-norms, i.e., the maximum singular value of a transfer function matrix over all frequency points. Thus the source of conservatism in the margin and ν-gap computations can be identified as two characteristics of H_∞-norm being

- the supremum over frequencies and
- a scalar measure of a matrix property.

The first conservatism can be removed through frequency-by-frequency analysis. However, to ameliorate the second type of conservatism, we must resort to use of scaling

matrices. Relative signal magnitudes or measurement units pertaining to the input and output signals greatly affect the size of the maximum singular value. Indeed, the singular value of a stable transfer function, T, is square root of the energy gain in the worst direction of input and output vectors,

$$\overline{\sigma}(T) = \sup_{u \neq 0} \frac{\|Tu\|_2}{\|u\|_2} = \sup_{u \neq 0} \frac{\|y\|_2}{\|u\|_2}.$$

Thus, if the system is not scaled appropriately and magnitude of any input or output signal is extremely larger than other magnitudes of signals then, the maximum singular value can be correspondingly very large. These reflect the conservatism of the H_∞-norm as a MIMO stability margin. The scalings in the generalized stability margin and the ν-gap metric computations have a stability analysis purpose and we can say the scaling reveals what the generalized stability margin should look like. The scaling problem for the generalized stability margin can be formulated as a convex optimization. This optimization problem is readily solved using LMI methods minimizing norms by scaling as in (Boyd, Ghaoui, Feron & Balakrishnan 1994). Whereas, scaling of the ν-gap metric cannot be formulated as a convex optimization. To tackle non-convex optimization, we modify the XY-centering algorithm (Iwasaki & Skelton 1995). We propose simultaneous scaling selections that attempt to maximize the generalized stability margin and to minimize the ν-gap jointly. Let us consider square matrices, W_i and W_o, namely an input and output scaling matrix, respectively. Then the inference inequality (1.1) can be rewritten as a scaled version,

$$\begin{aligned} &\arcsin b_{W_o P W_i, W_i^{-1} C_j W_o^{-1}} \\ &\qquad \geq \arcsin b_{W_o P W_i, W_i^{-1} C_i W_o^{-1}} - \arcsin \delta_\nu (W_i^{-1} C_i W_o^{-1}, W_i^{-1} C_j W_o^{-1}). \end{aligned} \tag{1.2}$$

Since W_i and W_o that improve $b_{W_o P W_i, W_i^{-1} C W_o^{-1}}$ cannot always make $\arcsin \delta_\nu (W_i^{-1} C_i W_o^{-1}, W_i^{-1} C_j W_o^{-1})$ smaller or, at least, same with $\delta_\nu(C_i, C_j)$, the input and output scaling martices that try to increase $b_{W_o P W_i, W_i^{-1} C W_o^{-1}}$ and to decrease $\arcsin \delta_\nu (W_i^{-1} C_i W_o^{-1}, W_i^{-1} C_j W_o^{-1})$ simultaneously must be considered for efficient controller certification.

Another important component for efficient controller certification will be studied in Chapter 4. Along with less conservative computations of the generalized stability margin and the ν-gap, estimating the generalized stability margin with an accurate error

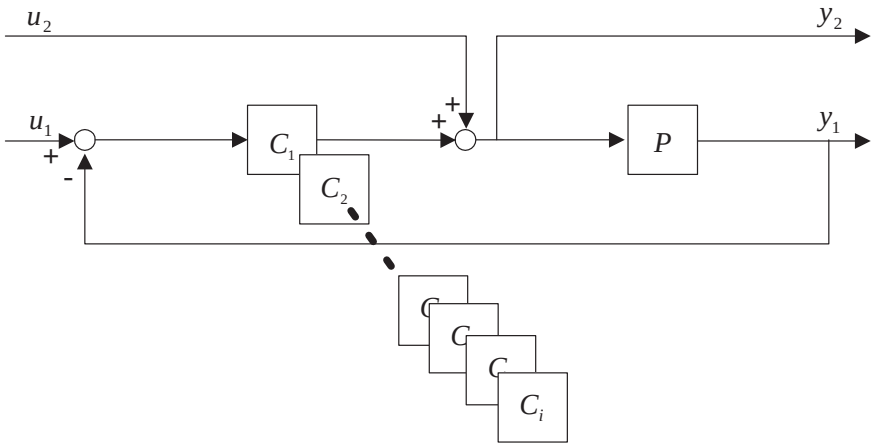

Figure 1.1: A feedback loop with a large number of candidate controllers.

bound has a significant impact on controller certification. At a fixed frequency point, we analyze an error bound on the generalized stability margin as the infinity norm of the MIMO empirical transfer function estimate (ETFE). We also provide, by bounding the interpolation error bound between any two frequency points, an upper bound on the error on a continuous frequency interval. Input signal design to reduce the error of the estimate is also studied. The swept-sine signal is used as a scalar test input signal. For MIMO estimation, we conduct as many experiments as the number of inputs. Each vector input can be generated by multiplying the scalar input by each column vector of a full rank matrix so that invertibility of the input DFT matrix can be assured. The magnitude of estimation error depends on several factors, such as the number of samples in the DFT computation, the energy in the input DFT at a specific frequency, the number of samples of pre-experimental running, and downsampling so on. We suggest running the system for a certain amount of time prior to recording of each output data set. The assured upper bound of estimation error can be tuned by the amount of the pre-experiment.

1.2 Outline of Dissertation

In Chapter 2, as shown in Figure 1.1, we consider an uncertain plant, P, with a single model, $\hat{P}$, and a ***large*** set of candidate controllers, C_i, each designed to achieve

internal stability with the model. The unknown plant, P, probably be a non-linear system and the model, $\hat{P}$, would be a local representation of P. According to the active physical constraints, a single particular controller C_i is employed in the feedback loop. The problem studied in Chapter 2 is to select a ***small*** subset of controllers, so that through experimental tests the complete set is guaranteed or not to achieve a certain level of stability with the unknown real plant. A controller, C, is said to be ***certified*** at level α, if the generalized stability margin of the unknown plant and the controller pair (P, C) is shown to be greater than a pre-specified margin level $\alpha \in [0, 1)$,

$$b_{P,C} > \alpha.$$

On the other hand, a controller C is said to be ***rejected*** at level $\beta \in [0, 1)$ if

$$b_{P,C} \leq \beta.$$

Let us assume we have two controllers, C_0 and C_1, and b_{P,C_0} is already estimated from closed-loop data. Then, if the ν-gap distance between two controller is bounded as in the following inequality,

$$\arcsin \delta_\nu(C_0, C_1) < \arcsin b_{P,C_0} - \arcsin \alpha,$$

certification of C_1 ($b_{P,C_1} > \alpha$) can be inferred without doing an extra experiment for estimation. Rejection of C_1 ($b_{P,C_1} \leq \beta$) can also be guaranteed if $b_{P,C_0} \leq \beta$ and

$$\arcsin \delta_\nu(C_0, C_1) \leq \arcsin \beta - \arcsin b_{P,C_0}.$$

In Chapter 2, we provide algorithms to reduce the number of experiments to certify/reject a large number of controllers using the above two inequalities.

In Chapter 3, computational considerations for the generalized stability margin and the ν-gap metric as considered. As shown in Figure 1.2, we use the input scaling, W_i, and the output scaling, W_o, to attempt to reduce conservatism in those computations. Three interesting classes of scaling function matrices arise naturally:

1) W_i, W_o positive definite symmetric matrices, constant over frequency $\omega \in \mathbb{R}$,

2) W_i, W_o positive definite hermitian matrices at a fixed frequency ω_n, and

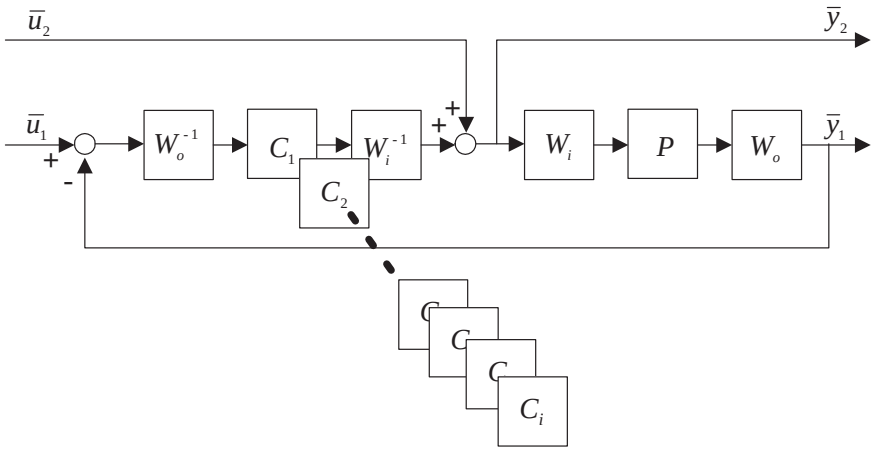

Figure 1.2: A feedback loop with the input and output scaling matrices.

3) $W_i(s)$, $W_o(s)$ bistable and bi-proper transfer function matrices interpolating W_i, W_o at a sequence of frequency values $\{\omega_n\}$.

We shall consider the first two kinds of scaling matrices in Chapter 3. We will present the formulation of a convex optimization problem to find the input/output weights for maximization of $b_{\hat{P},C}$. This optimization problem is readily solved using LMI methods minimizing norms by scaling as in (Boyd, Ghaoui, Feron & Balakrishnan 1994). With the analysis in (Fielding, Varga, Bennani & Selier 2002), conservatism of $b_{\hat{P},C}$ can be reduced fairly well.We also propose an approach to simultaneous alleviation of the conservatism in both of the $b_{\hat{P},C}$ and ν-gap metric computations.

In Chapter 4, we consider estimation of the generalized stability margin from closed-loop data using the MIMO empirical transfer function estimate (ETFE). Consider N-point of experimental data, $\{x(0), x(1), \cdots, x(N-1)\}$. Then the function X_N^l is defined as,

$$X_N^l = \frac{1}{\sqrt{N}} \sum_{t=0}^{N-1} x(t) e^{-j\frac{2\pi l}{N}t},$$

with $l = 0, 1, \cdots, N-1$ forming the discrete fourier transform (DFT) of the finite data sequence, $\{x(0), x(1), \cdots, x(N-1)\}$. For SISO system, we will identify the residual error, R_N^l, in the following DFT relationship,

$$R_N^l = Y_N^l - \left(G(e^{j\frac{2\pi l}{N}}) U_N^l + V_N^l \right)$$

where, Y_N^l, U_N^l, and V_N^l are the DFT of the output, $y(t)$, input, $u(t)$, and noise signal, $v(t)$.

and formulate a bound on R_N^l(not true).

and suggest an appropriate input signal to maintain the size of error due to the initial conditions and additive measurement noise. We extend the SISO result to MIMO error analysis using a full rank matrix, e.g., the Hadamard matrix.

1.3 Contributions

The contributions of this dissertation can be summarized as follows:

(1) Development of the stability inference tool that establishes the generalized stability margin of a large number of controllers by performing tests on a small subset. (Chapter 2)

- Identifying the ν-gap metric as a MIMO controller certification tool.
- Derivation of a radius of a ball in the Euclidean parameter space in which the controllers will guarantee a certain level of stability.
- Providing the certification algorithm and the rejection algorithm for a finite set of MIMO controllers.
- Providing the certification algorithm for an infinite set of SISO controllers.

(2) Numerical considerations for the generalized stability margin and the ν-gap metric computations for efficient MIMO Controller Certification(Chapter 3)

- Reducing conservatism in computations of the generalized stability margin and the ν-gap metric individually and simultaneously through scalings.
- Formulating the frequency dependent LMIs yielding the input and output scalings that can be used to find the maximal inferred generalized stability margin.

(3) Experiment design for the generalized stability margin estimation with an accurate error bound (Chapter 4)

- Derivation of the error bound in estimating the generalized stability margin from closed-loop data
- Reducing the error bound by conducting the pre-experiments before each recording of measurement for the DFT
- Designing vector inputs for MIMO ETFE

2

Controller Certification

A modern problem from aerospace control involves the certification of a large set of potential controllers with either a single plant or a fleet of potential plant systems, with both plants and controllers being MIMO and, for the moment, linear. Experiments on a limited number of controller/plant pairs should establish the stability and a certain level of margin of the complete set. We consider this certification problem for a set of controllers and provide algorithms for selecting an efficient subset for testing. This is done for a finite set of candidate controllers and, at least for SISO plants, for an infinite set. In doing this, the ν-gap metric will be the main tool. Computational examples are given, including one of certification of an aircraft engine controller. The overarching aim is to introduce truly MIMO margin calculations and to understand their efficacy in certifying stability over a set of controllers and in replacing legacy single-loop gain and phase margin calculations.

2.1 Introduction

We consider a single but uncertain plant system, P, with a fixed model, $\hat{P}$, with a "large" set, $\mathcal{C}$, of candidate controllers, C_i, designed to achieve internal stability and performance on $\hat{P}$. The problem studied is to select a "small" subset, $\{C_i\} \subset \mathcal{C}$, so that through experimental testing of pairs (P, C_i) the complete set $\mathcal{C}$ is certified, meaning that all pairs (P, C_j) are guaranteed to achieve internal stability with a prescribed margin. This problem is termed *Controller Certification*.

This problem was formulated in the aerospace industry, where a single engine is required to operate at a large number of possible constraint points depending on task. Typically, Dynamic Inversion and/or Model Predictive Control are applied to generate linearized engine controllers to maintain stability and control at one of a large number of possible operating constraints (Davies, Holt & Griffin 2006, Holt 2006). Particularly in jet engine control for a Short Takeoff and Vertical Landing (STOVL) aircraft, constraints are connected with the engine hardware limits such as actuator amplitude/rate limits, operating temperature limits, cooling flow pressure ratio limits, and compressor stall margin. The upper limits will not be active at the same time as lower limits on the one variable. The engines are necessarily highly coupled MIMO systems. The same engine operates in low altitude, low velocity, high power demand for short takeoff and in supersonic flight, leading to dramatically different constraint sets operating. For example if there were 20 constraints and up to four were active at any one instance, there are 6196 possible combinations of constraints, and hence roughly this many different controllers. The plant model also must be adjusted for operating points. However, this latter variation is not yet our concern, nor do we consider time-varying stability due to controller change or operating point change since this requires at least stability at each stationary value. In practice, the plant-controller testing will need to be fully MIMO and to permit the computation of generalized stability margin, $b_{P,C}$ (to be introduced later), as a function of frequency. This will require H_∞-norm estimation, see (Chen & Gu 2000), which is a data-intensive and therefore costly experimental test for each controller. This motivates our desire to minimize the number of necessary test points.

The aim is to use controller validation to determine a feasible subset of tests of the most informative controllers – as determined using the plant model $\hat{P}$ – and thereby to reduce the requisite number of overall physical tests. This certification of controllers is a central part of the commissioning of new high-performance multi-input/multi-output (MIMO) engine controllers, which historically has been conducted using single-loop closed-loop tests based on approved gain and phase margins.

The approach which we consider here is based on linear multivariable control ideas using Vinnicombe's ν-gap metric tools. It extends earlier approaches from single-input/single-output (SISO) loop consideration to a full MIMO problem. It remains linear

at this stage, although there are techniques being developed based on Sum-of-Squares methods (Papachristodoulou & Prajna 2002) for extension to nonlinear systems.

Recently this safety issue was studied by Action Group 11 of GARTEUR (Group for Aeronautical Research and Technology in Europe) who explored advanced clearance techniques to prove, before the aircraft is tested in flight, that a flight control system is safe and has the desired performance under all possible flight conditions and in the presence of certain controller failures (Fielding, Varga, Bennani & Selier 2002). In Chapter 18 of the book (Fielding, Varga, Bennani & Selier 2002), Steele and Vinnicombe used the ν-gap metric to obtain a linearized approximate model of a nonlinear system with parametric uncertainty.

The importance of using experimental evaluation of designed controllers is also advocated by controller unfalsification (Safonov & Tsao 1997). By using experimental input-output data of a plant, the unfalsified control theory sifts the controllers that are demonstrably unrobust from a set of candidate controllers. In this paper, however, using experimental data, we guarantee certified controllers to have the required degree of stability and margin. Quantitative Feedback Theory (QFT) (Horowitz & Sidi 1972) has been proposed as a computational approach to deal with a related problem of determining whether a controller is capable of stabilizing a number of different plants. Here the roles of plant and controller are reversed, but the method otherwise is related. The tack taken here is ideologically similar to QFT, which is based typically on Nichols charts and frequency response data. However we use analytical tools such as the frequency-dependent Vinnicombe ν-gap metric as a more formal tool which deals rationally and computationally with the MIMO nature of the problem and further lays the groundwork for extension to dealing with aircraft fleet variability.

The first category of the problem is certification of a finite candidate controller set, $\mathcal{C}$, which is considered in Section 3. In Section 4 an illustrative example of solving this first category is provided based on the F-100 jet engine and a parametrized set of LQG PI controllers. This example is purely computational and uses a full-order 'truth model' P and a reduced-order $\hat{P}$. A fully practical example is as yet not possible, because the development of a guaranteed certification process remains a hurdle to the full implementation of MIMO engine controllers. The second class of problems that we

consider is the finite certification of an infinite (but ν-gap compact) controller set, which is considered in Section 5. In this section, we are able to give for the SISO case alone an algorithm and an example of certification for $\mathcal{C}$ with infinite cardinality but parametrized by a finite-dimensional parameter. We point to central issues with the parametrization of MIMO controllers, which limits the extension of this approach to the MIMO case. In the next section we provide basic definitions and a theorem for stability and margin guarantees based on the ν-gap metric.

2.2 Definitions and a guarantee

The ν-gap metric (Vinnicombe 1993, Zhou & Doyle 1998, Vinnicombe 2001), $\delta_\nu(\cdot,\cdot)$ measures the distance between two systems yielding a number $\delta_\nu(C_i, C_j) \in [0,1]$.

Definition 2.2.1. *(The Winding Number Condition; WNC). Two controllers, $C_0(s)$ and $C_1(s)$, satisfy the Winding Number Condition if*

$$\begin{aligned} \det(I + C_1^* C_0)(j\omega) \neq 0,\ \forall\omega \ \textit{and} \\ \text{wno}\ \det(I + C_1^* C_0) + \eta(C_0) - \eta(C_1) = 0, \end{aligned} \tag{2.1}$$

where wno$(\cdot)$ *indicates the winding number of the Nyquist diagram of the scalar transfer function evaluated on a contour enclosing the right-half-plane and indented along the imaginary axis to the right around any pure imaginary poles, and $\eta(C)$ is the number of open right-half-plane poles of* $\det(C)$.

Definition 2.2.2 (κ function)**.** *Given two commensurate transfer function matrices, $C_0(s)$ and $C_1(s)$,*

$$\kappa(C_0, C_1) = \left\| (I + C_1 C_1^*)^{-\frac{1}{2}} (C_1 - C_0)(I + C_0^* C_0)^{-\frac{1}{2}} \right\|_\infty . \tag{2.2}$$

Definition 2.2.3 (Vinnicombe's ν-gap metric)**.**

$$\delta_\nu(C_0, C_1) = \begin{cases} \kappa(C_0, C_1), & \textit{if the WNC holds} \\ 1, & \textit{else} \end{cases} \tag{2.3}$$

The *generalized sensitivity function* of the plant-controller feedback pair (P, C) is given by

Definition 2.2.4 (Generalized Sensitivity Function)**.**

$$T(P,C) = \begin{pmatrix} P(I+CP)^{-1}C & P(I+CP)^{-1} \\ (I+CP)^{-1}C & (I+CP)^{-1} \end{pmatrix}. \tag{2.4}$$

Then the *generalized stability margin* of (P, C) is defined by the generalized sensitivity function as follows.

Definition 2.2.5 (Generalized Stability Margin)**.**

$$b_{P,C} = \begin{cases} (\|T\|_\infty)^{-1}, & \text{if } (P,C) \text{ is stable,} \\ 0, & \text{else.} \end{cases} \tag{2.5}$$

McFarlane and Glover (McFarlane & Glover 1989) used $b_{P,C}$ to denote a neighborhood of perturbations about the normalized coprime factors of P stabilized by C such that the perturbed closed-loop system will remain stable. $b_{P,C}$ has a value between $[0, 1]$ and the fact that $b_{P,C} > 0$ indicates the feedback pair (P, C) is stable and a higher value of $b_{P,C}$ is equivalent to the fact that the pair (P, C) retains stability for larger deviations in controller, as measured by the ν-gap metric. The definitions of the stability margin and the ν-gap metric may be extended from an infinity norm over all frequencies to singular values at each specific frequency, yielding frequency dependent quantities $b_{P,C}(\omega)$ and $\delta_\nu(C_i, C_j, \omega)$ (Vinnicombe 2001). The values $b_{P,C}$ $b_{P,C}(\omega)$ can be retrieved from experimental data, as will be shown in Chapter 4. The key relation of the ν-gap metric follows.

Theorem 2.2.1 (Vinnicombe(Vinnicombe 1993, Vinnicombe 2001))**.** *Consider a plant P and two controllers C_i and C_j, with C_i stabilizing P. Then the following results hold.*

Stability guarantee: *(P, C_j) is stable if*

$$\delta_\nu(C_i, C_j) < b_{P,C_i}. \tag{2.6}$$

Margin guarantee: *If $\delta_\nu(C_i, C_j) < b_{P,C_i}$ then*

$$\arcsin b_{P,C_j} \geq \arcsin b_{P,C_i} - \arcsin \delta_\nu(C_i, C_j), \tag{2.7}$$

and further,

$$\begin{aligned} \delta_\nu(C_i, C_j) &\leq \|T(P,C_i) - T(P,C_j)\|_\infty \\ &\leq \frac{\delta_\nu(C_i, C_j)}{b_{P,C_i} b_{P,C_j}}. \end{aligned} \tag{2.8}$$

Notice that Theorem 2.2.1 is only a sufficient condition for stability guarantee, i.e., at a ν-distance greater than b_{P,C_i} from C_i, there might exist a controller that stabilizes the plant, P. Further note that equipping the set of controller systems with a metric creates a metric space within which one may define neighborhoods. Using the ν-gap metric and the generalized stability margin, we can define the largest neighborhood of controllers about a given stabilizing controller for which a minimum level of margin (or performance measured by $\|T\|_\infty^{-1}$) is guaranteed with the plant.

2.3 Vinnicombe's Winding Number is not Transitive

In this section, we show non-transitivity of the winding number condition and its impacts on controller certification. The ν-gap metric computation consists of two pieces: checking a winding number condition, and computing a frequency-domain norm, $\kappa(\cdot,\cdot)$. Again, the aim of certification is establishing a certain level of the generalized stability margin of a large number candidate controllers with as few experiments as possible. The certification algorithm which will be introduced in Section 2.5 requires computation of the ν-gap distance between every pair of controllers. If the winding number condition were transitive, then we could eliminate the computational burden of checking the winding number condition in the ν-gap computations for the entire controller certification for the large set. The positive aspect is that non-transitivity could be warranty for searching for a controller that can certify at least two other controllers C_0 and C_1 even with $\delta_\nu(C_0, C_1) = 1$ so that all controllers might be certified by a single experiment. We will go into this issue in detail in the following section.

Cautious adaptation and the YK-homotopy

Anderson & Gevers (1998) proposed an approach to the selection of a new controller in which the inclusion of a ν-gap limit is easily feasible. This is based on the use of the Youla-Kucera parametrization of stabilizing controllers. Here we develop this slightly by using a normalized coprime factorization for the definition of the homotopy.

Definition 2.3.1 (YK-homotopy)**.** *Suppose we are given:*

– *A plant model P_0 with normalized coprime factorizations $P_0 = XY^{-1} = \tilde{Y}^{-1}\tilde{X}$,*

– *P_0-stabilizing and P-stabilizing controller C_0 with right coprime factorization $C_0 = ND^{-1}$ satisfying $\tilde{Y}D + \tilde{X}N = I$,*

– *P_0-stabilizing candidate controller C_1 with right coprime factorization given by the Youla-Kucera parameter Q, $C_1 = (N - YQ) \cdot (D + XQ)^{-1}$.*

Then we define the YK-homotopy of P_0-stabilizing controllers by

$$\left\{ C_\rho = (N - \rho YQ)\,(D + \rho XQ)^{-1} :\ \rho \in [0,1] \right\}. \tag{2.9}$$

Theorem 2.3.1. *For two controllers within the same YK-homotopy we have*

$$\begin{aligned} \delta_\nu\left(C_{\rho_1}, C_{\rho_2}\right) &\le \left\| T(P_0, C_{\rho_1}) - T(P_0, C_{\rho_2}) \right\|_\infty \\ &= \left|\rho_1 - \rho_2\right| \left\| Q \right\|_\infty \end{aligned} \tag{2.10}$$

Proof: The first inequality comes from Theorem 2.2.1. The second is derived as follows from

$$\begin{aligned} T(P_0, C_0) &= \begin{pmatrix} N \\ D \end{pmatrix} \left(\tilde{Y}D + \tilde{X}N \right)^{-1} \begin{pmatrix} \tilde{X} & \tilde{Y} \end{pmatrix} \\ &= \begin{pmatrix} N \\ D \end{pmatrix} \begin{pmatrix} \tilde{X} & \tilde{Y} \end{pmatrix}. \end{aligned}$$

$$T(P, C_{\rho_1}) - T(P_0, C_{\rho_2}) = (\rho_1 - \rho_2) \begin{pmatrix} -Y \\ X \end{pmatrix} Q \begin{pmatrix} \tilde{X} & \tilde{Y} \end{pmatrix},$$

$$\begin{aligned} &\left\| T(P_0, C_{\rho_1}) - T(P_0, C_{\rho_2}) \right\|_\infty \\ &= \left|\rho_1 - \rho_2\right| \sup_\omega \lambda_{\max}^{\frac{1}{2}} \left[\begin{pmatrix} -Y \\ X \end{pmatrix} Q \begin{pmatrix} \tilde{X} & \tilde{Y} \end{pmatrix} \begin{pmatrix} \tilde{X}^\star \\ \tilde{Y}^\star \end{pmatrix} Q^\star \begin{pmatrix} -Y^\star & X^\star \end{pmatrix} \right] \\ &= \left|\rho_1 - \rho_2\right| \sup_\omega \lambda_{\max}^{\frac{1}{2}} \left[\begin{pmatrix} -Y^\star & X^\star \end{pmatrix} \begin{pmatrix} -Y \\ X \end{pmatrix} Q \begin{pmatrix} \tilde{X} & \tilde{Y} \end{pmatrix} \begin{pmatrix} \tilde{X}^\star \\ \tilde{Y}^\star \end{pmatrix} Q^\star \right] \\ &= \left|\rho_1 - \rho_2\right| \left\| Q \right\|_\infty. \end{aligned}$$

$\nabla\nabla\nabla$

This establishes the following property.

Corollary 2.3.1. *Within the YK-homotopy, $\delta_\nu(C_0, C_\rho)$ is continuous in ρ.*

Proof: From the theorem above and the triangle inequality of the ν-gap metric, we have

$$\begin{aligned} |\delta_\nu(C_0, C_{\rho+d\rho}) - \delta_\nu(C_0, C_\rho)| &\leq \delta_\nu(C_{\rho+d\rho}, C_\rho) \\ &\leq |d\rho| \, \|Q\|_\infty . \end{aligned}$$

$\nabla\nabla\nabla$

We have the immediate corollary, which marginally extends an idea of Anderson & Gevers (1998).

Corollary 2.3.2. *Given an arbitrary bound $\epsilon > 0$, it is always possible to choose a positive value $\rho_{\max} = \min[1, \epsilon/\|Q\|_\infty]$ such that $\delta_\nu(C_0, C_\rho) < \epsilon$ for all $\rho < \rho_{\max}$.*

This corollary may be used to develop cautious control adaptation by combining condition (2.6) with this bound on ρ. The result (2.10) further shows that the YK-homotopy provides a path between controllers C_0 and C_1 which is connected in the ν-gap metric. It further provides a bound on the deviation of the designed closed-loop performance with model P_0 as ρ is varied. Although this is less important than bounds on the performance with P, which are captured by (2.7).

Nontransitivity of the Winding Number Condition

Satisfaction of the winding number condition (WNC) by two controllers is a reflexive and symmetric relation. Reflexivity follows since $\det(I + C_0^\star C_0)(j\omega)$ is a strictly positive function whose winding number is therefore zero. Thus the pair (C_0, C_0) satisfies WNC. Symmetry follows from the conjugate-negation of $\operatorname{wno}\det(I + C_1^\star C_0)$. So that if (C_0, C_1) satisfies WNC, then so does (C_1, C_0). Transitivity would make satisfaction of the winding number condition an equivalence relation.

Transitivity of the WNC would validate the following implication.

$$\begin{aligned} &[(C_0, C_1) \text{ satisfies WNC}] \wedge [(C_1, C_2) \text{ satisfies WNC}] \\ &\implies [(C_0, C_2) \text{ satisfies WNC}] . \end{aligned}$$

We shall shortly demonstrate by example that this is false. However, were it to be true, then one would have from Corollary 2.3.2 that all controllers in the YK-homotopy

would satisfy pairwise the winding number condition. Then the search for guaranteed P-stabilizing controllers would need only to consider the computation of the frequency norm $\kappa(C_0, C_\rho)$ among the candidate controllers. As will be demonstrated in the example, the κ function can return close to zero as one explores the YK-homotopy for larger values of ρ than those given by Corollary 2.3.2. The fact that we need separately to verify WNC is a reflection of the coarseness of the ν-gap metric.

Example

We borrow a example from (Blondel, Gevers & Bitmead 1997), in which two dramatically different plant models are stabilized by the same constant controller, yielding very closely similar closed-loop responses. We consider the dual of the example.

$$\begin{aligned}
P(s) &= 5.918, \\
X(s) &= \tilde{X}(s) = 0.9860, \\
Y(s) &= \tilde{Y}(s) = 0.1666, \\
C_0(s) &= \frac{(s-1)}{(s-2)(s-3)}, \\
D(s) &= \tilde{D}(s) = \frac{(s-2)(s-3)}{0.1666s^2 + 0.1530s + 0.0137}, \\
N(s) &= \tilde{N}(s) = \frac{(s-1)}{0.1666s^2 + 0.1530s + 0.0137}, \\
C_1(s) &= \frac{-1.22}{s + 7.32}, \\
Q(s) &= \frac{2.22s^2 + 0.22s}{0.0278s^3 + 0.0283s^2 + 0.048s + 0.0002},
\end{aligned}$$

These transfer functions satisfy the conditions required for us to develop the YK-homotopy of controllers, $\{C_\rho(s)\}$. Figure 2.1 shows two curves. The solid curve depicts $\delta_\nu(C_0, C_\rho)$ versus ρ, and the dashed curve shows $\delta_\nu(C_1, C_\rho)$ versus ρ. A zoomed version of the region in the neighborhood of $\rho = 0.383$ is shown in Figure 2.2. In these figures, a value of δ_ν less than one indicates that the winding number condition is satisfied by the two transfer functions. Thus from Figure 2.2, it is apparent that $(C_0, C_{0.383})$ and $(C_1, C_{0.383})$ satisfy WNC. A simple examination shows that (C_0, C_1) does not satisfy WNC. This establishes by example that WNC is not transitive.

Figure 2.3 shows the plot of $\kappa(C_0, C_\rho)$ as a function of ρ. For small values of

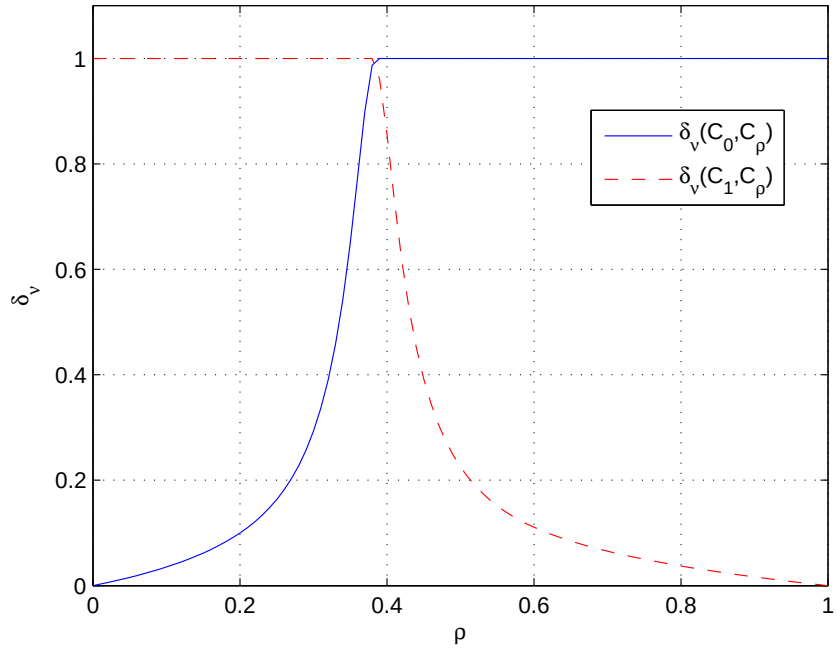

Figure 2.1: The ν-gap distance between C_0 and C_ρ (solid curve) and between C_1 and C_ρ as a function of ρ.

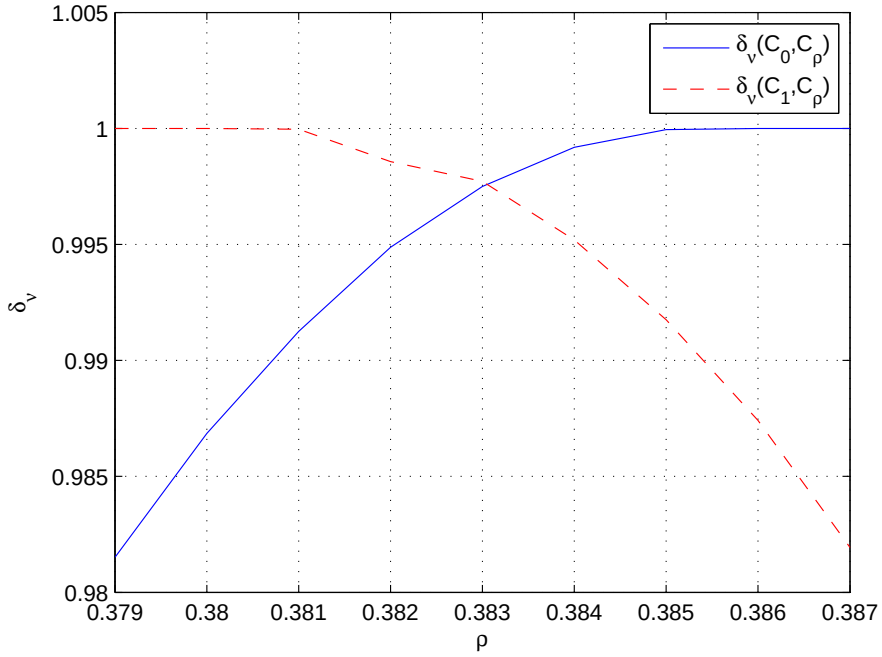

Figure 2.2: Zoomed image of the ν-gap metric plot.

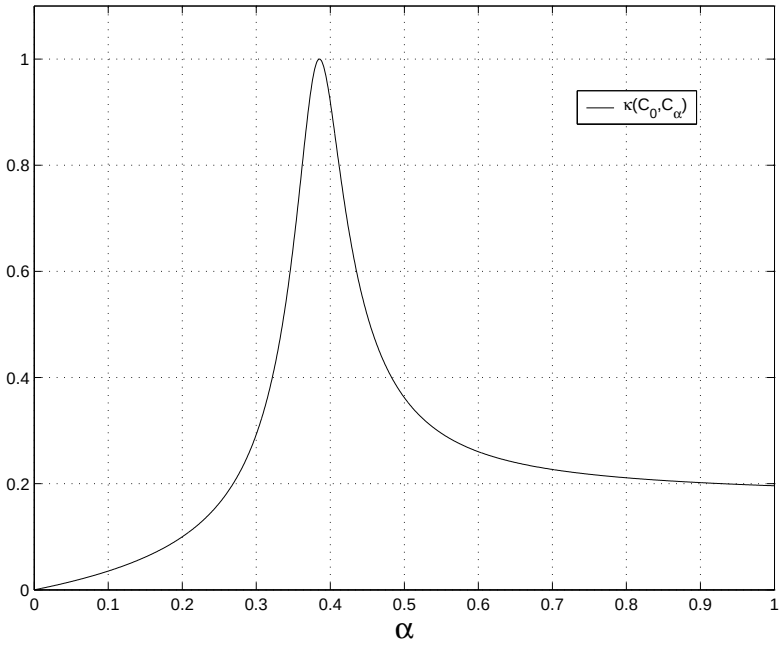

Figure 2.3: The frequency norm function $\kappa(C_0, C_\rho)$ versus ρ.

ρ it follows the $\delta_\nu(C_0, C_\rho)$ curve, of course. However, for larger ρ the function κ fails to indicate the dissatisfaction of WNC.

2.4 The Generalized Stability Margin Inference

Definition 2.4.1. *Given a set of controllers, not necessarily finite, $\mathcal{C} = \{C\}$, each element of which is designed to stabilize the fixed plant model $\hat{P}$, a particular controller C is said to be certified at level α if, using experimental data with the unknown actual plant P, we can guarantee that the generalized stability margin of the pair (P, C) is greater than a pre-specified performance level $\alpha \in [0, 1)$,*

$$b_{P,C} > \alpha. \tag{2.11}$$

Definition 2.4.2. *A controller C is said to be rejected at level β if*

$$b_{P,C} \leq \beta. \tag{2.12}$$

Note that controllers might remain neither certified nor rejected after an experiment.

Clearly, one could certify or reject all candidate controllers in a finite set by testing experimentally all pairs (P, C_j). Our aim here is to devise a systematic procedure for testing only a small subset of the candidate controllers and thence certifying all the remaining controllers. For an infinite controller set, one must rely on certification based on tests involving finite subsets of the candidates. The central tool that we shall apply in controller certification is the ν-gap metric. We have the following immediate result.

Lemma 2.4.1. *Given stabilizing plant-controller pair (P, C_i) with $b_{P,C_i} > \alpha$, if*

$$\arcsin \delta_\nu(C_i, C_j) < \arcsin b_{P,C_i} - \arcsin \alpha, \tag{2.13}$$

then C_j is certified at level α. On the other hand, if $0 < b_{P,C_i} \leq \beta$ and

$$\arcsin \delta_\nu(C_i, C_j) \leq \arcsin \beta - \arcsin b_{P,C_i}, \tag{2.14}$$

then C_j is rejected at level β.

From Theorem 2.2.1, if $\delta_\nu(C_i, C_j) = 1$, neither controller can guarantee the stability of the other with the plant, no matter how big their generalized stability margins might be. In this case, it seems that we must conduct the experiment twice to find whether both b_{P,C_i} and b_{P,C_j} are sufficiently large. However, there could exist a controller, C_k, such that $\delta_\nu(C_i, C_k) < 1$ and $\delta_\nu(C_k, C_j) < 1$, because the winding number condition associated with the ν-gap metric is not transitive as shown in Section 2.3. Furthermore, if b_{P,C_k} is sufficiently larger than α so that the controller, C_k, is able to satisfy both

$$\arcsin \delta_\nu(C_i, C_k) < \arcsin b_{P,C_k} - \arcsin \alpha$$
$$\arcsin \delta_\nu(C_k, C_j) < \arcsin b_{P,C_k} - \arcsin \alpha$$

then both $b_{P,C_i} > \alpha$ and $b_{P,C_j} > \alpha$ are guaranteed by Lemma 2.4.1. Thus if we perform an experiment to retrieve b_{P,C_k}, the certification for both C_i and C_j could be confirmed by a single experiment. From this fact, we notice that the total number of experiments for solving the certification problem depends on the choice of specific controllers. For a fixed P and given α, the number of experiments will decrease as the generalized stability margin of the chosen controller, C_k, increases and the number of candidate controllers in the δ_ν-neighborhood of the chosen controller, C_k, increases. In the next section, we will first develop an algorithm to search for such a controller C_k in a finite set. In Section 5, this will be generalized to an infinite but ν-gap-compact controller set.

2.4.1 Estimating $b_{P,C}$ from closed-loop data

An indispensable ingredient in controller certification is the estimation of the ∞-norm of the sensitivity matrix $T(P, C)$ which involves a matrix version of estimating a frequency response of a SISO transfer function. An H_∞ identification problem seeks an identification algorithm estimating frequency response values from closed-loop input-output data and managing maximal bounds on the error (Chen & Gu 2000). Satisfactory identification requires some prior information on the systems to be identified. As we will discuss in Chapter 4, this *a priori* information is usually in the form of relative stability of the system and an upper bound of the noise level. The reader is also referred to source material in (Gu & Khargonekar 1992, Helmicki, Jacobson & Nett 1993, Ninness & Goodwin 1995, Parker & Bitmead 1987) and the associated references.

From an experiment design perspective, for a MIMO system with a wide-band analysis, estimating the stability margin will be both difficult and expensive in its requirement of a large number of data samples collected under many different experimental conditions. This reinforces the need to minimize the number of experiments. We will provide more detailed experiment design in Chapter 4.

2.5 Algorithms for a Finite Controller Set

In this section the candidate controller set has a finite number of elements, i.e. $\mathcal{C} = \{C_0, C_1, \cdots, C_n\}$. To certify a collection of controllers, we need to guarantee the generalized stability margins $b_{P,C_i} > \alpha$ for all $C_i \in \mathcal{C}$. Since the transfer functions of the plant model, $\hat{P}$, and all the controllers are known, the ν-gap distances of candidate controller pairs and the $b_{\hat{P},C}$ can be easily calculated. However, the $b_{P,C}$ can only be evaluated through an experiment which is a relatively time consuming and expensive process. Instead of b_{P,C_i}, we will let $b_{\hat{P},C_i}$ guide us to determine which subset of controllers should be tested so that we can reduce the number of experiments required to finish certification of the whole set. If a nominal plant model $\hat{P}$ sufficiently approximates an unknown real plant P, the $b_{\hat{P},C_i}$ provide good guidance to solve the certification problem.

2.5.1 Algorithm - Certification

Before starting certification for the collection of candidate controllers, $\mathcal{C}$, we need to compute $b_{\hat{P},C_i}$ for all $i = 0, 1, \cdots, n$. This could be a likely by-product of the design process for C_i. Other data we need to prepare are a numerical table comprising the ν-gap distances $\delta_\nu(C_i, C_j)$ for all controller pairs in $\mathcal{C}$. Since the ν-gap is a metric, this table will have a form of an $n \times n$ symmetric matrix whose diagonal elements are zero. The $\delta_\nu(C_i, C_j)$ computation for $\mathcal{C}$ requires $\frac{n(n-1)}{2}$ times the $\delta_\nu(\cdot, \cdot)$ calculation. This could be a significant amount of computation if the number of controllers is very large. However, if we take into account the computational complexity of high fidelity simulations or difficulties of experiments to evaluate b_{P,C_i} for all $i = 0, 1, \cdots, n$, the $\delta_\nu(C_i, C_j)$ calculation is significantly preferable. The following algorithm yields a finite subset of controllers for test to manage the number of experiments. In the algorithm, α is the margin specification.

Step 1(Search) For each uncertified controller, C_i, with $b_{\hat{P},C_i} > \alpha$, count the number of uncertified controllers, C_j, that satisfy,

$$\arcsin \delta_\nu(C_i, C_j) < \arcsin b_{\hat{P},C_i} - \arcsin \alpha. \tag{2.15}$$

Then choose the controller, C_i, with the most controllers, C_j, satisfying (2.15). If several controllers have same number of controllers that satisfy (2.15), then choose C_i with the maximal $b_{\hat{P},C_i}$.

Step2(Experiment) Perform the experiment on (P, C_i) to retrieve b_{P,C_i} from closed-loop data.

Step 3A(Certify) If $b_{P,C_i} > \alpha$, certify the controllers, C_j, satisfying (2.16) of Lemma 2.4.1,

$$\arcsin \delta_\nu(C_i, C_j) < \arcsin b_{P,C_i} - \arcsin \alpha, \tag{2.16}$$

and exclude these candidate controllers from further tests. That is, for those controllers, C_j, we have shown that $b_{P,C_j} > \alpha$.

Step 3B(Reject) If $b_{P,C_i} \leq \alpha$, reject the controllers, C_j, satisfying (2.14) of Lemma 2.4.1,

$$\arcsin \delta_\nu(C_i, C_j) \leq \arcsin \alpha - \arcsin b_{P,C_i},$$

and exclude these candidate controllers from further tests. That is, for those controllers, C_j, we have shown that $b_{P,C_j} \leq \alpha$.

Loop If uncertified or unrejected controllers with $b_{\hat{P},C_i} > \alpha$ remain in the collection $\mathcal{C}$, iterate from Step 1 to Step 3 until all controllers are certified or rejected.

Notice that the only difference between (2.15) and (2.16) is that pre-computed $b_{\hat{P},C}$ is used in (2.15), while experimentally retrieved $b_{P,C}$ is used in (2.16).

2.5.2 Algorithm - Rejection

Step 3B of the Certification Algorithm introduces the idea of using the rejection test of Lemma 2.4.1 to explore implied rejection of untested controllers. Clearly, in a circumstance where $b_{\hat{P},C_i} < \alpha$ one could develop an efficient rejection algorithm along the same lines as the certification algorithm. Although, this would imply an incipient margin problem even at the design stage.

In the certification algorithm, we can observe the ν-gap radius of the ball in which one controller C_i certifies its neighbors C_j shrinks as the value of α approaches b_{P,C_i}. In other words, in (2.16), the admissible value of $\delta_\nu(C_i, C_j)$ decreases as the α gets close to the b_{P,C_i}. This is the same case in the rejection algorithm. The upshot of this observation, as will be illustrated in a later example, is that around the edge of the stabilizing region where $b_{P,C_i} = \alpha$, the certification or rejection balls shrink in radius and a very large number of experimental tests is necessary. Indeed, it is clear from Lemma 2.4.1 that a controller satisfying $b_{P,C_i} = \alpha$ is unable either to certify or reject any other controllers, no matter how ν-gap-close. Thus, the capacity is limited for resolving the exact boundary of the stabilizing region with a small number of tests. This shall become apparent in both subsequent computed examples, where fine resolution of this boundary requires exhaustive local testing. Of course, one might skirt around this problem by combining a certification test at level $\alpha - \triangle\alpha$, say, with a rejection test at level $\alpha + \triangle\alpha$ for a small positive $\triangle\alpha$.

2.6 Numerical Examples for Finite Controller Set

In this section, we develop two certification examples. The first example shows certification of SISO controllers that are parametrized by two parameters. The second certification example of an F100 jet engine puts more emphasis on MIMO characteristics.

2.6.1 Certification of SISO Control System

In this section, we will show a computer example of a controller certification of a SISO control system using the algorithm developed in the previous section. We consider that the controllers are parametrized by $(\rho_1;\ \rho_2)$ and presume that the range of parameters that stabilizes the nominal plant $\hat{P}(z)$ is given from a separate controller synthesis process.

$$C(z) = \frac{\rho_1 z}{z + \rho_2} \tag{2.17}$$

Let us assume, the unknown real plant $P(z)$ is

$$P(z) = \frac{0.1z^2(z - 0.3)}{(z - 0.8)(z^2 - 0.4z + 0.85)(z^2 - 1.2z + 0.72)}. \tag{2.18}$$

The stability margin b_{P,C_i} can be estimated from closed-loop data. Although, in this example, because the mathematical expression (2.18) of the real plant $P(z)$ is available, the experiment estimating the stability margin b_{P,C_i} will be substituted by computation of (2.5). We obtain the plant model $\hat{P}$ from model reduction of the real plant $P(z)$.

$$\hat{P}(z) = \frac{0.002985z^2 + 0.08012z + 0.1259}{z^3 - 1.123z^2 + 1.014z - 0.394}. \tag{2.19}$$

Since $\delta_\nu(P(z), \hat{P}(z)) = 0.1917$, which is an unknown value, the maximum difference between b_{P,C_i} and $b_{\hat{P}C_i}$ is guaranteed to be less than 0.1917 by Theorem 2.2.1. In this example the actual maximum difference between b_{P,C_i} and $b_{\hat{P}C_i}$ is 0.1874.

In Figure 2.4, the axes measure controller parameters ρ_1 and ρ_2. The thicker line depicts the boundary of the stabilizing region for the model $\hat{P}(z)$ and the thinner line delineates the $P(z)$-stabilizing region. Notice, once again, that we presume the boundary for the $P(z)$-stabilizing region is unknown. Inside the thick solid line, we select 74 points of $(\rho_1;\ \rho_2)$, i.e. 74 model-based controllers, which are represented by rectangles with their

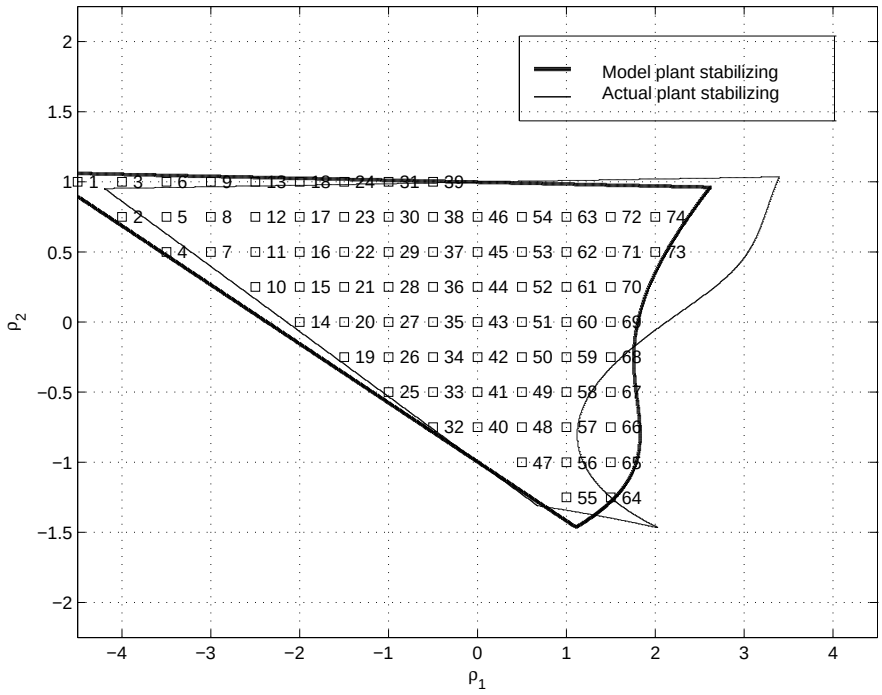

Figure 2.4: Stabilizing region for the real plant $P(z)$ and the nominal plant $\hat{P}(z)$ and selected controller parameters.

indices. From the figure 2.4, we can expect several controllers should not be used in real operation since they are outside stabilizing region of the actual plant. As a preparation step we calculate $\delta_\nu(C_i, C_j)$ for all pairs of controllers in $\mathcal{C}$ so that we can use these distances when we check for the certification conditions (2.15) or (2.16). Using (2.5), the generalized stability margins $b_{\hat{P}C_i}$ of all the controllers $\mathcal{C}$ with the nominal plant $\hat{P}$ are calculated in advance.

Certification for Stability

As a minimum requirement, the candidate controllers should guarantee stability when they are applied to the actual feedback loop. Certification for stability is accomplished by letting $\alpha = 0$ in (2.15) or (2.16). The key step in the controller certification procedure is the choice of the specific sequence of controllers for experiments. Hence we start the controller certification by counting the number of controllers satisfying (2.15) at each of the 74 candidates. Figure 2.5a shows the number of controllers, C_j, that

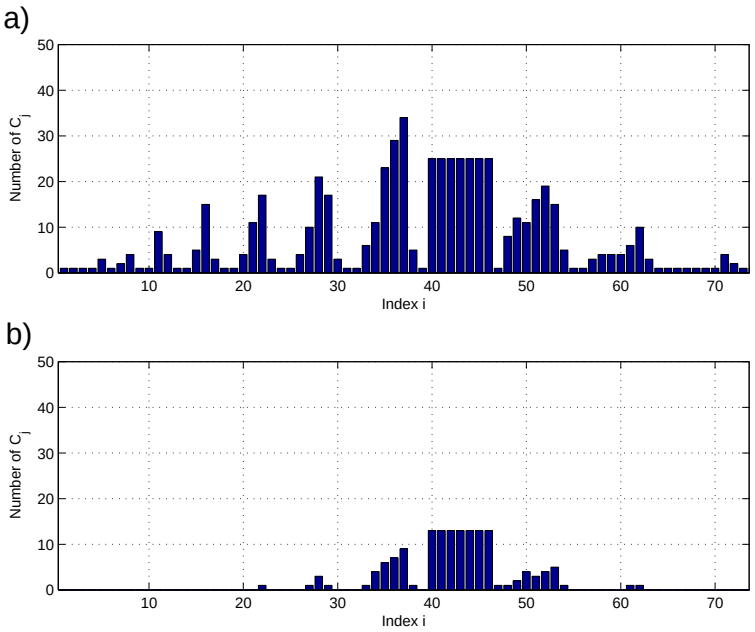

Figure 2.5: Numbers of C_j satisfying (2.15) after 1st searching using $b_{\hat{P},C_i}$,
a) $\alpha = 0$, b) $\alpha = 0.3$.

satisfy (2.15) with each C_i for $i = 1 \cdots, 74$. After calculating $b_{\hat{P},C_i}$ we count the number of controllers C_j. Figure 2.5a shows that $b_{\hat{P},C_j}$ advises us that the 37th controller could potentially certify 34 other controllers from the $\hat{P}$-stabilizing region. After retrieving $b_{P,C_{37}}$ from the closed-loop data, we realize that actually 21 controllers satisfy (2.16). In Figure 2.6a the controllers inside and on the line are those certified controllers.

We iterate this search and experiment process until all controllers in the set $\mathcal{C}$ are certified or rejected. Before searching for the next controller to be tested, we need to exclude the certified controllers in the previous iteration from $\mathcal{C}$ and search for the best remaining controller for the second experiment. In this manner, as shown in Figure 2.6, we complete the certification process for all 74 controllers in 31 experiments. In Figure 2.6a, the filled circle corresponds to the test controller and the other 20 hollow circles represent the controllers whose positive generalized stability margins ($b_{P,C_j} > 0$) have been inferred without requiring further experiments. For those controllers inside and on the solid line, the certification criterion (2.11) is satisfied. From Figure 2.6d, we can see that inside and on the line there are 60 certified controllers out of 74 candidate

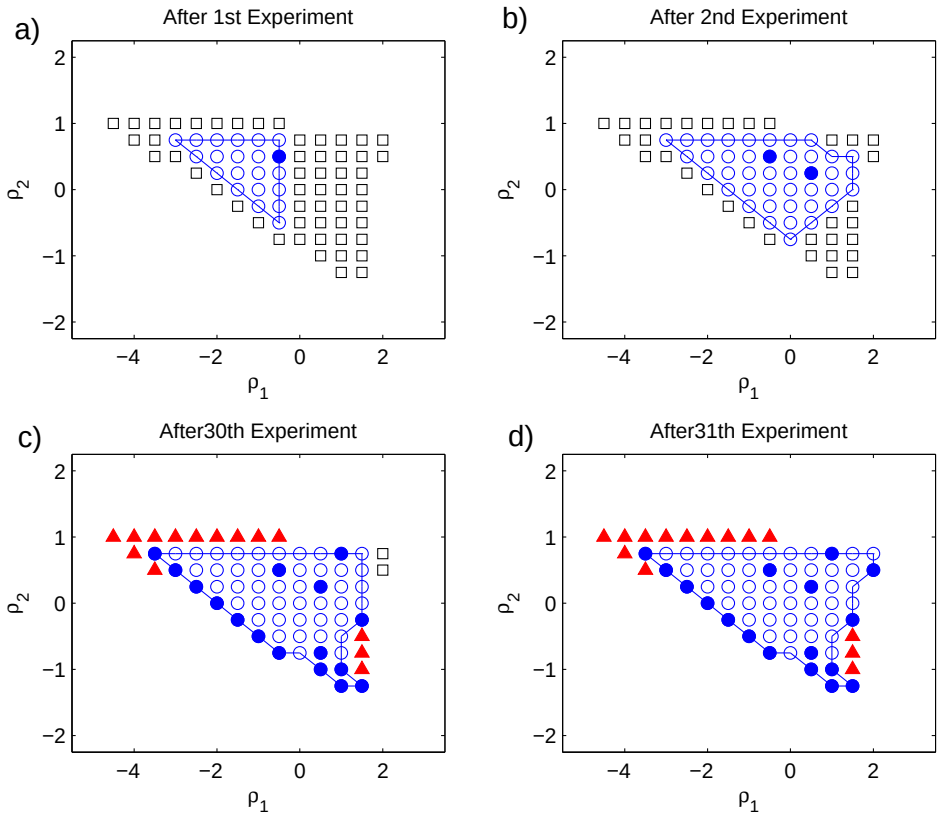

Figure 2.6: Certification process for stability ($\alpha = 0$, $\square$: untested, $\circ$: certified, $\bullet$:tested & certified, $\blacktriangle$: tested & rejected)

controllers. 14 red triangles represent the tested and rejected controllers ($b_{P,C_j} = 0$).

Since we are exhaustively testing all 74 possible controllers which extend outside the stabilization region for P, and since we are applying a sufficient condition for stability, it is necessary to test experimentally all rejected controllers as well as many near the stabilization boundary. Figure 2.6b indicates that two experiments yield the certification of the bulk of the certifiable controllers.

Certification for Performance

It is important in controller certification not only to guarantee stability, but also to achieve a specified level of performance. When $\|T(P, C_i) - T(\hat{P}, C_i)\|_\infty$ is large, the controller based on the model $\hat{P}$ cannot guarantee good performance with an actual

plant P. The dual inequality of (2.8), with $\delta_\nu(P,\hat{P}) < 1$, is

$$\begin{aligned} \delta_\nu(P,\hat{P}) &\leq \left\| T(P,C_i) - T(\hat{P},C_i) \right\|_\infty \\ &\leq \frac{\delta_\nu(P,\hat{P})}{b_{P,C_i} b_{\hat{P},C_i}}. \end{aligned} \tag{2.20}$$

For any particular $\delta_\nu(P,\hat{P})$, if we find a certain controller that makes $b_{\hat{P},C_i}$ large, then the $\|T(P,C_i) - T(\hat{P},C_i)\|_\infty$ may be smaller, which means we can achieve a better performance level with the chosen controller C_i. By increasing α in (2.15) and (2.16), we would expect better performance in the certified controllers. Figure 2.5b shows the numbers of controllers satisfying (2.15) after the first search for the best controller, when $\alpha = 0.3$. This figure tells us that there are 47 controllers that the algorithm will not try to certify since $b_{\hat{P},C} \leq 0.3$ for those controllers. Figure 2.7 shows the process of certification for 74 controllers with $\alpha = 0.3$ and shows that 27 controllers are certified in 7 experiments by the suggested algorithm.

2.6.2 Certification of the F-100 Engine Control System

In this section, we develop a certification example for a set of controllers for the F100 jet engine. The F100 engine controllers are legacy systems which were certified using single-loop gain and phase margin calculations. We have chosen to conduct our computational experiments using this engine model and a representative controller set in order to establish a correspondence between the old scalar margins and the more modern MIMO stability margins. Some calculations in (Vinnicombe 2001) suggest that joint single-loop gain margin of 2.69 dB and phase margin of 17.5° correspond to a MIMO margin of $b_{P,C} > 0.3$. However, the appropriateness of this numerical value is really yet to be demonstrated.

The F100 jet engine model was chosen at sea level static flight conditions with a power lever angle (PLA) of 36° (Merrill, Beattie, LaPrad, Rock & Akhter 1984). In Appendix 2.9.1, we provide the state space representation of the F100 engine and we assume that this full-order engine model is the unknown real plant for this example. The 2nd-order plant model $\hat{P}$ is obtained by model reduction from this engine model P and $\hat{P}$ is used in the subsequent controller design. The $\hat{P}$-stabilizing multivariable Proportional-plus-Integral controller is designed in the LQR framework.

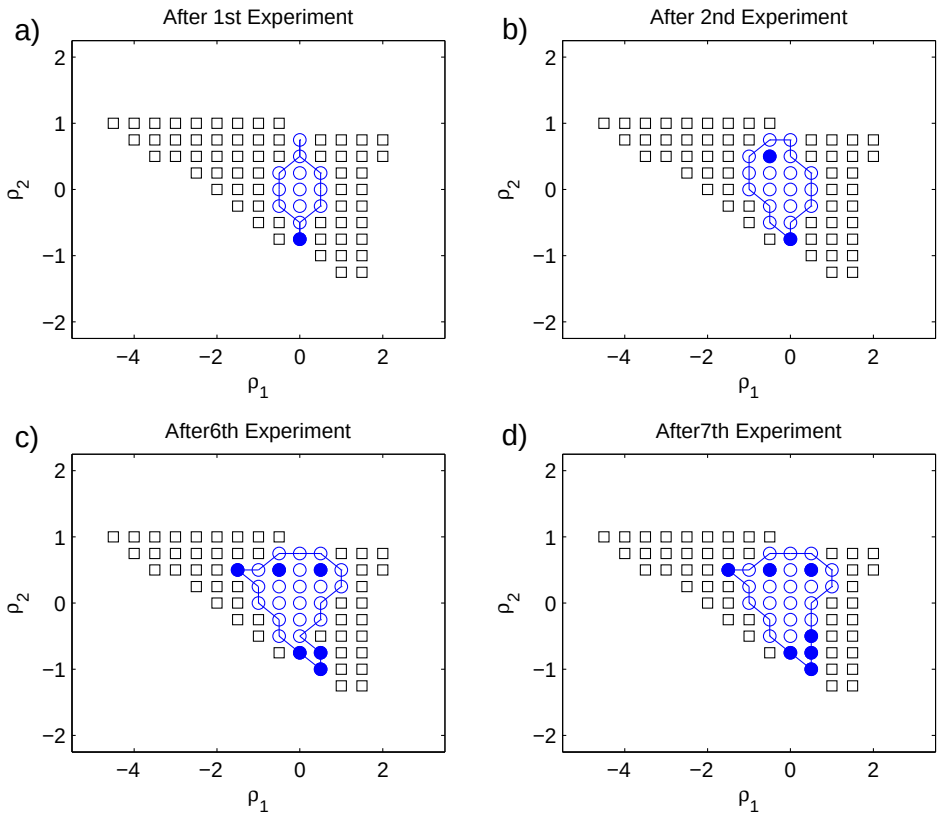

Figure 2.7: Certification process for performance ($\alpha = 0.3$, $\square$: untested, $\circ$: certified, $\bullet$:tested & certified).

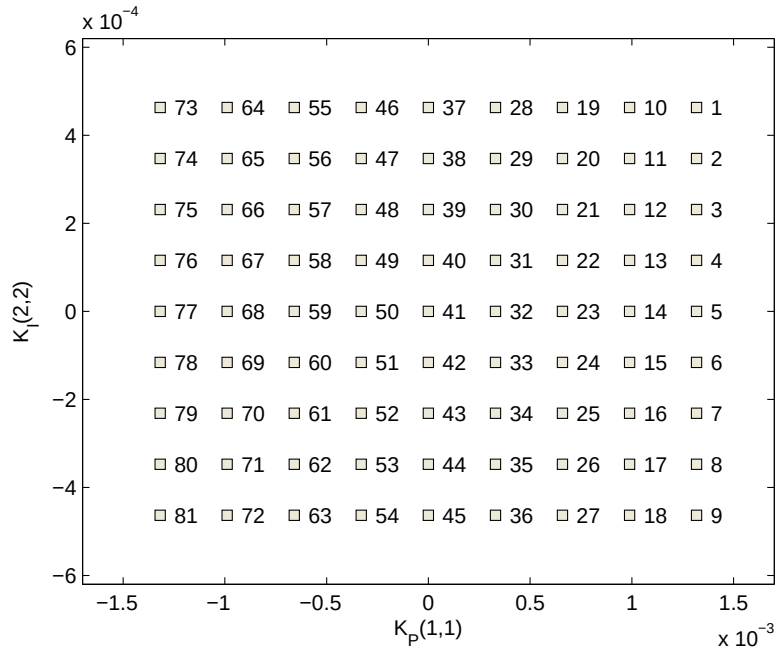

Figure 2.8: The set of candidate F100 jet engine controllers.

$$C(s) = K_P + \frac{1}{s}K_I \tag{2.21}$$

The nominal proportional gain and integral gain matrices are given in Appendix 2.9.2. For easy graphical representation of certification results, we certify only two parameters among the elements of the two 5×5 matrices K_P and K_I. The first parameter is $K_P(1,1)$ and the other is $K_I(2,2)$. Each parameter changes up to $\pm30\%$ from its original value. In Figure 2.8, the axes measure controller parameters $K_P(1,1)$ and $K_I(2,2)$. In this 2-dimensional parameter space, we select 81 points, i.e. we have 81 model-based controllers to be tested which are represented by rectangles with their indices.

Input and Output Scaling for $b_{\hat{P},C_i}$ Computation

Computation of the generalized stability margin (2.5) involves calculation of the singular values of a matrix. This is sensitive to the selection of relative signal magnitudes or measurement units pertaining to the input and output signals; in the MIMO case, this problem is exacerbated by the need to manage the relative scaling of all the signals. To accommodate this, we consider the re-scaling of each input and output channel in order that we might calculate the most favorable stability margin. Likewise, one may consider

using different scalings at different frequencies to improve minimal margins. Some of these issues are broached in (Fielding, Varga, Bennani & Selier 2002) for MIMO metric computations. In Chapter 3, the input and output scaling will be explored in detail.

In our computations, we consider the incorporation of constant diagonal input/output matrices, W_o and W_i. Thus the plant model, $\hat{P}$, is weighted as $W_o\hat{P}W_i$ and the controller is $W_i^{-1}C_iW_o^{-1}$ instead of C_i. The W_o and W_i yield a weighted generalized stability margin $b_{W_o\hat{P}W_i,W_i^{-1}C_iW_o^{-1}}$. The use of W_o and W_i makes it possible to scale engineering units of signals with closed-loop performance analysis in mind. These input and output scaling matrices are important even for SISO systems with these margin and metric calculations, since $T(P,C)$ is a 2×2 block transfer function matrix. If we use scaling matrices, the searching inequality (2.15) for test controllers becomes

$$\arcsin\delta_\nu(C_i',C_j') < \arcsin b_{\hat{P}',C_i'} - \arcsin\alpha.$$

where, $C_i' = W_i^{-1}C_iW_o^{-1}$, $C_i' = W_i^{-1}C_iW_o^{-1}$, and $\hat{P}' = W_o\hat{P}W_i$. The constant scaling matrices do not alter the stability of $T(\hat{P}',C')$ and it is straightforward to show $T(\hat{P}',C')$ is stable if and only if $T(\hat{P},C)$ is stable.

Certification of Stability

As with SISO certification, the controller certification starts with counting the number of controllers satisfying (2.15) at each point of Figure 2.8; that is, the number of other controllers that would be certified by an experiment on the $\hat{P}$ and C_j pair. In this example, the first experiment of retrieving b_{P,C_1} says that b_{P,C_j} of every controller ($j = 1\cdots 81$) is greater than 0, which means all of 81 controllers stabilize the real F100 engine. This highly efficient certification result is due to the sufficient level of b_{P,C_j} over all controllers and relatively small ν-gap distance between any two candidates. Nevertheless, this is what one would expect from many practical designs.

Certification of Margin

In Figure 2.9 the circles represent certified controllers and the filled circles indicate those tested. In Figure 2.9a, since C_{19} is the controller which satisfies (2.15) for the greatest number of other controllers , the first experiment is performed to retrieve

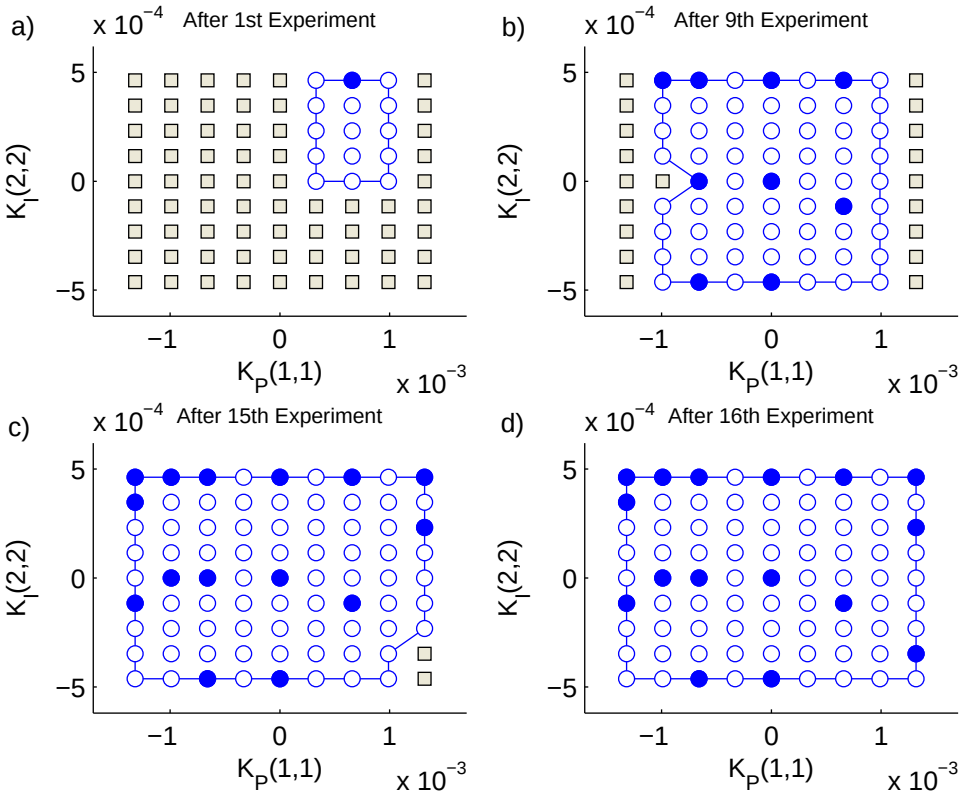

Figure 2.9: Certified parameters at the level $\alpha = 0.2$. (○: certified, ●:tested & certified)

$b_{P,C_{19}}$. From the closed-loop data it turns out actually 15 controllers are certified at the level of 0.2. By the certification algorithm, we iterate the search and experiment process until all controllers in the parameter space in Figure 2.8 are certified or rejected. In this manner, as shown in Figure 2.9 the certification of all 81 controllers at the level of 0.2 is completed in 16 tests.

Rejection

Because of the discrepancy between the real and nominal generalized stability margins, b_{P,C_i} and $b_{\hat{P},C_i}$, the b_{P,C_i} can be less than the target certification level α. Even in this situation, the b_{P,C_i} can give valuable information on the candidate controllers. After a closed-loop experiment, if the b_{P,C_i} is less than α, we can recycle the b_{P,C_i} to reject the controllers that have less b_{P,C_j} than α. The rejection algorithm can avoid exhaustive experiments on the parameters outside the region $b_{\hat{P},C_i} > \alpha$. Figure 2.10 shows the process of rejection at the level of 0.23. In Figure 2.10 the triangles represent rejected controllers and the filled triangles indicate those tested.

2.7 Infinite Controller Set

2.7.1 Topological Preliminaries

In the previous section the proposed algorithm certified only a finite number of points in the parameter space and therefore infinitely many untested parameters remain. We now move from a finite set to an infinite controller set and consider the modification of the preceding enumerative algorithm. However, we restrict ourselves to SISO plants and controllers. Extension to MIMO is nontrivial because of issues dealing with the parametrization of MIMO systems and the proper understanding of coprimeness in a parametrized MIMO setting (Hannan & Deistler 1998).

The key idea is to use the properties of the $(\mathcal{C}, \delta_\nu)$ metric space to develop a sequence of controllers $\{C_0, C_1, \cdots\}$ for experimental test which validate all candidate controllers in an open neighborhood of $\mathcal{C}$. In this section we provide answers to the main issues in developing an algorithm which eventually certifies the whole continuous parameter space without testing exhaustively. Anderson et al (Anderson, Brinsmead,

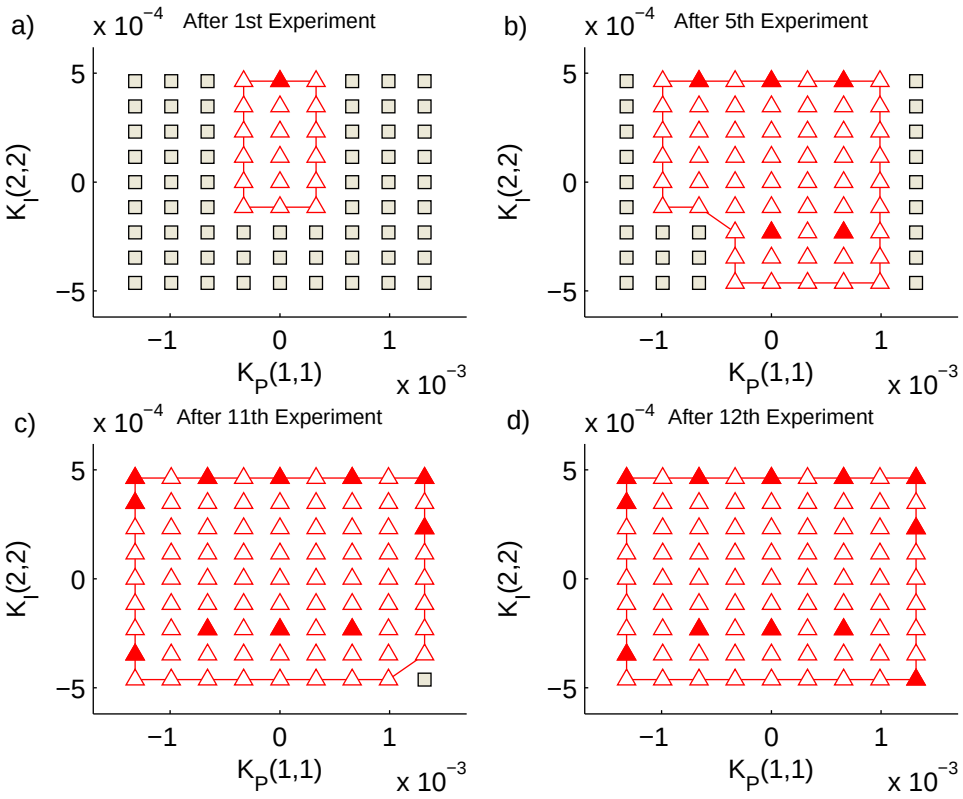

Figure 2.10: Rejection procedure at the level of $\alpha = 0.23$.

De Bruyne, Hespanha, Liberzon & Morse 2000) establish that for a controller set $\mathcal{C}$ continuously parametrized by parameter θ in a compact set Θ, it is possible to construct a finite open covering of $\mathcal{C}$ by δ_ν-balls about centers $\{C_0, C_1, \cdots\}$. This relies on the Heine-Borel property and pivots on continuity and compactness. However, it is important to note that the factorization of controllers must maintain coprimeness when they continuously move from one parameter to another in Θ. If the set of SISO rational functions of a fixed degree n (without common factors) is topologized in a natural way, the set is the disjoint union of $n+1$ open sets (Brockett 1976). When a controller moves from one of these open sets to another, it must pass through a region of common factors. If there are unstable common factors, the controllers cannot cross from one controller set to another without an unstable pole-zero cancellation which causes violation of coprimeness of controllers. Thus the certification algorithm should restrict one individual δ_ν-ball to be contained in only one disjoint set. These disjoint sets contain transfer functions with the same Cauchy index.

We shall apply these ideas here to explore this construction for a specific natural parametrization associated with the controller certification problem. Let us assume the candidate controllers are parametrized as follows

$$\begin{aligned} C(\theta_0) &= \frac{b_{0,0} + b_{1,0}z^{-1} + \cdots + b_{n,0}z^{-n}}{1 + a_{1,0}z^{-1} + \cdots + a_{n,0}z^{-n}} \triangleq \frac{n_0}{d_0}, \\ C(\theta_1) &= \frac{b_{0,1} + b_{1,1}z^{-1} + \cdots + b_{n,1}z^{-n}}{1 + a_{1,1}z^{-1} + \cdots + a_{n,1}z^{-n}} \triangleq \frac{n_1}{d_1}. \end{aligned} \tag{2.22}$$

And define an infinite collection of controllers to be certified,

$$\mathcal{C} \triangleq \{C(\theta_i) | \theta_i \in \Theta \quad i = 0, 1, \cdots\},$$

where θ_i is a parameter vector such that

$$\theta_i = (a_{1,i}, a_{2,i}, \cdots, a_{n,i}, b_{0,i}, b_{1,i}, \cdots, b_{n,i})^T \in \Theta, \tag{2.23}$$

and $\Theta \subset \mathbb{R}^{2n+1}$ is the controller parameter space which must be assumed to be compact. Suppose the known plant model has normalized coprime factorizations,

$$\hat{P} = XY^{-1} = \tilde{Y}^{-1}\tilde{X}. \tag{2.24}$$

Define unit transfer functions such that

$$U_0 \triangleq n_0 X + d_0 Y, \quad U_1 \triangleq \tilde{X} n_1 + \tilde{Y} d_1.$$

Then, $I = U_0^{-1} n_0 X + U_0^{-1} d_0 Y, \quad I = \tilde{X} n_1 U_1^{-1} + \tilde{Y} d_1 U_1^{-1}$. Choose $\tilde{N}_0$, $\tilde{D}_0$, N_1, and D_1 such that $\tilde{N}_0 = U_0^{-1} n_0$, $\tilde{D}_0 = U_0^{-1} d_0$, $N_1 = n_1 U_1^{-1}$, and $D_1 = d_1 U_1^{-1}$. This provides coprime factorizations of $C(\theta_0) = \tilde{D_0}^{-1} \tilde{N}_0$ and $C(\theta_1) = N_1 D_1^{-1} = [N_0 - QY][D_0 + QX]^{-1}$ with Youla-Kucera parameter,

$$Q = \tilde{N}_0 D_1 - \tilde{D}_0 N_1 = U_0^{-1} \left(n_0 d_1 - d_0 n_1 \right) U_1^{-1}. \tag{2.25}$$

Let us define Δd and Δn such that, $d_1 = d_0 + \Delta d$, $n_1 = n_0 - \Delta n$, then $n_0 d_1 - n_1 d_0 = n_0 \Delta d + d_0 \Delta n = S_C(\theta_1 - \theta_0)$, where $S_C = \begin{pmatrix} 1 & z^{-1} & \cdots & z^{-2n+1} & z^{-2n} \end{pmatrix} \times V$ and the matrix, V, is a Sylvester matrix of two polynomials n_0 and d_0. Therefore, from (2.25), Q can be represented in terms of the difference of two parameter vectors, $\theta_1 - \theta_0$,

$$Q = U_0^{-1} S_C(\theta_1 - \theta_0) U_1^{-1}. \tag{2.26}$$

Suppose a parameter vector θ_0 is selected then so is U_0. Thus we have only two variables in (2.26), θ_1 and U_1. Further simple manipulation of the unit transfer function U_1 makes (2.26) a combination of only $(\theta_1 - \theta_0)$ and other known terms. Let the plant model $\hat{P} = \frac{p_0 + p_1 z^{-1} + \cdots + p_n z^{-n}}{1 + q_1 z^{-1} + \cdots + q_n z^{-n}} = XY^{-1} = \frac{p(z)}{r(z)} \left(\frac{q(z)}{r(z)} \right)^{-1}$, where as above X and Y are a normalized coprime factorization of the plant model. Then $U_1 = n_1 X + d_1 Y = U_0 + S_P(\theta_1 - \theta_0) r^{-1}$ where the vector $S_P = \begin{pmatrix} 1 & z^{-1} & \cdots & z^{-2n} \end{pmatrix} \times V_P$, and V_P is a Sylvester matrix for $-p$ and q. Therefore,

$$Q = \left(U_0^{-1} S_C \left(\theta_1 - \theta_0 \right) \right) \left(U_0 + S_P \left(\theta_1 - \theta_0 \right) r^{-1} \right)^{-1} \tag{2.27}$$

Now we show that, in the δ_ν-gap metric space, there exists a finite covering of the compact set of controllers, $\mathcal{C}$, by ϵ-balls. For every controller $C(\theta_\rho)$ contained in the ball $\mathcal{B}(C(\theta_i), \epsilon)$, which is centered at $C(\theta_i)$ with the δ_ν-radius of ϵ, if we choose ϵ less than $b_{P,C(\theta_i)}$, then $\delta_\nu(C(\theta_i), C(\theta_\rho)) < b_{P,C(\theta_i)}$. In addition, if this $C(\theta_i)$ stabilizes P, every controller $C(\theta_\rho)$ in the ball $\mathcal{B}(C(\theta_i), \epsilon)$ stabilizes the unknown actual plant P by Theorem 2.2.1. Thus if the δ_ν-radius ϵ is strictly positive, we are able to construct a finite number of non-vanishing balls such that,

$$\mathcal{C} \subset \bigcup_{i=0}^{N} \mathcal{B}(C(\theta_i), \epsilon),$$

where N is a finite number. We will find a radius of the ball in the Euclidean parameter space, Θ, instead of the the ν-gap metric space, so that all candidate controllers will

satisfy (2.15) in the ball. Thus,

$$\begin{aligned}\delta_\nu(C(\theta_0), C(\theta_1)) &\leq ||T(\hat{P}, C(\theta_0)) - T(\hat{P}, C(\theta_1))||_\infty \\ &= ||Q||_\infty \\ &= \left\| \frac{U_0^{-1} S_C \left(\theta_1 - \theta_0\right)}{U_0 + S_P \left(\theta_1 - \theta_0\right) r^{-1}} \right\|_\infty\end{aligned}$$

and we need to find an upper limit on $|\theta_1 - \theta_0|$ satisfying

$$\begin{aligned}&\arcsin \delta_\nu(C(\theta_0), C(\theta_1)) \\ &\qquad \leq \arcsin \left\| \frac{U_0^{-1} S_C \left(\theta_1 - \theta_0\right)}{U_0 + S_P \left(\theta_1 - \theta_0\right) r^{-1}} \right\|_\infty \\ &\qquad \leq \arcsin b_{\hat{P}, C(\theta_0)} - \arcsin \alpha.\end{aligned}$$

The following theorem gives us the radius of a ball in Euclidean space which contains only certified controllers.

Theorem 2.7.1. *Let* $\arcsin \hat{\gamma} = \arcsin b_{\hat{P}, C(\theta_0)} - \arcsin \alpha$.
If

$$|\theta_1 - \theta_0| \leq \frac{\hat{\gamma}}{\|U_0^{-2} S_C\|_\infty + \hat{\gamma} \|r^{-1} U_0^{-1} S_P\|_\infty}, \tag{2.28}$$

then

$$\arcsin \delta_\nu(C(\theta_0), C(\theta_1)) \leq \arcsin b_{\hat{P}, C(\theta_0)} - \arcsin \alpha.$$

Proof.

$$\begin{aligned}|\theta_1 - \theta_0| \left(\|U_0^{-2} S_C\|_\infty + \hat{\gamma} \|r^{-1} U_0^{-1} S_P\|_\infty \right) &\leq \hat{\gamma} \\ \|U_0^{-2} S_C (\theta_1 - \theta_0)\|_\infty + \hat{\gamma} \|r^{-1} U_0^{-1} S_P (\theta_1 - \theta_0)\|_\infty &\leq \hat{\gamma} \\ \frac{\|U_0^{-2} S_C (\theta_1 - \theta_0)\|_\infty}{1 - \|r^{-1} U_0^{-1} S_P (\theta_1 - \theta_0)\|_\infty} &\leq \hat{\gamma} \\ \frac{\|U_0^{-2} S_C (\theta_1 - \theta_0)\|_\infty}{\|1 + r^{-1} U_0^{-1} S_P (\theta_1 - \theta_0)\|_\infty} &\leq \hat{\gamma} \\ \left\| \frac{U_0^{-2} S_C (\theta_1 - \theta_0)}{1 + r^{-1} U_0^{-1} S_P (\theta_1 - \theta_0)} \right\|_\infty &\leq \hat{\gamma}\end{aligned}$$

Since $\delta_\nu(C(\theta_0), C(\theta_1)) \leq \left\| \frac{U_0^{-2} S_C (\theta_1 - \theta_0)}{1 + r^{-1} U_0^{-1} S_P (\theta_1 - \theta_0)} \right\|_\infty$, we have $\delta_\nu(C(\theta_0), C(\theta_1)) \leq \hat{\gamma}$.
Therefore $\arcsin \delta_\nu(C(\theta_0), C(\theta_1)) \leq \arcsin b_{\hat{P}, C(\theta_0)} - \arcsin \alpha$. □

Using this theorem, in the next section we will construct a finite cover for an infinite set of certified controllers.

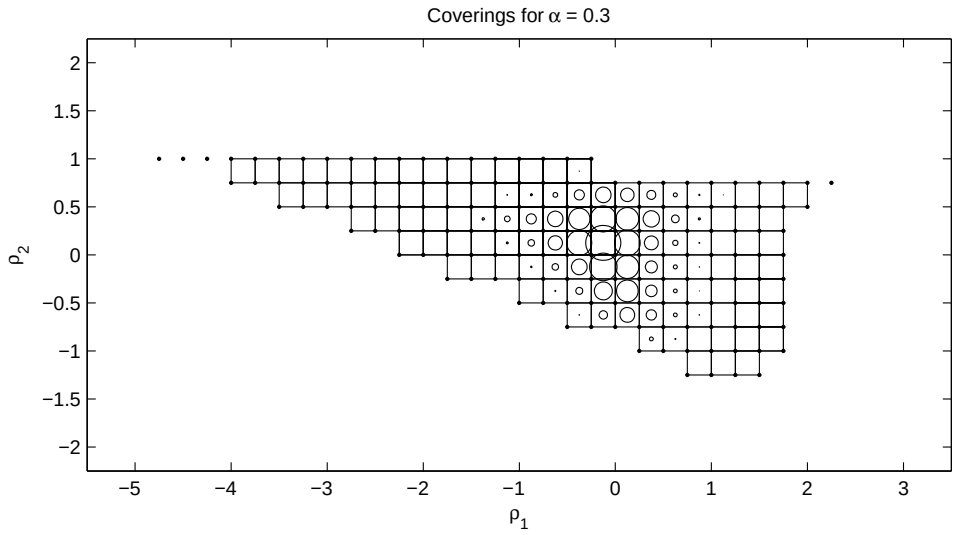

Figure 2.11: Initial squares with circles by computation of (2.28).

2.7.2 Certification Algorithm and Numerical Example for an Infinite Controller Set

A k-cell (also known as a rectangle or l_∞-ball) is a set of all points $x = \{x_1, \cdots, x_k\}$ such that $a_i \le x_i \le b_i$ $(1 \le i \le k)$ for given $\{a_i, b_i\}$. We require $|a_i - b_i|$ to be the same for all i for simplicity here. We divide the candidate controller set $\mathcal{C}$ into small k-cells and then we certify the $\mathcal{C}$ on a subset by subset basis. After determining k-cells inside $\mathcal{C}$, we pick one of the centers of the k-cells as the experimental parameter. In the case of $k = 2$ and $|a_1 - b_1| = |a_2 - b_2|$, the k-cell is simply a square.

Certification Algorithm: In Euclidean coordinates, a k-cell is a convex polygon, thus to show the k-cell is covered by a ball it suffices to check the the all vertices of the k-cell are enclosed by the ball. Before starting the certification, we make initial grids on the candidate controller set, $\mathcal{C}$, as Figure 2.11 shows.

Step 1(Search) For each uncertified k-cell, pick the centroid of the k-cell as a test controller parameter, θ_i, with $b_{\hat{P},C(\theta_i)} > \alpha$ and measure the radius of the certifying cover of the $C(\theta_i)$,

$$\frac{\hat{\gamma}}{\|U_i^{-2} S_C\|_\infty + \hat{\gamma}\|r^{-1} U_i^{-1} S_P\|_\infty},$$

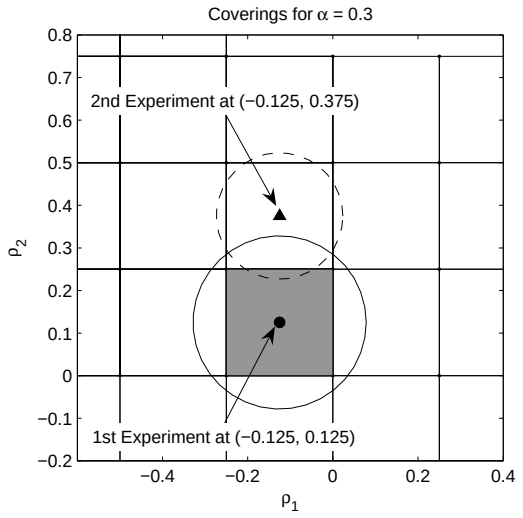

Figure 2.12: 1st certified square.

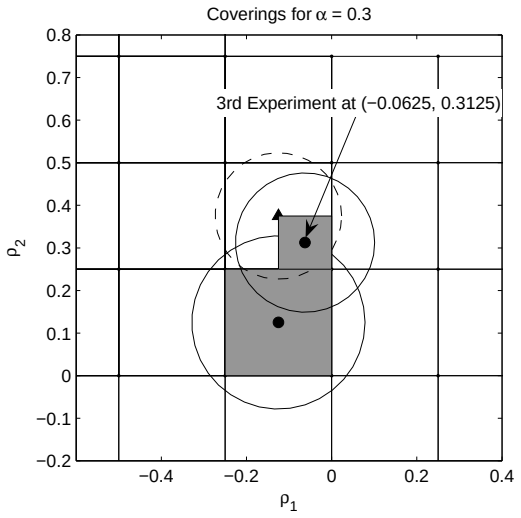

Figure 2.13: 2nd certified square.

where $\arcsin\hat{\gamma} = \arcsin b_{\hat{P},C(\theta_i)} - \arcsin\alpha$. Then choose the controller, $C(\theta_i)$, with the largest radius of the cover.

Step 2(Experiment) Perform the experiment on $(P, C(\theta_i))$ to retrieve $b_{P,C(\theta_i)}$, $\|U_i^{-2}S_C\|_\infty$, and $\|r^{-1}U_i^{-1}S_P\|_\infty$ from closed-loop data.

Step 3(Certify) Certify the k-cell that contains all controllers, $C(\theta_j)$, satisfying,

$$|\theta_j - \theta_i| \leq \frac{\gamma}{\|U_i^{-2}S_C\|_\infty + \gamma\|r^{-1}U_i^{-1}S_P\|_\infty},$$

where $\arcsin\gamma = \arcsin b_{P,C(\theta_i)} - \arcsin\alpha$. Exclude the k-cell from further tests. That is, for those controllers in the k-cell, $C(\theta_j)$, we have shown that $b_{P,C(\theta_j)} > \alpha$.

Step 4(Refinement of the Grids) If the cover generated at θ_i does not enclose all of the vertices of the k-cell then divide the k-cell into 2^k identical k-cells. If the divided k-cell is smaller than a prescribed size then exclude the k-cell from the candidate set. Otherwise, if there is any uncertified k-cell with center controller, $C(\theta_i)$ and $b_{\hat{P},C(\theta_i)} > \alpha$ in the refined grids, then go to Step 1.

Numerical Example: Here we provide a certification example for a set of continuously parametrized discrete-time controllers. We use the same SISO plant and

model with Section 2.6.1: the actual plant,

$$P = \frac{0.1z^2(z-0.3)}{(z-0.8)(z^2-0.4z+0.85)(z^2-1.2z+0.72)},$$

the plant model,

$$\hat{P} = \frac{0.002985z^2+0.08012z+0.1259}{z^3-1.123z^2+1.014z-0.394},$$

and the controllers,

$$C = \frac{\rho_1 z}{z+\rho_2}.$$

Here ρ_1 and ρ_2 are controller parameters to be certified, thus $k = 2$ in this example. The radii of circles in Figure 2.11 are computed with the plant model using (2.28) and the center of the circle having the largest radius is chosen as the first parameter to be evaluated. In Figure 2.12, we represent this point, $(\rho_1, \rho_2) = (-0.125, 0.125)$, as a filled small circle. Through the first experiment on the actual plant with controller $C(\theta_0) = \frac{-0.125z}{z+0.125}$ we find $b_{P,C(\theta_0)}$, $\|U_0^{-2}S_C\|_\infty$ and $\|r^{-1}U_0^{-1}S_P\|_\infty$. We then draw a circle centered at (-0.125, 0.125) with radius of 0.2034. The first square is certified, since this solid lined circle has a radius greater than the distance from the center of square to the vertices. After certifying the first square, we look for the next parameter by searching for the center of the square that has the largest radius excluding the already certified square(s). In Figures 2.12, 2.13, and 2.14, we filled the certified square with gray color. In Figure 2.12, after the second experiment, we can draw a dashed line circle having a radius of 0.1484 on $(-0.125, 0.375)$. Since the radius of the dashed line circle is less than the distance from the center of the initial square to the vertices, the second square is not certifiable. So we need to divide the second square into 4 smaller identical squares and then try to certify smaller squares. Figure 2.13 shows that the third experiment at $(-0.0625, 0.3125)$ certifies the refined square. In this way, as is shown in Figure 2.14, we construct a cover for certifiable parameters that guarantees $\alpha > 0.3$. As was identified at the end of Section 2.5, the radii of the certifying circles diminishes as they approach the certification boundary. This is evident in Figure 2.14 by the fracturing of the k-cells towards the edge of the set of certifiable controllers. To avoid an excessive number of experiments in the edge area, we excluded the squares if the radius of ball located at the centroid of the square was less than 0.03.

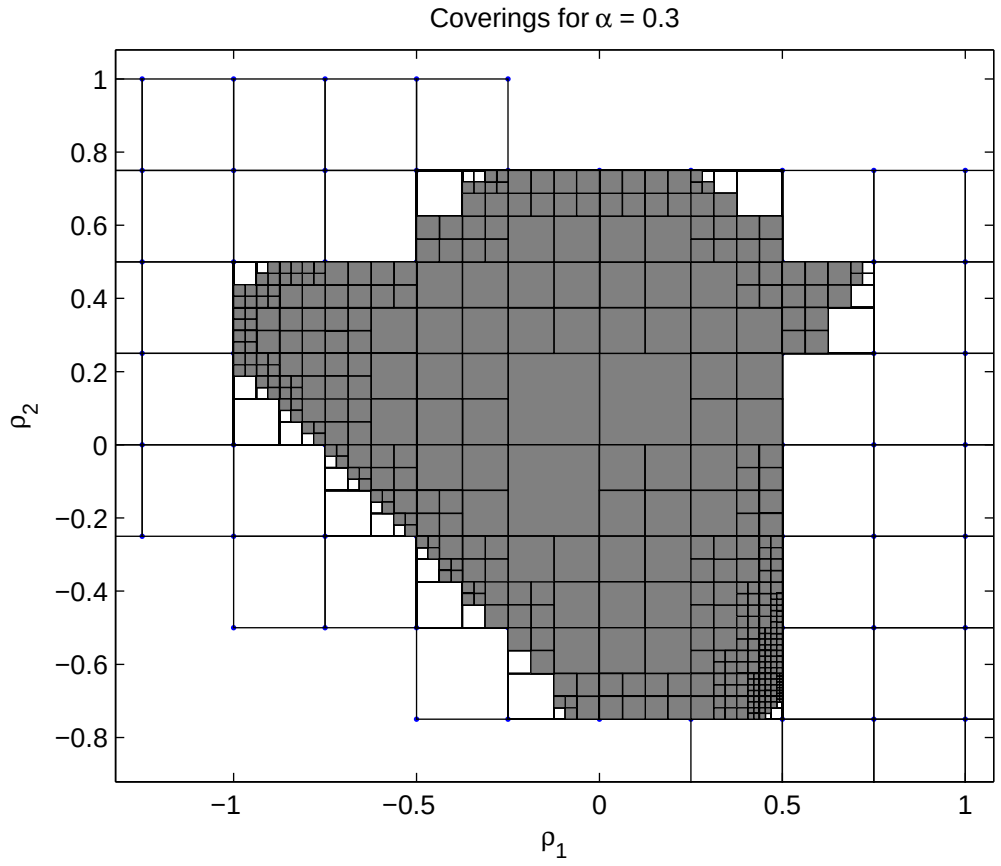

Figure 2.14: Certification covering for $\alpha = 0.3$.

2.8 Conclusions

We have developed a search method for a subset of designed controllers to reduce the number of experiments required in controller certification. By doing experiments only on a small subset of controllers, we can solve the certification problem for a large or, in the SISO case at least, an infinite set of candidate controllers in an efficient fashion. Precomputed design quantities such as $b_{\hat{P},C}$ and $\delta_\nu(C_i, C_j)$ are used to guide the search for controllers to be tested experimentally with the actual plant to yield certification of the complete set $\mathcal{C}$. A required margin for the controller certification can be maintained as we appropriately choose α in (2.11). For the SISO case when the candidate controller set has an infinite number of controllers, we have shown that only a finite number of experiments are required to solve the certification problem. We provided a theorem restricting the radius of a ball in Euclidean space and we gave an example that the controller will guarantee a prescribed level of stability and performance if parameters of a scalar controller are contained in that ball.

Further work required in this area is apparent to explore joint approaches to incorporating controller certification and fleet variability. There remain many open questions about extension to nonlinear systems and about the inclusion of significant time-variation among either or both the plants and controllers. From a practical perspective, questions still needing resolution are concerned with the experimental calculation of a useful tight bound on $b_{P,C}$ from data, and for the refinement of margins and ν-gaps to yield the least conservative values in MIMO problems through appropriate scaling. Some of these issues are introduced in (Fielding, Varga, Bennani & Selier 2002), but there still remains a wealth of problems. In Chapter 3, we will explore this issue fully. Clearly, extension of the SISO results for continuously parametrized sets of MIMO controllers will require significant technical work. Although, from a practical perspective, this might be subsumed by the enumerated solution.

Of particular interest is the extension of these results dealing with stability and stability margins to cover issues of guaranteed closed-loop performance. Already, weighting functions are used in the computation of MIMO margins and it is clear that weighting functions also play a central role in loop-shaping control designs.

2.9 Appendices

2.9.1 State Space Data of the F100 Jet Engine

The following model is at the F100 jet engine model of sea level static flight conditions with a power level angle (PLA) of 36 degrees. This comes from the report (Merrill, Beattie, LaPrad, Rock & Akhter 1984). The model itself is provided in Imperial/English units in the report; the symbol $^\circ R$ refers to temperature in degrees Rankine, the Fahrenheit equivalent of Kelvin.

```
A=[ -3.9180e+0  4.1886e+0 -4.1148e-2 1.2279e-1;
    -1.8061e-1 -2.1480e+0  1.5853e-1  6.6994e-4;
    -1.3190e-1 -2.4056e-1 -6.6630e-1  2.3770e-4;
    -3.8191e-1 -1.0501e+0 -6.7400e-2 -2.0000e+0];
B=[  5.1991e-1  1.1942e+0  2.1974e-1 -2.4990e-2 -1.7226e-2;
     3.6266e-1  1.0836e-1  7.2562e-3 -1.2133e-2 -7.2114e-3;
     2.8427e-1  3.3231e-2  5.7770e-3  5.7672e-3  1.6319e-3;
     9.3743e-1  7.3072e-2  1.7417e-2  2.0418e-2  1.0634e-1];
C=[  2.2043e+1          0          0          0;
             0  2.7339e+1          0          0;
     3.7700e+1  1.0341e+1 -7.6298e-3 -4.3237e-3;
     8.0543e+0  3.1436e-1 -6.6634e-2 -3.7135e-2;
    -2.9070e+0 -7.9884e+0 -5.1265e-1  2.6855e-3];
D=[          0          0          0          0          0;
             0          0          0          0          0;
     1.0036e+0 -8.2350e-1 -1.5200e-1 -5.6233e-2 -5.8600e-2;
     9.7674e-1 -5.7450e+0 -3.8500e-1  9.5762e-3 -2.2963e-2;
     7.1316e+0  5.5560e-1 1.32470e-1  1.5533e-1  4.8290e-2];
```

The states of system are: x_1 = fan speed [rpm], x_2 = compressor speed [rpm], x_3 = burner exit slow response temperature [$^\circ R$], and x_4 = fan turbine inlet slow response temperature [$^\circ R$].

The engine control inputs are: u_1 = main burner fuel flow [lb/hr], u_2 = nozzle jet area [ft^2], u_3 = fan guide vane angle [deg], u_4 = compressor stator vane angle [deg], and u_5 = compressor bleed flow [%].
The engine outputs are: y_1 = fan speed [rpm], y_2 = compressor speed [rpm], y_3 = burner pressure [psia], y_4 = augmentor pressure [psia], and y_5 = fan turbine inlet temperature [$^\circ R$].

2.9.2 Controller Gain Matrices

```
Kp=[-4.3945e-3  3.9063e-3          0  1.1719e-2  5.8594e-3;
     1.9531e-3 -2.9297e-3          0 -1.9531e-3  9.7656e-3;
    -2.5391e-2  1.5625e-2 -6.2500e-2  6.2500e-2 -9.3750e-2;
     2.3438e-1 -1.2500e-1 -5.0000e-1 -2.5000e-1          0;
    -4.5313e-1  5.0000e-1  1.5000e+0  7.5000e-1  2.0000e+0];
Ki=[ 2.4826e-4  6.6527e-3 -3.3803e-3  9.0337e-4  2.1197e-3;
     9.2531e-5 -1.5441e-3  8.1495e-3 -8.8501e-3  1.2418e-3;
     2.5726e-2 -2.3225e-2 -5.5274e-2  4.4241e-2 -3.6174e-3;
    -2.2895e-2 -4.8496e-1  4.9878e-1 -7.8880e-2  1.3700e-1;
     4.8743e-2  8.6349e-1 -1.0482e+0  1.0015e-1 -1.0255e-1];
```

2.9.3 Implementation of Controller Certification

The GUIs in Figure 2.15 and Figure 2.16 were developed in collaboration with SC Solutions Inc. at Sunnyvale, CA. The main GUI, in Figure 2.15, is responsible for

- computing and displaying the generalized stability margins,
- finding input and output scalings, and
- interpreting the generalized stability margin as the gain margin and phase margin.

The certification GUI, in Figure 2.16, using the certification algorithm, suggests the best parameters for next tests and shows the overall certification procedure.

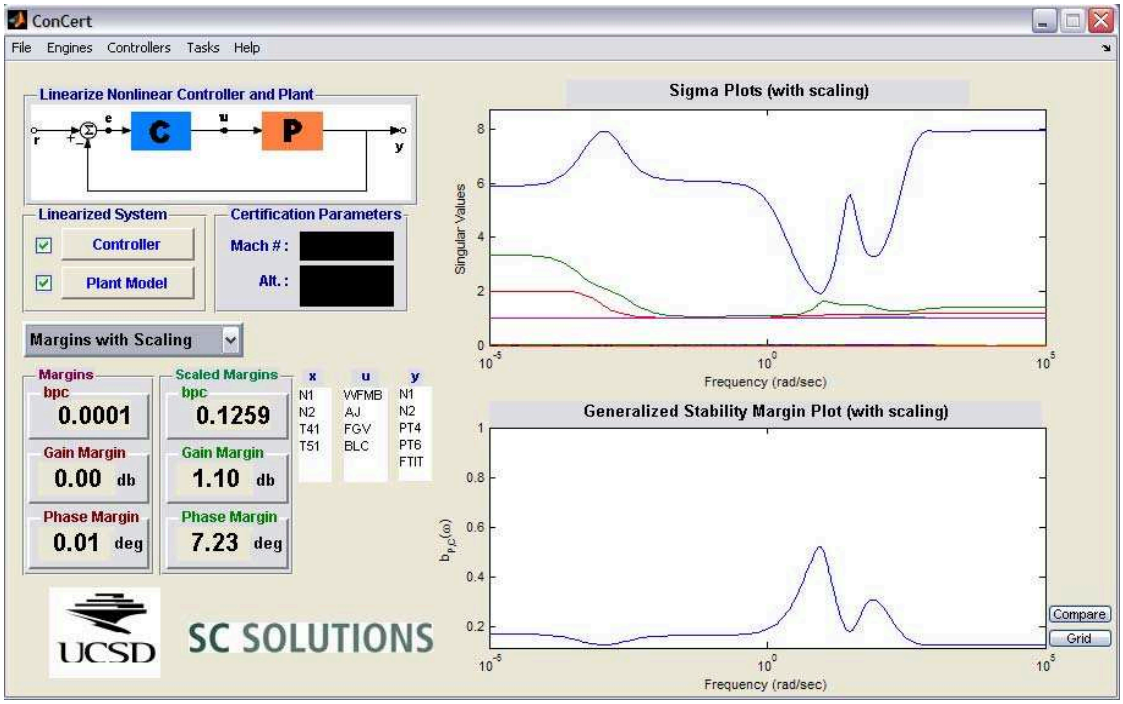

Figure 2.15: Main Certification GUI.

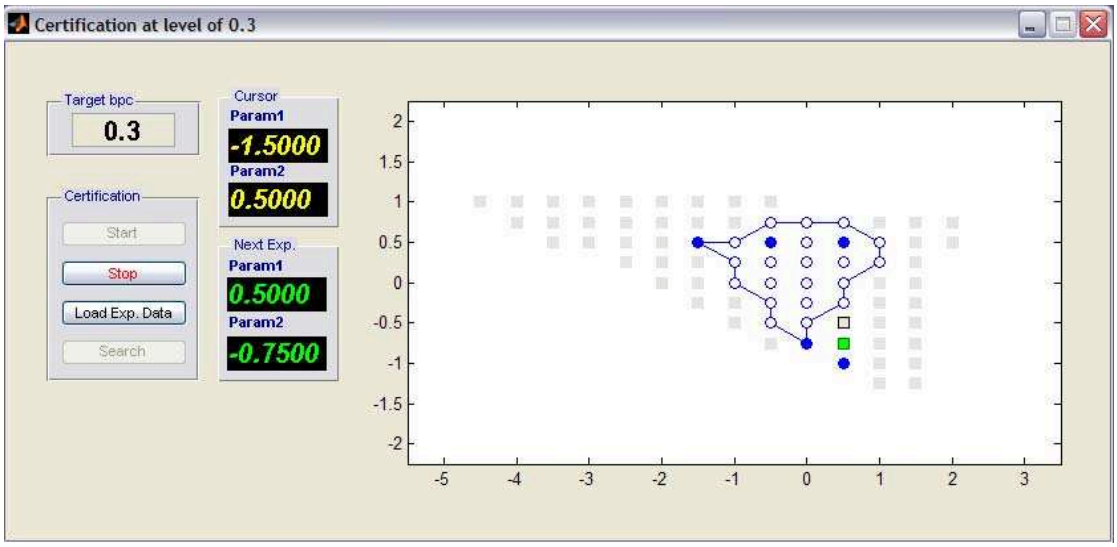

Figure 2.16: Certification at $\alpha = 0.3$.

This chapter is in part a reprint of the materials as is appears in,

Jisang Park, Robert R. Bitmead - *Controller Certification*, Automatica, Vol. 44 No. 1, Jan. 2008, pp.167–176.

Jisang Park, Robert R. Bitmead - *Controller Certification*, 44th IEEE Conference on Decision and Control, and European Control Conference in Seville, Spain, Dec., 2005. pp. 6442–6447

Jisang Park, Robert R. Bitmead - *Vinnicombe's Winding Number Condition is not Transitive: Impacts for Adaptive Control*, IFAC Workshop on Adaptation and Learning in Control and Signal Processing in Yokohama, Japan, Aug., 2004. pp. 783–787

The dissertation author was the primary author and the co-author listed in these publications directed and supervised the research.

3

Simultaneous Scaling for MIMO Controller Certification

We consider methods for the computation of; maximal MIMO stability margins $b_{\hat{P},C}$, minimal ν-gap metrics δ_ν, and the maximal difference between these two values, through the use of scaling and weighting functions. We propose simultaneous scaling selections that attempt to maximize the generalized stability margin and minimize the ν-gap to facilitate controller certification developed in Chapter 2. The minimization of the ν-gap by scaling involves a non-convex optimization. We modify the XY-centering algorithm to handle this non-convexity.

3.1 Introduction

Controller certification (Park & Bitmead 2008) was introduced as a decision support tool that reduces the number of time-consuming and expensive experiments that are required to establish the stability margin of a large set of multiple-input/mulitple-output (MIMO) controllers, $\mathcal{C}$. Vinnicombe introduced the ν-gap metric (Vinnicombe 1993) to provide MIMO stability and performance robustness guarantees. In this chapter, we investigate effects of scalings on these stability margin and ν-gap computations for controller certification and propose a simultaneous scaling matrix for computation of the margin and ν-gap to expedite a controller certification. Crucial ingredients of controller certification are computations of the generalized stability margin, $b_{\hat{P},C_i}$ and the ν-gap

between the C_i, and other controllers, $C_j \in \mathcal{C}$.

3.1.1 Computation of Margin and ν-gap

Computation of the generalized stability margin, $b_{\hat{P},C_i}$, involves calculation of the singular values of a transfer function matrix. This singular value computation is sensitive to the selection of relative signal magnitudes or measurement units pertaining to the input and output signals in each channel. To accommodate this, Steele and Vinnicombe (Fielding, Varga, Bennani & Selier 2002) considered constant diagonal scaling of all input and output channels in order that a favorable stability margin might be calculated. Likewise, one may consider using different scalings at different frequencies to improve minimal margins. Finding close to the maximal $b_{\hat{P},C_i}$ uses the same analysis with computation of an upper bound of the structured singular values. Both problems can be solved by a convex optimization.

The ν-gap metric computation between MIMO systems also suffers the sensitivity problem of computing a singular value. However, differently from the optimization of $b_{\hat{P},C_i}$, scaling of the ν-gap metric calculation cannot be done by a convex optimization. This is where the main difficulty arises. To tackle this non-convex optimization, we modify the XY-centering algorithm (Iwasaki & Skelton 1995). Iwasaki and Skelton (Iwasaki & Skelton 1995) formulated the matrix inequality problem for static output feedback controller synthesis as a dual LMI problem. We propose simultaneous scaling selections that attempt to maximize the generalized stability margin and to minimize the ν-gap. We say controller certification for the candidate controller set, $\mathcal{C}$, is *efficient* when we are able to examine whether the generalized stability margins, b_{P,C_j} of $\mathcal{C}$, are larger than a pre-specified stability margin level, α, with as small a number of experiments as possible.

3.1.2 Problem Settings

Figure 3.1a depicts the MIMO feedback loop for the control system whose stability is under consideration. Figure 3.1b shows the same loop with weightings introduced. W_i is the input weighting and W_o is the output weighting, which correspond to defining new scaled input and output signals as shown. Three interesting classes of

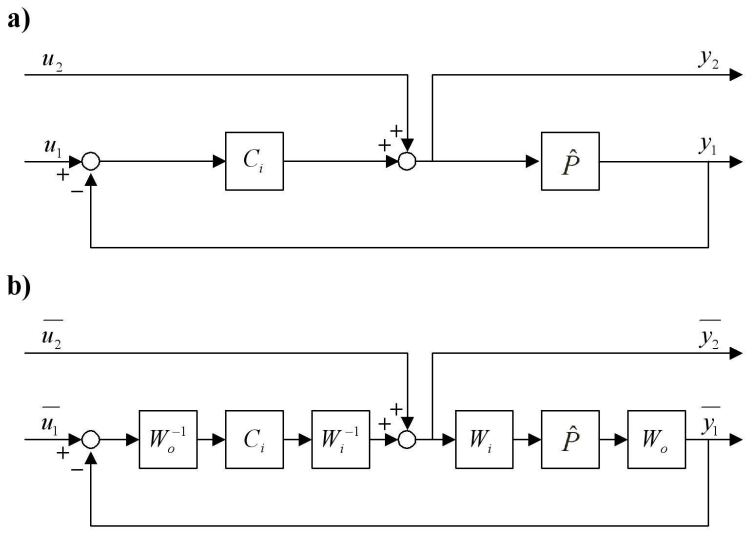

Figure 3.1: a) Feedback loop of $T(\hat{P}, C_i)$ b) Scaled feedback loop

scaling function matrices arise naturally:

1) W_i, W_o positive definite symmetric matrices, constant over frequency $\omega \in \mathbb{R}$,

2) W_i, W_o positive definite hermitian matrices at a fixed frequency ω_n, and

3) $W_i(s)$, $W_o(s)$ bistable and bi-proper transfer function matrices interpolating W_i, W_o at a sequence of frequency values $\{\omega_n\}$.

We shall consider the first two kinds of scaling matrices in this thesis. The following assumption allows us to extend the input/output scalings from a finite number of frequency points of the second type problem to all frequency range.

Assumption 3.1.1. *Satisfaction of the certification inequality (2.16),*

$$\arcsin \delta_\nu(C_i, C_j) < \arcsin b_{P,C_i} - \arcsin \alpha$$

at a finite number of frequencies, $\{\omega_n\}$, implies satisfaction of this inequality over the complete frequency range.

Smoothness of the frequency response of $T(\hat{P}, C_i)(j\omega)$ and $\kappa(C_i, C_j)(j\omega)$ will support Assumption 3.1.1. The internal stability of both the loops in Figures 3.1a and 3.1b is identical, although the techniques sufficient for demonstrating stability can vary

between the two loops. In Figure 3.1b, if $\hat{P}$ and C are scalar transfer functions, then the gain margin (GM) and the phase margin (PM) of the feedback-loop between input $\overline{u}_1$ and output $\overline{y}_1$ are invariant to the choice of scalings W_o and W_i. However $b_{\hat{P},C}$ depends not merely on stability from $\overline{u}_1$ to $\overline{y}_1$, but also on the maximum singular value of the 2×2 block transfer function matrix. Therefore, $b_{\hat{P},C}$ can be small with a poorly scaled SISO system even though $(\hat{P}, C)$ is well behaved and has good scalar margins. This fact reflects the conservatism of $b_{\hat{P},C}$ as a stability margin. The more detailed relationship between $b_{\hat{P},C}$ and the SISO GM and PM can be found in Chapter 2 and Appendix ?? as well as (Vinnicombe 2001, Glover, Vinnicombe & Papageorgiou 2000).

We will present the formulation of a convex optimization problem to find the input/output weights for maximization of $b_{\hat{P},C}$ in Section 3.2. This optimization problem is readily solved using LMI methods minimizing norms by scaling as in (Boyd, Ghaoui, Feron & Balakrishnan 1994). With the analysis in (Fielding, Varga, Bennani & Selier 2002), conservatism of $b_{\hat{P},C}$ can be reduced fairly well. However, merely improving conservatism of the generalized stability margin computation cannot always promise successful controller certification. This is simply because the input/output scalings on $b_{\hat{P},C}$ are not necessarily the optimal ones for the ν-gap metric computation and do not necessarily positively affect the implied bounds on $b_{\hat{P},C_j}$. In Section 3.4, we propose an approach to simultaneous alleviation of the conservatism in both of the $b_{\hat{P},C}$ and ν-gap metric computations. A numerical example is given in Section 3.5.

3.2 LMI formulation for Scaling $b_{\hat{P},C}$

In this Section, a short LMI formulation for $b_{\hat{P},C_i}$ minimization by input and output scalings is developed for application in the XY-centering framework in Section 3.4.1. As depicted in Figure 3.1b, if the scaling matrices W_i and W_o are involved in the $b_{\hat{P},C_i}$ computation using the $T(\hat{P}, C_i)$, the frequency-wise generalized sensitivity function of the scaled feedback loop in Figure 3.1 b) is given by,

$$
\begin{aligned}
&T(W_o\hat{P}W_i, W_i^{-1}C_iW_o^{-1})(j\omega) \\
&= \begin{bmatrix} W_o & 0 \\ 0 & W_i^{-1} \end{bmatrix} \begin{bmatrix} \hat{P}(I+C\hat{P})^{-1}C & \hat{P}(I+C\hat{P})^{-1} \\ (I+C\hat{P})^{-1}C & (I+C\hat{P})^{-1} \end{bmatrix} (j\omega) \begin{bmatrix} W_o^{-1} & 0 \\ 0 & W_i \end{bmatrix} \\
&= \begin{bmatrix} W_o & 0 \\ 0 & W_i^{-1} \end{bmatrix} T(\hat{P}, C_i)(j\omega) \begin{bmatrix} W_o^{-1} & 0 \\ 0 & W_i \end{bmatrix},
\end{aligned} \tag{3.1}
$$

where $T(\hat{P}, C_i)(j\omega)$ is used to denote the frequency-wise generalized sensitivity function, $T(\hat{P}(j\omega), C_i(j\omega))$. Using (3.1), $\|T\|_\infty = \sqrt{\lambda_{\max}(T^*T)}$ and $\lambda_{\max}(AB) = \lambda_{\max}(BA)$, the reciprocal of the scaled generalized stability margin is represented as following,

$$
\begin{aligned}
&\left(b_{W_o\hat{P}W_i, W_i^{-1}C_iW_o^{-1}}\right)^{-1} \\
&= \|T(W_o\hat{P}W_i, W_i^{-1}C_iW_o^{-1})(j\omega)\|_\infty \\
&= \sup_{\omega\in\mathbb{R}} \lambda_{max}^{1/2} \left(\begin{bmatrix} W_o^{*-1} & 0 \\ 0 & W_i^* \end{bmatrix} T(\hat{P}, C_i)^*(j\omega) \begin{bmatrix} W_o^* & 0 \\ 0 & W_i^{*-1} \end{bmatrix} \cdot \right. \\
&\qquad\qquad \left. \begin{bmatrix} W_o & 0 \\ 0 & W_i^{-1} \end{bmatrix} T(\hat{P}, C_i)(j\omega) \begin{bmatrix} W_o^{-1} & 0 \\ 0 & W_i \end{bmatrix} \right) \\
&= \sup_{\omega\in\mathbb{R}} \lambda_{max}^{1/2} \left(\begin{bmatrix} (W_o^*W_o)^{-1} & 0 \\ 0 & W_iW_i^* \end{bmatrix} T(\hat{P}, C_i)^*(j\omega) \cdot \right. \\
&\qquad\qquad \left. \begin{bmatrix} W_o^*W_o & 0 \\ 0 & (W_iW_i^*)^{-1} \end{bmatrix} T(\hat{P}, C_i)(j\omega) \right).
\end{aligned} \tag{3.2}
$$

The scaling matrices W_i and W_o in (3.2) are computed by solving an optimization at each point on a frequency grid. Note that at a specific interesting frequency point ω_n, (3.2) can be solved, even though finding a solution on an infinite frequency grid is unrealistic.

3.2.1 Frequency Dependent Scaling of $b_{\hat{P},C}$

From the following theorem, we can obtain a lower bound on the scaled $b_{\hat{P},C}$ at a given frequency ω_n.

Theorem 3.2.1. *At a fixed frequency ω_n, consider positive definite hermitian matrices W_i and W_o with $X_o = W_o^* W_o$ and $Y_i = (W_i W_i^*)^{-1}$. If a solution (X_o, Y_i) of the following LMI,*

$$\begin{aligned} &\textit{minimize} \quad \gamma_1^2 \\ &\textit{subject to} \quad \gamma_1^2 \begin{bmatrix} X_o & 0 \\ 0 & Y_i \end{bmatrix} - T(\hat{P}, C)^*(j\omega_n) \begin{bmatrix} X_o & 0 \\ 0 & Y_i \end{bmatrix} T(\hat{P}, C)(j\omega_n) > 0, \\ &\qquad\qquad X_o > 0, \quad Y_i > 0. \end{aligned} \tag{3.3}$$

exists with achieved objective value γ_1, then the scaled $b_{\hat{P},C}$ at ω_n is bounded below by γ_1^{-1}

$$b_{W_o \hat{P} W_i, W_i^{-1} C W_o^{-1}}(j\omega_n) > \gamma_1^{-1}.$$

Proof. At a fixed frequency point, ω_n, using a solution $(X_o, Y_i) = (W_o^* W_o, (W_i W_i^*)^{-1})$, the equation (3.3) can be rewritten in the following minimization form,

$$\begin{aligned} &\text{minimize} \quad \gamma_1^2 \\ &\text{subject to} \left(\begin{bmatrix} (W_o^* W_o)^{-1} & 0 \\ 0 & W_i W_i^* \end{bmatrix} T(\hat{P}, C)^*(j\omega_n) \right. \\ &\qquad\qquad \left. \begin{bmatrix} W_o^* W_o & 0 \\ 0 & (W_i W_i^*)^{-1} \end{bmatrix} T(\hat{P}, C)(j\omega_n) \right) < \gamma_1^2 I, \\ &\qquad W_o^* W_o > 0, \quad W_i W_i^* > 0. \end{aligned} \tag{3.4}$$

Since the optimal value γ_1 is an upper bound of (3.2), we have

$$\left(b_{W_o \hat{P} W_i, W_i^{-1} C W_o^{-1}}(j\omega_n) \right)^{-1} < \gamma_1.$$

□

Since $\lambda_{\max}(AB) = \lambda_{\max}(BA)$, by defining $X_i = Y_i^{-1} = W_i W_i^*$ and $X_o = Y_o^{-1} = W_o^* W_o$, an alternative formulation of (3.3) is

$$\begin{aligned} &\text{minimize} \quad \gamma_1^2 \\ &\text{subject to} \quad \gamma_1^2 \begin{bmatrix} Y_o & 0 \\ 0 & X_i \end{bmatrix} - T(\hat{P}, C)(j\omega_n) \begin{bmatrix} Y_o & 0 \\ 0 & X_i \end{bmatrix} T(\hat{P}, C)^*(j\omega_n) > 0, \\ &\qquad\qquad X_i > 0, \quad Y_o > 0. \end{aligned} \tag{3.5}$$

The optimization in (3.3) and (3.5) can be performed iteratively using bisection on γ_1^2 by solving feasibility problems as in (Boyd & Vandenberghe 2004). Either (3.3) or (3.5) can be used in the algorithm in Section 3.4.1.

3.2.2 Constant Scaling Over All Frequencies

As noted in the previous section, computing solutions over an infinite frequency gridding is impractical. Steele (Steele 2001) used a result from (Rantzer 1996) to find a constant scaling over all frequencies by replacing a frequency domain infinite family of LMIs with a single LMI. Define $M = \begin{bmatrix} W_o^* W_o & 0 \\ 0 & (W_i W_i^*)^{-1} \end{bmatrix}$ and let (A, B, C, D) be a state space realization of $T(\hat{P}, C)$. Then the scaling matrix M to maximize the $b_{\hat{P},C}$ can be obtained by solving,

$$\begin{aligned} &\text{minimize} \quad \gamma_1^2 \\ &\text{subject to} \\ &\begin{bmatrix} (j\omega I - A)^{-1}B \\ I \end{bmatrix}^* \begin{bmatrix} C & D \\ 0 & I \end{bmatrix}^* \begin{bmatrix} M & 0 \\ 0 & -\gamma_1^2 M \end{bmatrix} \begin{bmatrix} C & D \\ 0 & I \end{bmatrix} \begin{bmatrix} (j\omega I - A)^{-1}B \\ I \end{bmatrix} < 0 \quad \forall \omega, \\ &M > 0. \end{aligned} \tag{3.6}$$

Corollary 3.2.1. *Over all frequencies $\omega \in \mathbb{R}$, consider constant positive definite hermitian matrices W_i and W_o with $M = \begin{bmatrix} W_o^* W_o & 0 \\ 0 & (W_i W_i^*)^{-1} \end{bmatrix}$. If a solution M of the following LMI,*

$$\begin{aligned} &\textit{minimize} \quad \gamma_1^2 \\ &\textit{subject to} \quad \begin{bmatrix} C^* \\ D^* \end{bmatrix} M \begin{bmatrix} C & D \end{bmatrix} + \begin{bmatrix} QA + A^*Q & PB \\ Q^*\hat{P} & 0 \end{bmatrix} < \gamma_1^2 \begin{bmatrix} 0 & 0 \\ 0 & M \end{bmatrix}, \\ &\qquad M > 0, \quad Q = Q^* \end{aligned} \tag{3.7}$$

exists with achieved objective value γ_1, then the scaled $b_{\hat{P},C}$ is bounded below by γ_1^{-1}

$$b_{W_o P W_i, W_i^{-1} C W_o^{-1}} \geq \gamma_1^{-1}.$$

By applying the theorem on the KYP lemma in (Rantzer 1996), the LMI in (3.6) can be transformed into the LMI in (3.7). As noted in (Rantzer 1996), the equivalence for strict inequality of (3.6) and (3.7) holds even if (A, B) is not controllable. LMI (3.7) also can be solved using bisection on γ_1^2 with iterative feasibility solution on M and Q. Note (3.7) cannot be incorporated into the algorithm we will present in the next section. Corollary 3.2.1 provides a guaranteed lower bound on the scaled $b_{\hat{P},C}$.

3.3 LMI formulation for Scaling $\delta_\nu(C_i, C_j, \omega_n)$

The input/output scaling methods in Section 3.2 may reduce the conservatism in the $b_{\hat{P},C}$ computation. However the use of scaling matrices without carefully considering how W_o and W_i will alter $\delta_\nu(W_i^{-1}C_iW_o^{-1}, W_i^{-1}C_jW_o^{-1})$ can bring unfavorable ramifications to the controller certification. This is because $\delta_\nu(W_i^{-1}C_iW_o^{-1}, W_i^{-1}C_jW_o^{-1})$ need not be smaller than $\delta_\nu(C_i, C_j)$, since W_o and W_i in Section 3.2.1 and 3.2.2 are intended to reduce conservatism of the computation of $b_{\hat{P},C_i}$ only. In Section 3.3.1, we provide an example showing that certain scalings can cause violation of the winding number condition (WNC) (2.1).

3.3.1 The winding number condition and scaling matrices

The value of $\delta_\nu(W_i^{-1}C_iW_o^{-1}, W_i^{-1}C_jW_o^{-1}, \omega_n)$ depends on the scaling matrices W_o and W_i. Indeed, the satisfaction of WNC can be affected by the weighting matrices. In some cases, the input/output scalings cause a violation of WNC.

Consider a plant $\hat{P} = \frac{1}{s+1}$, $\hat{P}$-stabilizing controllers $C_0 = 1$ and $C_1 = k$ ($k > -1$). If we choose the following scalings,

$$W_i = W_o = \frac{s+1}{as+1}, \tag{3.8}$$

where $a > 0$, then from (2.1),

$$\begin{aligned}
&\det(1 + W_o^{*-1} C_1^* W_i^{*-1} W_i^{-1} C_0 W_o^{-1})(j\omega) \\
=&1 + k \left(\frac{-aj\omega + 1}{-j\omega + 1} \right)^2 \left(\frac{aj\omega + 1}{j\omega + 1} \right)^2 \\
=&\frac{(a^4 k + 1)\omega^4 + 2(a^2 k + 1)\omega^2 + (k + 1)}{\omega^4 + 2\omega^2 + 1} \\
\triangleq&X(\omega).
\end{aligned}$$

Note $\lim_{\omega \to \infty} X(\omega) = a^4 k + 1$, and $\lim_{\omega \to 0} X(\omega) = k + 1$. If

$$-1 < k < -\frac{1}{a^4}, \text{ then } \lim_{\omega \to \infty} X(\omega) < 0$$

and, since $k > -1$,

$$\lim_{\omega \to 0} X(\omega) > 0.$$

Since $X(\omega)$ is real and continuous in ω, $X(\omega) = 0$ for some ω. Therefore, WNC is not preserved by the scalings (3.8). The non-invariance of WNC to scaling in this example immediately implies non-invariance in MIMO. In order to ensure satisfaction of WNC for specific choices of weighting matrices, we can rely on the following result.

Lemma 3.3.1 ((Vinnicombe 2001) p. 136)**.** *Let $\hat{P}$, C_i, and C_j be given such that the feedback pair $(\hat{P}, C_i)$ is stable and $\kappa(C_i, C_j)(j\omega) < b_{\hat{P}, C_i}(j\omega)$ for all ω, then $(\hat{P}, C_j)$ is stable if, and only if, the winding number condition holds.*

Since the scalings W_i and W_o do not change stability of the feedback loops in Figure 3.1, stability of the scaled feedback pair $(W_o \hat{P} W_i, W_i^{-1} C_i W_o^{-1})$ and $(W_o \hat{P} W_i, W_i^{-1} C_j W_o^{-1})$ is also maintained. Thus, by Lemma 3.3.1, $\kappa(W_i^{-1} C_i W_o^{-1}, W_i^{-1} C_j W_o^{-1})(j\omega) < b_{W_o \hat{P} W_i, W_i^{-1} C_i W_o^{-1}}(j\omega)$ for all ω will suffice to establish satisfaction of WNC between $W_i^{-1} C_i W_o^{-1}$ and $W_i^{-1} C_j W_o^{-1}$. We shall define in Section 3.4 an iterative algorithm for successive optimization of scaling matrices and we will need to consider whether these matrices might violate WNC in the successive procedure. This algorithm provides monotonic decrease of an upper bound of $\kappa(W_i^{-1} C_i W_o^{-1}, W_i^{-1} C_j W_o^{-1})(j\omega_n)$ and monotonic increase of a lower bound of $b_{W_o \hat{P} W_i, W_i^{-1} C_i W_o^{-1}}(j\omega_n)$ at a specific frequency ω_n. At a finite number of frequency points, once the algorithm establishes that the lower bound of $b_{W_o \hat{P} W_i, W_i^{-1} C_i W_o^{-1}}(j\omega_n)$ is greater

than the upper bound of $\kappa(W_i^{-1}C_iW_o^{-1}, W_i^{-1}C_jW_o^{-1})(j\omega_n)$, Assumption 3.1.1 extends this result over the complete frequency range. Then Lemma 3.3.1 with Assumption 3.1.1 can ensure satisfaction of WNC between two scaled controllers. However, if we want to minimize $\delta_\nu(W_i^{-1}C_iW_o^{-1}, W_i^{-1}C_jW_o^{-1})(j\omega_n)$ only at a specific frequency of interesting, the algorithm needs to check violation of WNC (2.1) of the weighted $C_i(s)$ and $C_j(s)$ during entire iteration of the algorithm.

Assumption 3.3.1. *If weighting matrices $W_i(\omega_n)$ and $W_o(\omega_n)$ can be found satisfying*

$$\delta_\nu(W_i^{-1}C_iW_o^{-1}, W_i^{-1}C_jW_o^{-1})(j\omega_n) < b_{W_o\hat{P}W_i, W_i^{-1}C_iW_o^{-1}}(j\omega_n)$$

then the interpolating weighting function $W_i(\omega)$ and $W_o(\omega)$ satisfy

$$\delta_\nu(W_i^{-1}C_iW_o^{-1}, W_i^{-1}C_jW_o^{-1})(j\omega) < b_{W_o\hat{P}W_i, W_i^{-1}C_iW_o^{-1}}(j\omega)$$

for all ω and hence, by Lemma 3.3.1, $W_i^{-1}C_iW_o^{-1}$ and $W_i^{-1}C_jW_o^{-1}$ satisfy WNC.

If Assumption 3.3.1 is not satisfied, one may resort to testing the satisfaction of WNC over all frequencies for each constant scaling $W_i(\omega_n)$ and $W_o(\omega_n)$.

3.3.2 LMI Formulation of ν-gap minimization

Define the following matrices ϕ and ψ,

$$\phi(Y_i, X_o, \gamma_1) \triangleq \gamma_1^2 \begin{bmatrix} X_o & 0 \\ 0 & Y_i \end{bmatrix} - T(\hat{P}, C_i)^*(j\omega_n) \begin{bmatrix} X_o & 0 \\ 0 & Y_i \end{bmatrix} T(\hat{P}, C_i)(j\omega_n), \tag{3.9}$$

$$\psi(X_i, Y_i, X_o, Y_o, \gamma_2) \triangleq \begin{bmatrix} \gamma_2^2(X_i + C_jY_oC_j^*) & (C_j - C_i) \\ (C_j - C_i)^* & (X_o + C_i^*Y_iC_i) \end{bmatrix} (j\omega_n). \tag{3.10}$$

Then define two sets Φ and Ψ,

$$\Phi(\gamma_1) \triangleq \{Y_i, X_o : \phi(Y_i, X_o, \gamma_1) > 0\}, \tag{3.11}$$

$$\Psi(\gamma_2) \triangleq \{X_i, Y_i, X_o, Y_o : \psi(X_i, Y_i, X_o, Y_o, \gamma_2) > 0\}. \tag{3.12}$$

Then a guaranteed upper bound of the scaled ν-gap by W_o and W_i is given in Theorem 3.3.1.

Theorem 3.3.1. *At a fixed frequency $\omega_n \in \mathbb{R}$, consider the frequency response of a plant model $\hat{P}(j\omega_n)$, and stabilizing controllers $C_i(j\omega_n)$ and $C_j(j\omega_n)$ and consider positive definite hermitian matrices W_i and W_o with $X_o = Y_o^{-1} = W_o^* W_o$ and $X_i = Y_i^{-1} = W_i W_i^*$. If a solution (X_i, Y_i, X_o, Y_o) exists with achieved objective value γ_2 for the LMIs,*

$$\begin{gathered}\begin{bmatrix} \gamma_2^2(X_i + C_j Y_o C_j^*) & (C_j - C_i) \\ (C_j - C_i)^* & (X_o + C_i^* Y_i C_i) \end{bmatrix}(j\omega_n) > 0, \\ \begin{bmatrix} X_i & I \\ I & Y_i \end{bmatrix} > 0, \text{ and } \begin{bmatrix} X_o & I \\ I & Y_o \end{bmatrix} > 0.\end{gathered} \tag{3.13}$$

with the following properties,

$$\begin{cases} (X_i^{-1}, X_o) \in \Phi(\gamma_1) \\ (X_i, X_i^{-1}, X_o, X_o^{-1}) \in \Psi(\gamma_2) \end{cases} \text{or} \begin{cases} (Y_i, Y_o^{-1}) \in \Phi(\gamma_1) \\ (Y_i^{-1}, Y_i, Y_o^{-1}, Y_o) \in \Psi(\gamma_2) \end{cases}$$

then the scaled ν-gap metric at ω_n is bounded above by γ_2,

$$\delta_\nu(W_i^{-1} C_i W_o^{-1}, W_i^{-1} C_j W_o^{-1})(j\omega_n) < \gamma_2.$$

The weighted ν-gap minimization requires solving a non-convex matrix inequality. Provided the winding number condition (2.1) of two scaled controllers $W_i^{-1} C_0(s) W_o^{-1}$ and $W_i^{-1} C_1(s) W_o^{-1}$ is satisfied, the weighted ν-gap is expressed as follow,

$$\begin{aligned} &\delta_\nu(W_i^{-1} C_i W_o^{-1}, W_i^{-1} C_j W_o^{-1}) \\ =&\Big\| \left(I + W_i^{-1} C_j W_o^{-1} W_o^{*-1} C_j^* W_i^{*-1}\right)^{-\frac{1}{2}} W_i^{-1} (C_j - C_i) \\ &\qquad W_o^{-1} \left(I + W_o^{*-1} C_i^* W_i^{*-1} W_i^{-1} C_i W_o^{-1}\right)^{-\frac{1}{2}} \Big\|_\infty \\ =&\sup_{\omega \in \mathbb{R}} \lambda_{max}^{1/2} \Big(\left(W_i W_i^* + C_j W_o^{-1} W_o^{*-1} C_j^*\right)^{-1} \cdot (C_j - C_i) \\ &\qquad \cdot \left(W_o^* W_o + C_i^* W_i^{*-1} W_i^{-1} C_i\right)^{-1} \cdot (C_j - C_i)^* \Big)(j\omega). \end{aligned} \tag{3.14}$$

Using positive hermitian matrices

$$X_i = Y_i^{-1} = W_i W_i^* \text{ and } X_o = Y_o^{-1} = W_o^* W_o,$$

for a fixed frequency, ω_n, minimization of (3.14) can be formulated as the following

optimization problem. Find hermitian matrices $X_o,\ X_i$ such that

$$\begin{aligned} &\text{minimize} \quad \gamma_2^2 \\ &\text{subject to} \quad \left(\left(X_i + C_j Y_o C_j^*\right)^{-1} (C_j - C_i) \left(X_o + C_i^* Y_i C_i\right)^{-1} (C_j - C_i)^* \right) (j\omega_n) < \gamma_2^2 I, \\ &\qquad\qquad X_i = Y_i^{-1} > 0,\ X_o = Y_o^{-1} > 0. \end{aligned} \tag{3.15}$$

Then using the Schur complement, (3.15) is expressed as

$$\begin{aligned} &\text{minimize} \quad \gamma_2^2 \\ &\text{subject to} \quad \begin{bmatrix} \gamma_2^2 (X_i + C_j Y_o C_j^*) & (C_j - C_i) \\ (C_j - C_i)^* & (X_o + C_i^* Y_i C_i) \end{bmatrix} (j\omega_n) > 0, \\ &\qquad\qquad X_i = Y_i^{-1} > 0,\ X_o = Y_o^{-1} > 0. \end{aligned} \tag{3.16}$$

Note that $X_o + C_i^* Y_i C_i$ is positive by its structure. We use the XY-centering algorithm (Iwasaki & Skelton 1995) to handle the non-convexity in (3.16). To use the algorithm, optimization (3.16) is recast as the following problem,

$$\begin{aligned} &\text{minimize} \quad \gamma_2^2 \\ &\text{subject to} \quad \begin{bmatrix} \gamma_2^2 (X_i + C_j Y_o C_j^*) & (C_j - C_i) \\ (C_j - C_i)^* & (X_o + C_i^* Y_i C_i) \end{bmatrix} (j\omega_n) > 0 \\ &\qquad\qquad \begin{bmatrix} X_i & I \\ I & Y_i \end{bmatrix} > 0\ , \quad \begin{bmatrix} X_o & I \\ I & Y_o \end{bmatrix} > 0. \end{aligned} \tag{3.17}$$

The optimization problems (3.16) and (3.17) are identical except for the constraints on the (X_i, Y_i) pair and the (X_o, Y_o) pair. The XY-centering algorithm makes the discrepancy between those constraints smaller if possible. The algorithm, for example with the (X_i, Y_i) pair, pushes the constraint of $X_i \geq Y_i^{-1}$ in (3.17) to head towards $X_i = Y_i^{-1}$ in (3.16) by iterative minimization of $\lambda_{\max}(X_i Y_i)$. In the next section, we modify the algorithm to accommodate minimization problems (3.3) and (3.17) simultaneously.

3.4 Simultaneous Scaling of $b_{\hat{P},C}$ and ν-gap

For the certification purpose, W_i and W_o should not merely reduce conservatism of the $b_{W_o \hat{P} W_i, W_i^{-1} C_i W_o^{-1}}$ computation but rather maximize the following quantity

$$b_{W_o \hat{P} W_i, W_i^{-1} C_i W_o^{-1}} - \delta_\nu \left(W_i^{-1} C_i W_o^{-1}, W_i^{-1} C_j W_o^{-1} \right),$$

which can be interpreted as a simultaneous optimization problem of

$$\begin{aligned} &\underset{W_o,W_i}{\text{minimize}} \left(b_{W_o\hat{P}W_i,W_i^{-1}C_iW_o^{-1}}\right)^{-1} \\ \text{and} \quad &\underset{W_o,W_i}{\text{minimize}}\, \delta_\nu \left(W_i^{-1}C_iW_o^{-1}, W_i^{-1}C_jW_o^{-1}\right). \end{aligned} \tag{3.18}$$

As noticed in (Iwasaki & Skelton 1995), the XY-centering algorithm may not give a global solution to minimizing $\lambda_{\max}(X_iY_i)$. Then the main result of this chapter boils down to the following theorem.

Theorem 3.4.1. *At a fixed frequency ω_n, consider the frequency response of a plant model $\hat{P}(j\omega_n)$, and stabilizing controllers $C_i(j\omega_n)$ and $C_j(j\omega_n)$ and consider positive definite hermitian matrices W_i and W_o with $X_o = Y_o^{-1} = W_o^*W_o$ and $X_i = Y_i^{-1} = W_iW_i^*$. If a solution (X_i, Y_i, X_o, Y_o) exists with achieved objective values γ_1 and γ_2 for the LMIs,*

$$\begin{aligned} &\gamma_1^2 \begin{bmatrix} X_o & 0 \\ 0 & Y_i \end{bmatrix} - T(\hat{P}, C_i)^*(j\omega_n) \begin{bmatrix} X_o & 0 \\ 0 & Y_i \end{bmatrix} T(\hat{P}, C_i)(j\omega_n) > 0, \\ &\begin{bmatrix} \gamma_2^2(X_i + C_jY_oC_j^*) & (C_j - C_i) \\ (C_j - C_i)^* & (X_o + C_i^*Y_iC_i) \end{bmatrix} (j\omega_n) > 0, \\ &\begin{bmatrix} X_i & I \\ I & Y_i \end{bmatrix} > 0, \text{ and } \begin{bmatrix} X_o & I \\ I & Y_o \end{bmatrix} > 0. \end{aligned} \tag{3.19}$$

with either of the following properties,

$$\begin{cases} (X_i^{-1}, X_o) \in \Phi(\gamma_1) \\ (X_i, X_i^{-1}X_o, X_o^{-1}) \in \Psi(\gamma_2) \end{cases} \text{or} \quad \begin{cases} (Y_i, Y_o^{-1}) \in \Phi(\gamma_1) \\ (Y_i^{-1}, Y_iY_o^{-1}, Y_o) \in \Psi(\gamma_2) \end{cases}$$

then the scaled $b_{\hat{P},C}$ at ω_n is bounded below by γ_1^{-1} and the scaled ν-gap metric at ω_n is bounded above by γ_2,

$$\begin{aligned} b_{W_oPW_i,W_i^{-1}CW_o^{-1}}(j\omega_n) &> \gamma_1^{-1} \\ \delta_\nu(W_i^{-1}C_iW_o^{-1}, W_i^{-1}C_jW_o^{-1})(j\omega_n) &< \gamma_2. \end{aligned}$$

3.4.1 XY-Centering Algorithm for Simultaneous Scaling of $b_{\hat{P},C}$ and ν-gap

In this section, we provide an algorithm that minimizes γ_1 and γ_2 in (3.19). Consider a linear square matrix inequality,

$$F(x) = F_0 + \sum_{i=1}^{m} x_i F_i > 0,$$

where $x \in \mathbb{R}^m$ is the variable and $F_i = F_i^T \in \mathbb{R}^{n\times n}$ $i = 1, \cdots, m$ are symmetric matrices. The function $\xi(x)$ is a barrier function for the feasible set $\{x : F(x) > 0\}$,

$$\xi(x) \triangleq \begin{cases} \log\det F(x)^{-1} & F(x) > 0 \\ \infty & \text{otherwise.} \end{cases}$$

Definition 3.4.1 (Analytic Center of an LMI)**.** *Define the analytic center, x^*, of the LMI $F(x) > 0$ as*

$$x^* \triangleq \arg\min_x \xi(x).$$

Equivalently,

$$x^* = \arg\max_{F(x)>0} \det F(x).$$

Intuitively, the analytic center is the most feasible point of the set, $\{x : F(x) > 0\}$, in the sense that x^* is the point where the distance from the boundary of $\{x : F(x) > 0\}$ ($\det(F(x))$ is maximum. In the algorithm, at Step 3, we compute the analytic centers of the LMIs to make X_i and X_o close to Y_i^{-1} and Y_o^{-1} respectively. Furthermore, use of the analytic centers causes (Y_i, X_o) and (X_i, Y_i, X_o, Y_o) to be near the most feasible points in the sets $\Phi(\gamma_1)$ and $\Psi(\gamma_2)$, respectively, at each iteration. In Step 3, $ac\{\cdot\}$ denotes the analytic center of the LMI $\{\cdot\}$. For example, (X_{i_k}, X_{o_k}) is the analytic center of the LMI,

$$\begin{aligned}\operatorname{diag}\{&\alpha_k I - Y_{i_k}^{1/2} X_i Y_{i_k}^{1/2},\ Y_{i_k}^{1/2} X_i Y_{i_k}^{1/2} - I, \\ &\beta_k I - X_{o_k}^{1/2} Y_o X_{o_k}^{1/2},\ X_{o_k}^{1/2} Y_o X_{o_k}^{1/2} - I,\ \Phi(\gamma_1),\ \Psi(\gamma_2)\} > 0.\end{aligned}$$

Algorithm(Simultaneous Scaling):

Step 1. Choose parameters $0 < \theta_\lambda < 1$ and $0 < \theta_\gamma < 1$.

Step 2. Let the initial values, $\gamma_1 > 0$ and $\gamma_2 > 0$, be sufficiently large, and find initial values for $X_{i_1}, Y_{i_1}, X_{o_1}$ and Y_{o_1} such that,

$$(Y_{i_1}, X_{o_1}) \in \Phi(\gamma_1) \ \text{ and } \ (X_{i_1}, Y_{i_1}, X_{o_1}, Y_{o_1}) \in \Psi(\gamma_2).$$

Then initialize $k = 1$ and choose α_1 and β_1 such that,

$$\alpha_1 > \lambda_{\max}(X_{i_1} Y_{i_1}) \text{ and } \beta_1 > \lambda_{\max}(X_{o_1} Y_{o_1}).$$

Step 3. Compute the analytic centers,

$$\begin{aligned}(X_{i_k}, X_{o_k}) = ac\{&I < Y_{i_k}^{1/2} X_i Y_{i_k}^{1/2} < \alpha_k I, \\ &I < Y_{o_k}^{1/2} X_o Y_{o_k}^{1/2} < \beta_k I,\ X_o \in \Phi(\gamma_{1_k}), \text{ and } (X_i, X_o) \in \Psi(\gamma_{2_k})\} \\ (Y_{i_{k+1}}, Y_{o_{k+1}}) = ac\{&I < X_{i_k}^{1/2} Y_i X_{i_k}^{1/2} < \alpha_k I, \\ &I < X_{o_k}^{1/2} Y_o X_{o_k}^{1/2} < \beta_k I,\ Y_i \in \Phi(\gamma_{1_k}), \text{ and } (Y_i, Y_o) \in \Psi(\gamma_{2_k})\}\end{aligned}$$

Step 4. If (X_{ik}, X_{ok}) do not yield scaled $C_i(s)$ and scaled $C_j(s)$ which violate the WNC (2.1) and they satisfy the following,

$$(X_{i_k}^{-1}, X_{o_k}) \in \Phi(\gamma_1) \text{ and } (X_{i_k}, X_{i_k}^{-1}, X_{o_k}, X_{o_k}^{-1}) \in \Psi(\gamma_2),$$

or, if (Y_{ik}, Y_{ok}) do not yield scaled $C_i(s)$ and scaled $C_j(s)$ which violate the WNC (2.1) and they satisfy the following,

$$(Y_{i_k}, Y_{o_k}^{-1}) \in \Phi(\gamma_1) \text{ and } (Y_{i_k}^{-1}, Y_{i_k}, Y_{o_k}^{-1}, Y_{o_k}) \in \Psi(\gamma_2),$$

then

$$\gamma_{1_{k+1}} = (1 - \theta_\gamma)\Omega_\phi(X_{o_k}, Y_{i_k}) + \theta_\gamma \gamma_{1_k} \text{ and}$$

$$\gamma_{2_{k+1}} = (1 - \theta_\gamma)\Omega_\psi(X_{i_k}, Y_{i_k}, X_{o_k}, Y_{o_k}) + \theta_\gamma \gamma_{2_k},$$

where

$$\Omega_\phi(X_{o_k}, Y_{i_k}) = \min\{\gamma_1 : \phi(\gamma_1) \geq 0\} \text{ and}$$

$$\Omega_\psi(X_{i_k}, Y_{i_k}, X_{o_k}, Y_{o_k}) = \min\{\gamma_2 : \psi(\gamma_2) \geq 0\}.$$

Otherwise,

$$\alpha_{k+1} = (1 - \theta_\lambda)\lambda_{\max}(X_{i_k} Y_{i_{k+1}}) + \theta_\lambda \alpha_k$$

$$\beta_{k+1} = (1 - \theta_\lambda)\lambda_{\max}(X_{o_k} Y_{o_{k+1}}) + \theta_\lambda \beta_k.$$

Step 5. Stop, if $\alpha_{k+1} - 1 < \epsilon$, $\beta_{k+1} - 1 < \epsilon$, $\gamma_{1k+1} - \gamma_{1k} < \epsilon$ and $\gamma_{2k+1} - \gamma_{2k} < \epsilon$ for small ϵ. Otherwise $k = k + 1$ and go to Step 3.

3.5 Numerical Example

In this section, we provide an example of reducing computational conservatism in controller certification. Consider a state-space representation of a multivariable plant model $\hat{P}(s)$,

$$A_{\hat{P}} = \begin{bmatrix} -1 & 0 & 0 & 0 \\ 0 & -0.5 & 0 & 0 \\ 0 & 0 & -3 & 0 \\ 0 & 0 & 0 & -5 \end{bmatrix}, \; B_{\hat{P}} = \begin{bmatrix} 1 & 0 \\ 2 & 0 \\ 0 & 2 \\ 0 & 1 \end{bmatrix}, C_{\hat{P}} = \begin{bmatrix} 1 & 0 & 1 & 0 \\ 0 & 1.5 & 0 & 1 \end{bmatrix}, \; D_{\hat{P}} = \begin{bmatrix} 0 & 0 \\ 0 & 0 \end{bmatrix}.$$

We choose $\hat{P}$-stabilizing controllers, $C_0(s)$,

$$A_{C_0} = \begin{bmatrix} -1 & 0 \\ 0 & -1 \end{bmatrix}, \; B_{C_0} = \begin{bmatrix} 2 & 0 \\ 0 & 2 \end{bmatrix}, C_{C_0} = \begin{bmatrix} 0.5 & 0.5 \\ 0.5 & 0.5 \end{bmatrix}, \; D_{C_0} = \begin{bmatrix} 0 & 0 \\ 0 & 0 \end{bmatrix}.$$

and $C_1(s)$:

$$A_{C_1} = \begin{bmatrix} -1 & 0 \\ 0 & -1 \end{bmatrix}, \; B_{C_1} = \begin{bmatrix} 1 & 0 \\ 0 & 1 \end{bmatrix}, C_{C_1} = \begin{bmatrix} 0 & 1 \\ 1 & 0 \end{bmatrix}, \; D_{C_1} = \begin{bmatrix} 0.5 & 0 \\ 0 & 0.25 \end{bmatrix}.$$

Let us assume $\omega_n = 0.1$[rad/sec] is a frequency at which we want to investigate the stability margin of the feedback loop of Figure 3.1. Then from $\hat{P}(j\omega_n)$, $C_0(j\omega_n)$, and $C_1(j\omega_n)$, we compute unscaled values,

$$b_{\hat{P},C_0}(j\omega_n) = 0.5495, \quad \text{and} \quad \delta_\nu(C_0, C_1)(j\omega_n) = 0.5407.$$

These numbers allow us to state that C_1 stabilizes $\hat{P}$ but we are unable to provide a guarantee that the stability margin will exceed 0.0088.

3.5.1 Maximize only $b_{\hat{P},C_i}$

At ω_n, a scaled version of (2.16) is,

$$\begin{aligned} &\arcsin \delta_\nu(W_i^{-1}C_iW_o^{-1}, W_i^{-1}C_jW_o^{-1})(j\omega_n) \\ &\qquad < \arcsin b_{W_o\hat{P}W_i, W_i^{-1}C_iW_o^{-1}}(j\omega_n) - \arcsin \alpha. \end{aligned} \tag{3.20}$$

Using the scaling method in Section 3.2.1, we have the following scaling matrices for this example.

$$W_o = \begin{bmatrix} 1.3519 & 1.0086 - 0.0016i \\ 1.0086 + 0.0016i & 1.3073 \end{bmatrix},$$

$$W_i = \begin{bmatrix} 0.2088 & 0.0700 - 0.0025i \\ 0.0700 + 0.0025i & 0.3388 \end{bmatrix}.$$

In this example, the inclusion of the scalings into the $b_{\hat{P},C_0}$ increases, the generalized stability margin from 0.5495 to

$$b_{W_o\hat{P}W_i,W_i^{-1}C_0W_o^{-1}}(j\omega_n) = 0.9964.$$

However the ν-gap metric is also increased by these W_i and W_o from 0.5407 to

$$\delta_\nu(W_i^{-1}C_0W_o^{-1}, W_i^{-1}C_1W_o^{-1})(j\omega_n) = 0.9921.$$

This achieves nothing in terms of extending the guaranteed margin of $T(\hat{P}, C_1)$.

3.5.2 Simultaneous Scaling on $b_{\hat{P},C_i}$ and ν-gap

For the algorithm of Section 3.4.1, we chose the convergence speed parameters, $\theta_\lambda = 0.3$ and $\theta_\gamma = 0.7$. These values were selected after several trial computations to have appropriate convergence of γ_1 and γ_2 in Figure 3.2. We choose the initial values $\gamma_1 = \sqrt{2}\left(b_{\hat{P},C_0}(j\omega_n)\right)^{-1}$, $\gamma_2 = \sqrt{10}\delta_\nu(C_0, C_1)(j\omega_n)$. Then identity matrices are chosen as the initial values of X_i, Y_i, X_o, and Y_o since they satisfy (3.11) and (3.12). Figure 3.3 shows iterates of an upper bound of $\lambda_{\max}(X_iY_i)$ and $\lambda_{\max}(X_oY_o)$, at each iteration from their initial vales, $\alpha_k = \beta_k = 1.5$.

Then using the algorithm in Section 3.4.1, we have

$$X_i \cong Y_i^{-1} = \begin{bmatrix} 0.2954 & -0.0264 - 0.0134i \\ -0.0264 + 0.0134i & 1.3463 \end{bmatrix},$$

$$\lambda(X_iY_i) = 1.00043, 1.00056$$

$$X_o \cong Y_o^{-1} = \begin{bmatrix} 2.2905 & -0.1417 - 0.0398i \\ -0.1417 + 0.0398i & 0.8847 \end{bmatrix},$$

$$\lambda(X_oY_o) = 1.00001, 1.00001$$

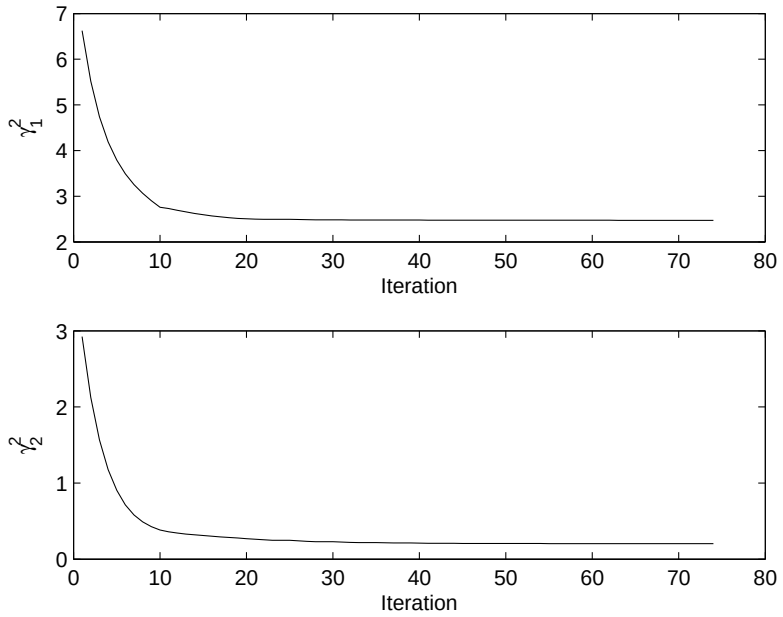

Figure 3.2: a) Achieved objective value of $b_{W_o\hat{P}W_i,W_i^{-1}C_iW_o^{-1}}(j\omega_n)$ b) Achieved objective value of $\delta_\nu(W_i^{-1}C_0W_o^{-1}, W_i^{-1}C_1W_o^{-1})(j\omega_n)$.

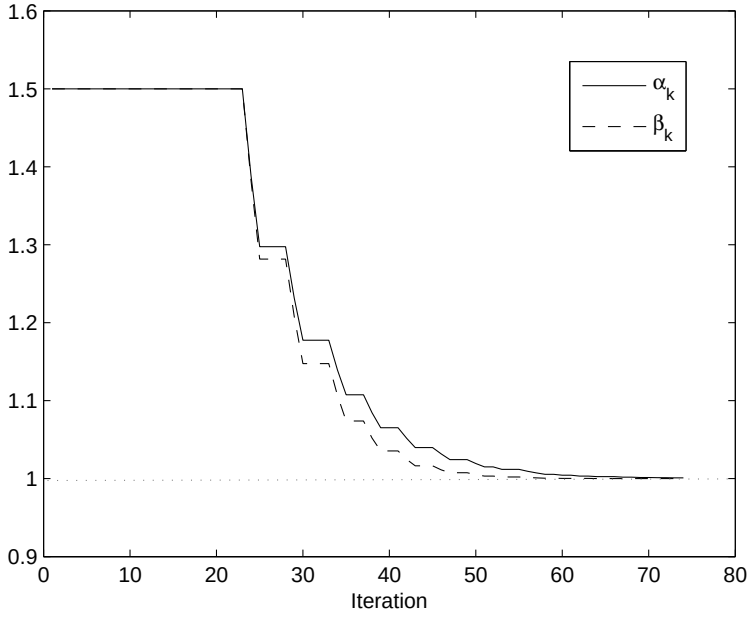

Figure 3.3: The upper bound of $\lambda_{\max}(X_iY_i),\ \alpha_k$, and the upper bound of $\lambda_{\max}(X_oY_o),\ \beta_k$.

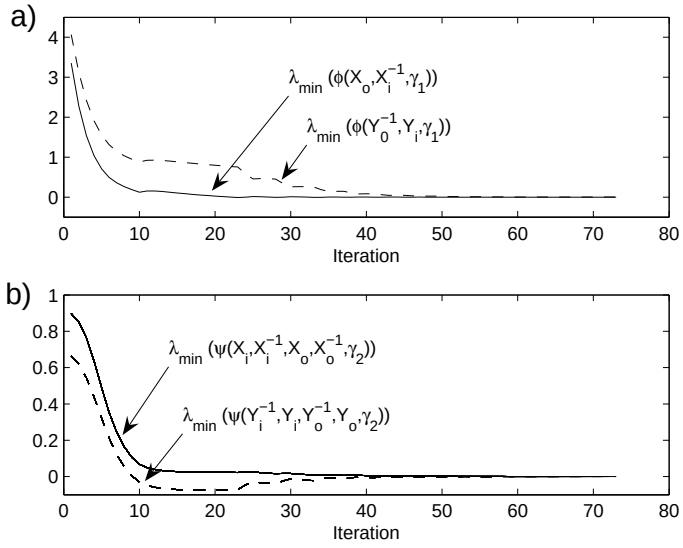

Figure 3.4: Minimum eigenvalues of ϕ in (3.9) and ψ in (3.10).

As shown in Figure 3.4, the proposed algorithm does not guarantee $(X_i^{-1}, X_o) \in \Phi(\gamma_1)$, $(X_i, X_i^{-1}, X_o, X_o^{-1}) \in \Psi(\gamma_2)$, $(Y_i, Y_o^{-1}) \in \Phi(\gamma_1)$ or $(Y_i^{-1}, Y_i, Y_o^{-1}, Y_o) \in \Psi(\gamma_2)$. The algorithm is supposed to guarantee only $(Y_i, X_o) \in \Phi(\gamma_1)$ and $(X_i, Y_i, X_o, Y_o) \in \Psi(\gamma_2)$. Thus once the algorithm stops, we need to decide whether to use X_i or Y_i for W_i and X_o or Y_o for W_o. For instance if $(X_i, X_i^{-1}, X_o, X_o^{-1}) \notin \Psi(\gamma_2)$, in other words, the minimum eigenvalue of $\psi(X_i, X_i^{-1}, X_o, X_o^{-1}, \gamma_2)$ is not positive then only Y_i and Y_o can be used to compute W_i and W_o respectively. For this specific example, we used Y_i and Y_o for computation of

$$b_{W_o \hat{P} W_i, W_i^{-1} C_0 W_o^{-1}}(j\omega_n) = 0.6362,$$

and

$$\delta_\nu(W_i^{-1} C_0 W_o^{-1}, W_i^{-1} C_1 W_o^{-1})(j\omega_n) = 0.4521.$$

Table 3.1 shows guaranteed $b_{\hat{P}, C_1}$ is improved by the simultaneous scaling. This shows choice of appropriate input/output scaling matrices may increase a number of certifiable controllers with the same choice of controller for margin test.

In this example, WNC (2.1) in Step 4 of Section 3.4.1 was never violated throughout the entire iteration. Indeed Steele and Vinnicombe in Chapter 4 of (Fielding, Varga, Bennani & Selier 2002), without considering WNC (2.1), investigated only the

Table 3.1: Scaling methods and the minimal attainable margin levels of $b_{\hat{P},C_1}$ at $\omega_n = 0.1$.

Scaling	$b_{\hat{P},C_0}$	$\delta_\nu(C_0, C_1)$	$b_{\hat{P},C_1}$ $\left(> \sin(\arcsin b_{\hat{P},C_0} - \arcsin \delta_\nu(C_0, C_1))\right)$
Without	0.5495	0.5407	> 0.0105
$b^{-1}_{\hat{P},C_0}$ only	0.9964	0.9921	> 0.0409
$b^{-1}_{\hat{P},C_0}$ and $\delta_\nu(C_0, C_1)$	0.6362	0.4521	> 0.2188

maximum of κ value for two scaled transfer functions in (3.14) at a specific frequency in lieu of the ν-gap metric.

3.6 Conclusions

We investigated the effects of scaling on the stability margin computation in controller certification. The input/output scaling effect on $b_{\hat{P},C_i}$ computation may reduce the conservatism in the $b_{\hat{P},C}$. However the use of scaling matrices without carefully considering how W_o and W_i will alter the ν-gap metric could unfavorably affect the controller certification. We proposed simultaneous scaling on $b_{\hat{P},C_i}$ and the ν-gap so that we can achieve an efficient controller certification. An area of further work is bi-stable and bi-proper transfer function matrices interpolating the set of frequency points, $\{\omega_n\}$.

This chapter is in part a reprint of the materials as is appears in,

Jisang Park, Robert R. Bitmead - *Simultaneous Scaling for MIMO Controller Certification*, Automatica, submitted, Oct. 2007.

Jisang Park, Robert R. Bitmead - *Simultaneous Scaling for MIMO Controller Certification*, 46th IEEE Conference on Decision and Control in New Orleans, LA, USA, Dec, 2007. pp. 4409–4414

The dissertation author was the primary author and the co-author listed in these publications directed and supervised the research.

4

Estimation of the Generalized Stability Margin

4.1 Introduction

Estimating the generalized stability margin with an accurate error bound has significant impact on controller certification. In Chapter 2, we introduced the stability inference inequality,

$$\arcsin b_{P,C_2} \geq \arcsin b_{P,C_1} - \arcsin \delta_\nu(C_1, C_2).$$

As shown in the above inequality, the inferred stability margin of controller C_2 relies on the estimated value of b_{P,C_1} and the computed value $\delta_\nu(C_1, C_2)$. At a fixed frequency point, we analyze an error bound of the generalized stability margin as the infinity norm of the MIMO empirical transfer function estimate (ETFE). We also provide, by interpolating the error bound between any two frequency points, the upper bound of error on a continuous frequency interval. Input signal design to reduce the error on the estimate is also studied. We suggest running the system for a certain length of time prior to recording of each output data set. The assured upper bound of estimation error can be tuned by the amount of the pre-experiment.

A scalar linear time invariant process is given by

$$y(t) = \sum_{n=0}^{\infty} g(n)u(t-n) + v(t) = G(z)u(t) + v(t) \tag{4.1}$$

where $y(t)$ is the observed output, $u(t)$ is the input, $v(t)$ is the disturbance that is uncorrelated with $u(t)$, and $g(n)$ is the impulse response of the exponentially stable transfer function,

$$G(z) = \sum_{n=0}^{\infty} g(n) z^{-n}. \tag{4.2}$$

Consider the N-point of experimental data record, $\{u(0), u(1), \cdots, u(N-1)\}$. Then the function U_N^l is defined as,

$$U_N^l = \frac{1}{\sqrt{N}} \sum_{t=0}^{N-1} u(t) e^{-j\frac{2\pi l}{N}t}, \tag{4.3}$$

with $l = 0, 1, \cdots, N-1$ forming the discrete Fourier transform (DFT) of the finite input sequence. By the inverse DFT, we can obtain time domain sequence $u(t)$, $t = 0, 1, \cdots, N-1$,

$$u(t) = \frac{1}{\sqrt{N}} \sum_{l=0}^{N-1} U_N^l e^{j\frac{2\pi l}{N}t}. \tag{4.4}$$

Fourier analysis leads us to the definition of the *periodogram*, the squared magnitude of $U_N(\omega)$,

$$|U_N(\omega)|^2.$$

Indeed the periodogram is an estimate of the power at frequency ω by filtering the data with a bandpass filter (Kay 1988). Through Parseval's theorem,

$$\sum_{k=0}^{N-1} |U_N(2\pi k/N)|^2 = \sum_{t=0}^{N-1} u(t)^2,$$

we can see clearly that, at a specific frequency $\omega = 2\pi k/N$, the periodogram is one component of the total energy of the signal $u(t)$ $t = 0, 1, \cdots, N-1$. It is observed that if $u(t)$ is zero mean white Gaussian noise, even though the average value of the periodogram of random data converges to the true value as the data record length increases, the variance of the periodogram of random signal is a constant no matter how many data might be taken into the computation. If it is the case that we have random data sequences, we may resort to the averaged periodogram to estimate the frequency response. Ljung (Ljung 1985, Ljung 1999) introduced the notation of the Empirical Transfer Function Estimation (ETFE) as an estimate of transfer function,

$$\widehat{G}(e^{j\frac{2\pi l}{N}}) = \frac{Y_N^l}{U_N^l}.$$

The accuracy of this estimate of the frequency response function has been studied by several researchers (Ljung 1999, Broersen 2004, Pintelon & Schoukens 2001, de Vries 1994). Broersen (Broersen 2004) provided formulations for bias and variance error of the ETFE with a stochastic input. He showed that the bias error could be eliminated by employing a periodic input. In the next section, we will show that, to remove the bias error from the frequency response estimation, an infinite length of data records must be used in the DFT computation. Pintelon and Schoukens (Pintelon & Schoukens 2001) quantified the bias and variance errors of the frequency response estimation due to correlated input/output errors. De Vries (de Vries 1994) suggested running a feedback system for a specific length of time prior to recording the input and output data to reduce the error due to unknown past inputs. In de Vries' analysis, he introduced a partly periodic signal which is a signal that has a duplication of the last part of the input at the first part. He extended the error analysis to MIMO estimation by using multiple of the channel-by-channel SISO error analyses and that correspondingly many error bounds. De Vries's MIMO error bound cannot be used in our framework directly since the generalized stability margin is a scalar representation of matrix property. Hence our need is a representation of MIMO frequency response error in a scalar. Differently from de Vries' MIMO error analysis, in this dissertation, we provide a single scalar value as the MIMO error bound.

4.2 Error Analysis of ETFE

In general, the following relationship does not hold.

$$Y_N^l = G(e^{j\frac{2\pi l}{N}})U_N^l + V_N^l, \tag{4.5}$$

where $Y_N(\omega)$, $U_N(\omega)$, and $V_N(\omega)$ are the M-point DFTs of $y(k)$, $u(k)$, and $v(k)$ respectively. Instead of (4.5), we should consider,

$$Y_N^l = G(e^{j\frac{2\pi l}{N}})U_N^l + R_N^l + V_N^l. \tag{4.6}$$

In this section, we will identify the term, R_N^l, formulate a bound on R_N^l and suggest an appropriate input signal to maintain the size error due to R_N^l. Another error source in

(4.6) is noise, $v(t)$, over which we do not have control. From (4.1) with the definition of the DFT, we have

$$\begin{aligned} Y_N^l &= \frac{1}{\sqrt{N}} \sum_{t=0}^{N-1} \left(G(z)u(t) + v(t)\right) e^{-j\frac{2\pi l}{N}t} \\ &= \frac{1}{\sqrt{N}} \sum_{t=0}^{N-1} \sum_{k=0}^{\infty} g(k) e^{-j\frac{2\pi l}{N}t} u(t-k) + V_N^l \end{aligned} \tag{4.7}$$

Using the change of variables, $\tau = t - k$.

$$\begin{aligned} Y_N^l &= \sum_{k=0}^{\infty} g(k) e^{-j\frac{2\pi l}{N}k} \cdot \frac{1}{\sqrt{N}} \sum_{\tau=-k}^{N-1-k} u(\tau) e^{-j\frac{2\pi l}{N}\tau} + V_N^l \\ &= \sum_{k=0}^{\infty} g(k) e^{-j\omega k} \cdot \left(U_N^l + \frac{1}{\sqrt{N}} \sum_{\tau=-k}^{N-1-k} u(\tau) e^{-j\frac{2\pi l}{N}\tau} - U_N^l \right) + V_N^l \\ &= G(e^{j\frac{2\pi l}{N}}) U_N^l + \sum_{k=0}^{\infty} g(k) e^{-j\frac{2\pi l}{N}k} \cdot \left(\frac{1}{\sqrt{N}} \sum_{\tau=-k}^{N-1-k} u(\tau) e^{-j\frac{2\pi l}{N}\tau} - U_N^l \right) + V_N^l. \end{aligned} \tag{4.8}$$

Then we define the residual error in (4.8) as the bias error, R_N^l,

$$R_N^l \triangleq \sum_{k=0}^{\infty} g(k) e^{-j\omega k} \cdot \left(\frac{1}{\sqrt{N}} \sum_{\tau=-k}^{N-1-k} u(\tau) e^{-j\omega\tau} - U_N^l \right)$$

Then bias error term, R_N^l can be rewritten as following,

$$\begin{aligned} R_N^l &= \sum_{k=0}^{\infty} g(k) e^{-j\frac{2\pi l}{N}k} \cdot \left(\frac{1}{\sqrt{N}} \sum_{\tau=-k}^{N-1-k} u(\tau) e^{-j\frac{2\pi l}{N}\tau} - \frac{1}{\sqrt{N}} \sum_{\tau=0}^{N-1} u(\tau) e^{-j\frac{2\pi l}{N}\tau} \right) \\ &= \sum_{k=0}^{\infty} g(k) e^{-j\frac{2\pi l}{N}k} \cdot \frac{1}{\sqrt{N}} \left(\sum_{\tau=-k}^{-1} u(\tau) e^{-j\frac{2\pi l}{N}\tau} - \sum_{\tau=N-k}^{N-1} u(\tau) e^{-j\frac{2\pi l}{N}\tau} \right) \\ &= \sum_{k=0}^{\infty} g(k) e^{-j\frac{2\pi l}{N}k} \cdot \frac{1}{\sqrt{N}} \left(\sum_{\tau=-k}^{-1} u(\tau) e^{-j\frac{2\pi l}{N}\tau} - \sum_{\tau=-k}^{-1} u(\tau+N) e^{-j\frac{2\pi l}{N}\tau} \right) \\ &= \sum_{k=0}^{\infty} g(k) e^{-j\frac{2\pi l}{N}k} \cdot \frac{1}{\sqrt{N}} \sum_{\tau=-k}^{-1} \left(u(\tau) - u(\tau+N) \right) e^{-j\frac{2\pi l}{N}\tau} \end{aligned} \tag{4.9}$$

From (4.9), we can recognize the bias error stems from the discrepancy between inputs $u(t)$ and $u(t+n)$ for $t \in [-\infty, -1]$. The DFT allows us to analyze frequency domain information contents from finite duration of time domain signal. The residual error is inevitable due to using a finite amount of data for computing the DFT in the estimation of the frequency response of $G(z)$. The DFT is calculated from a finite length data record but exact $G(e^{j\omega})$ would require knowledge of an infinite input sequence,

Broersen (Broersen 2004) mentioned that if $u(t)$ is a periodic input with period N, then $R_N^l = 0$. As shown, in (4.9), if $u(\tau)$ approaches to $u(\tau+N)$ for all $\tau \in [-\infty, -1]$, the bias error R_N^l approach to zero. Thus, as we mentioned earlier in this section, the bias error may not be removed completely from the estimation of the frequency response of $G(e^{j\frac{2\pi l}{N}})$ unless we have run the system with a periodic input signal from the infinite past. Of course, if the system's unforced response decays in the finite times, then an infinitely long periodic input signal would not be necessary to make R_N^l zero. We will use the property of a finite decay rate of the impulse response of the plant in designing a useful input signal for estimating the frequency response of $G(z)$ at $\omega = \frac{2\pi l}{N}$ with a manageable error.

4.2.1 Standard Test Signal

In this section, we will define a scalar probing signal for the error analysis and the excitation signal design in this chapter.

Definition 4.2.1 (The Standard Test Signal, $u(t)$)**.** *Consider a scalar signal, $u(t)$, for $t \in [-N_r, N-1]$ with integers N_r and N ($N_r \geq 0$ and $N > 1$). If $u(t)$ has following properties,*

1) frequency domain components: $U_N^l \neq 0$ for $k_1 \leq l \leq k_2$, where k_1, k_2 are integers,

2) time domain components: for $t \in [-N_r, -1]$,

$$u(t) = u(t+N). \tag{4.10}$$

then $u(t)$ is defined as the standard test signal.

In definition 4.2.1, the first property is the requirement on assurance of the ETFE computation within a fixed frequency range. In the second property, the integer N_r can be understood as the number of sample times while the output, $y(t)$, is not recorded yet. After N_r samples of waiting, the recording of output $y(t)$ starts. Then the each of DFT of $y(t)$ and $u(t)$ is computed from the output and input data collected for $t \in [0, N-1]$ respectively. We call the operation of feedback-loop for $t \in [-N_r, -1]$ as a *pre-experiment*. The purpose of this pre-experiments can be explained as a way of reducing the initial

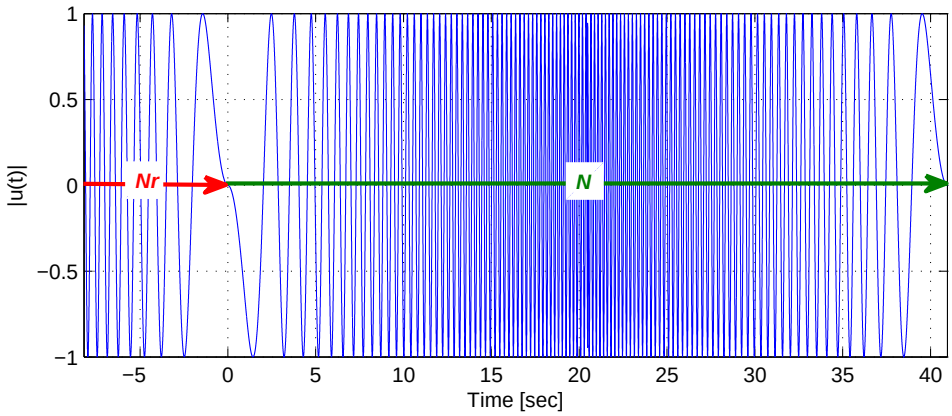

Figure 4.1: Implementation of the standard test signal.

condition from previous unknown operation. Figure 4.1 shows an implementation of the standard test signal. To satisfy the first property in Definition 4.2.1, the chirp up and down signal is chosen as $u(t)$ and it has the pre-experiment part in $t \in [-N_r, -1]$.

4.2.2 SISO Error Bound: Pre-experiment Analysis

Formulating (4.9) does not require any *a priori* information on the system. The residual error is directly derived from an LTI system only using the definition of the DFT. Since no assumption on the system is used in (4.9), it can be applied to any LTI system. However it is not obvious how to derive a bound on the residual error, (4.9). In this section, we will provide an error bound of the frequency response of a SISO transfer function $G(e^{j\frac{2\pi l}{N}})$ by employing a pre-experiment by running the system with an input before the recording (i.e. $t < 0$) of data for the DFT. In this section we will assume use of the standard test signal and show the connection between the length of the pre-experiment and the bound on the bias error. Note that the output is in the form of an infinite summation, (4.1).

Theorem 4.2.1. *Consider the measured output sequence, $y(t)$ for $t \in [0, N-1]$, given by (4.1),*

$$y(t) = \sum_{n=0}^{\infty} g(n)u(t-n) + v(t),$$

with the standard test signal, $u(t)$, for $t \in [-N_r, N-1]$. Define the N-point DFTs for

$l = 0, \cdots, N-1$

$$\begin{aligned} U_N^l =& \frac{1}{\sqrt{N}} \sum_{t=0}^{N-1} u(t) e^{-j\frac{2\pi l}{N}t} \\ Y_N^l =& \frac{1}{\sqrt{N}} \sum_{t=0}^{N-1} y(t) e^{-j\frac{2\pi l}{N}t} \\ V_N^l =& \frac{1}{\sqrt{N}} \sum_{t=0}^{N-1} v(t) e^{-j\frac{2\pi l}{N}t} \end{aligned} \tag{4.11}$$

and assume $U_N^l \neq 0$. *Assume we are given a bound on the impulse response,* $g(k)$,

$$|g(k)| \leq M\rho^k,$$

with $M > 0$ *and* $0 < \rho < 1$ *and a bound* $\overline{V}_N^l$ *on* V_N^l. *Assume there exists a bound on input* $u(t)$,

$$|u(t)| \leq \begin{cases} \overline{u} & \text{for } t < -N_r \\ u^{\max} & \text{for } t \in [0, N-1] \end{cases}.$$

Denote the empirical transfer function estimate of $G\left(e^{j\frac{2\pi l}{N}}\right)$,

$$\widehat{G}\left(e^{j\frac{2\pi l}{N}}\right) = \frac{Y_N^l}{U_N^l}.$$

Then the following error bound is satisfied

$$\begin{aligned} &\left| G\left(e^{j\frac{2\pi l}{N}}\right) - \widehat{G}\left(e^{j\frac{2\pi l}{N}}\right) \right| \\ &\qquad \leq \frac{1}{\sqrt{N}|U_N^l|} \left(u^{\max} + \overline{u}\right) \frac{M\rho^2}{(1-\rho)^2} \rho^{N_r}(1-\rho^N) + \frac{\overline{V}_N^l}{|U_N^l|}. \end{aligned} \tag{4.12}$$

Proof. See Appendix 4.7.1. □

4.2.3 Guidance on SISO ETFE estimation

Energy in U_N^l

To find the frequency where b_{P,C_i} is achieved, iterative experiments may be required. Initially, the input signal should have a wide bandwidth so that the resultant ETFE can show at least a rudimentary range of frequencies where the peak value of magnitude of the ETFE might exist. The use of a periodic swept-sine wave is recommended, since periodicity is also required. In addition, at the early stage, the constant $|U_N^l|$ over

$l = 0, 1, \cdots, N-1$ can be used in an experiment for ETFE with roughly fixed signal to noise ratio(SNR). After having a crude range of frequencies where the peak value of b_{P,C_i} estimate exists, a narrower bandwidth can be used to refine the frequency range of the input signal. The magnitude of $|U_N^l|$ can be increased in a certain frequency range to improve the SNR. The first term in the right hand side of (4.12) represents a bound on the bias error and the second term indicates a bound on the estimate error due to noise. By increasing $|U_N^l|$, in (4.12), both errors can be decreased at the frequency $\omega = \frac{2\pi l}{N}$.

Length of Pre-experiment, N_r

One could imagine selecting N_r so as to maintain the first term on the right hand side of (4.12) roughly equal to the second term, thereby keeping the systematic error bound approximately equal to the noise error bound. For a smaller estimate error bound in (4.12), we need to keep the number of pre-excitation samples large since the error bound (4.12) decreases geometrically with N_r.

Downsampling

The second term of the right hand side of (4.12) is due to the additive measurement noise, $v(t)$. Downsampling is one remedy of limiting the noise effect. The following simple relationship shows that down a smpling is equivalent to increasing the energy in the DFT of the input signal. For $l = 0, \cdots, N-1$,

$$|U_{rN}^{rl}| = \sqrt{r}|U_N^l|$$

where r is an integer, and assume $u(t)$ in N-periodic. Thus the DFT of r periods of a periodic signal is $\sqrt{r}$ times larger than the DFT of one period of $u(t)$. However, downsampling decreases the number of data points in the DFT computations, which results an increase of the first term of the right hand side of(4.12). In Appendix 4.7.3, we prove Theorem 4.7.1 that shows the equivalence between downsampling and averaging.

4.2.4 MIMO Error Bound

A causal q-input p-output process is given by

$$\vec{y}(t) = \sum_{n=0}^{\infty} H(n)\vec{u}(t-n) + \vec{v}(t) = \mathbb{G}(z)\vec{u}(t) + \vec{v}(t)$$

where $\vec{y}(t)$ is the $p \times 1$ observed output signal vector, $\vec{u}(t)$ is the $q \times 1$ observed input signal vector, $\vec{v}(t)$ is $p \times 1$ output noise vector, and $H(n)$ is the $p \times q$ impulse response matrix,

$$H(n) = \begin{bmatrix} h_{11}(n) & h_{12}(n) & \cdots & h_{1q}(n) \\ h_{21}(n) & h_{22}(n) & \cdots & h_{2q}(n) \\ \vdots & \vdots & \cdots & \vdots \\ h_{p1}(n) & h_{p2}(n) & \cdots & h_{pq}(n) \end{bmatrix},$$

where $h_{ij}(n)$ is the impulse response from the j-th input to the i-th output, with the exponentially stable transfer function matrix

$$\mathbb{G}(z) = \sum_{n=0}^{\infty} H(n) z^{-n}. \tag{4.13}$$

The next theorem extends the result of Theorem 4.2.1 to a error bound for a MIMO system.

Theorem 4.2.2. *Consider the p-output, q-input Linear MIMO system*

$$\vec{y}(t) = \sum_{n=0}^{\infty} H(n)\vec{u}(t-n) + \vec{v}(t), \tag{4.14}$$

and the standard test signal, $u(t)$ for $t \in [-N_r, N-1]$. Define the N-point DFT

$$U_N^l = \frac{1}{\sqrt{N}} \sum_{t=0}^{N-1} u(t) e^{-j\frac{2\pi l}{N}t}, \quad l = 0, 1, \cdots, N-1.$$

Next consider q distinct experiments with vector input signals,

$$\vec{u}_i(t) = \vec{q}_i u(t), \quad t \in [-N_r, N-1]$$

and the corresponding output measurements,

$$\vec{y}_i(t), \quad t \in [0, N-1]$$

Define: the $q \times q$ matrix,

$$Q = [\vec{q}_1, \vec{q}_2, \cdots, \vec{q}_q],$$

the N-point vector DFTs, for $l = 0, \cdots, N-1$, $i = 1, \cdots, q$

$$\begin{aligned}
\vec{Y}_{Ni}^{l} =& \frac{1}{\sqrt{N}} \sum_{t=0}^{N-1} \vec{y}_i(t) e^{-j\frac{2\pi l}{N}t}, \\
\vec{U}_{Ni}^{l} =& \frac{1}{\sqrt{N}} \sum_{t=0}^{N-1} \vec{u}_i(t) e^{-j\frac{2\pi l}{N}t} = \vec{q}_i U_N^l, \\
\vec{V}_{Ni}^{l} =& \frac{1}{\sqrt{N}} \sum_{t=0}^{N-1} \vec{v}_i(t) e^{-j\frac{2\pi l}{N}t}.
\end{aligned} \tag{4.15}$$

Consider the matrices,

$$\begin{aligned}
\mathbb{Y}_N^l &\triangleq \left[\vec{Y}_{N1}^{l}, \vec{Y}_{N2}^{l}, \cdots, \vec{Y}_{Nq}^{l}\right] \in \mathbb{C}^{p\times q} \\
\mathbb{U}_N^l &\triangleq \left[\vec{U}_{N1}^{l}, \vec{U}_{N2}^{l}, \cdots, \vec{U}_{Nq}^{l}\right] \in \mathbb{C}^{q\times q} = QU_N^l \\
\mathbb{V}_N^l &\triangleq \left[\vec{V}_{N1}^{l}, \vec{V}_{N2}^{l}, \cdots, \vec{V}_{Nq}^{l}\right] \in \mathbb{C}^{p\times q}
\end{aligned} \tag{4.16}$$

Assume the following,

- $U_N^l \neq 0$ *for* $l = 0, \cdots, N-1$.
- *Bounds on the test function are known*

$$|u(t)| \leq \begin{cases} \overline{u} & \text{for } t < -N_r \\ u^{\max} & \text{for } t \in [0, N-1] \end{cases}.$$

- $\overline{\sigma}(Q)$ *is bounded and* Q *is invertible*
- *A bound on the maximum singular value of the impulse response matrices,* $H(n)$*, is given,*

$$\overline{\sigma}(H(n)) \leq \tilde{M}\tilde{\rho}^n, \tag{4.17}$$

  with $\tilde{M} > 0$ *and* $0 < \tilde{\rho} < 1$*, and* $n \geq 0$.

- *A bound on the maximum singular value of the matrix of the N-point DFT* $\mathbb{V}_N^l$ *of the noise* $v(t)$*,*

$$\overline{\sigma}(\mathbb{V}_N^l) \leq \overline{V}_N^l.$$

Define the MIMO ETFE as

$$\widehat{\mathbb{G}}\left(e^{j\frac{2\pi l}{N}}\right) = \mathbb{Y}_N^l (\mathbb{U}_N^l)^{-1} = \frac{1}{U_N^l} \mathbb{Y}_N^l Q^{-1}. \tag{4.18}$$

Then the following error bound is satisfied

$$\begin{aligned}\overline{\sigma}\left(\mathbb{G}\left(e^{j\frac{2\pi l}{N}}\right)-\widehat{\mathbb{G}}\left(e^{j\frac{2\pi l}{N}}\right)\right)\\ \leq\frac{1}{\sqrt{N}|U_N^l|}\frac{\overline{\sigma}(Q)}{\underline{\sigma}(Q)}\left(u^{\max}+\overline{u}\right)\frac{\tilde{M}\tilde{\rho}^2}{(1-\tilde{\rho})^2}\tilde{\rho}^{N_r}(1-\tilde{\rho}^N)+\frac{\overline{V}_N^l}{\underline{\sigma}(Q)|U_N^l|}.\end{aligned} \tag{4.19}$$

Proof. See Appendix 4.7.2. □

As in the SISO ETFE error bound given by (4.12), the MIMO ETFE error bound (4.19) can also be tuned with energy in U_N^l and the number of samples of the periodic pre-excitation, N_r. Furthermore, the bias error in MIMO ETFE is affected by the condition number of the matrix Q.

4.2.5 Interpolating the Error Bounds

At fixed frequencies, $\omega = \frac{2\pi l}{N}$, $l = 0, \cdots, N-1$, (4.12) and (4.19) provide the error bounds on the ETFE. These bounds apply to the ETFE at the frequency points only. In order to bound excursions of $G(e^{j\omega}$ between these points, we require a farther bound on the inter-frequency interpolation. The next proposition provides a bound on error between the fixed frequency points.

Proposition 4.2.1. *Consider a stable transfer function matrix given by (4.13),*

$$\mathbb{G}(e^{j\omega}) = \sum_{n=0}^{\infty} H(n)e^{-j\omega n}.$$

Assume that a bound on the maximum singular value of the impulse response matrix, $H(n)$, as in (4.17),

$$\overline{\sigma}(H(n)) \leq \tilde{M}\tilde{\rho}^n,$$

with $\tilde{M} > 0$ and $0 < \tilde{\rho} < 1$, and $n \geq 0$. Then

$$\overline{\sigma}\left(\mathbb{G}\left(e^{j\frac{2\pi(l+r)}{N}}\right)-\mathbb{G}\left(e^{j\frac{2\pi l}{N}}\right)\right) \leq \frac{\tilde{M}\tilde{\rho}}{(1-\tilde{\rho})^2}\frac{\pi}{N} \tag{4.20}$$

with $l = 0, 1, \cdots, N-1$ and $-\frac{1}{2} \leq r \leq \frac{1}{2}$.

Proof.

$$\begin{aligned}\frac{d\mathbb{G}(e^{j\omega})}{d\omega} &= \sum_{n=0}^{\infty}(-jn)H(n)e^{-j\omega n}\\ &\leq \sum_{n=0}^{\infty} n\overline{\sigma}(H(n))\\ &= \frac{\tilde{M}\tilde{\rho}}{(1-\tilde{\rho})^2}\end{aligned}$$

From the Taylor series,

$$\mathbb{G}\left(e^{j\frac{2\pi(l+r)}{N}}\right) = \mathbb{G}\left(e^{j\frac{2\pi l}{N}}\right) + \frac{d\mathbb{G}(e^{j\omega})}{d\omega}\left(\frac{2\pi r}{N}\right),$$

where the second term of the right hand side of the equation is the remainder term of the truncated Taylor series. □

The next theorem provides an error bound on the frequency response function between a MIMO ETFE and the true value of the frequency response.

Corollary 4.2.1. *Consider a stable transfer function matrix as given in (4.13),*

$$\mathbb{G}(z) = \sum_{n=0}^{\infty} H(n)z^{-n},$$

and the ETFE of $\mathbb{G}(e^{j\omega})$ *of (4.18) with* $l = 0, 1, \cdots, N-1$

$$\widehat{\mathbb{G}}\left(e^{j\frac{2\pi l}{N}}\right) = \mathbb{Y}_N^l(\mathbb{U}_N^l)^{-1}.$$

Assume a bound on the maximum singular value of the impulse response matrix, $H(n)$*, as in (4.17),*

$$\overline{\sigma}(H(n)) \leq \tilde{M}\tilde{\rho}^n,$$

with $\tilde{M} > 0$ *and* $0 < \tilde{\rho} < 1$*, and* $n \geq 0$*. Then*

$$\begin{aligned}\overline{\sigma}\left(\mathbb{G}\left(e^{j\frac{2\pi(l+r)}{N}}\right)\right) &\leq \overline{\sigma}\left(\widehat{\mathbb{G}}\left(e^{j\frac{2\pi l}{N}}\right)\right)\\ &+ \frac{\tilde{M}\tilde{\rho}}{(1-\tilde{\rho})^2}\left(\frac{\pi}{N} + \frac{1}{\sqrt{N}|U_N^l|}\frac{\overline{\sigma}(Q)}{\underline{\sigma}(Q)}\left(u^{\max}+\overline{u}\right)\tilde{\rho}^{N_r+1}(1-\tilde{\rho}^N)\right) + \frac{\overline{V}_N^l}{\underline{\sigma}(Q)|U_N^l|}\end{aligned}$$

with $l = 0, 1, \cdots, N-1$ *and* $-\frac{1}{2} \leq r \leq \frac{1}{2}$*. Therefore,*

$$\begin{aligned}\|G(z)\|_\infty \leq \max_l \Bigg\{&\overline{\sigma}\left(\widehat{\mathbb{G}}\left(e^{j\frac{2\pi l}{N}}\right)\right)\\ &+\frac{\tilde{M}\tilde{\rho}}{(1-\tilde{\rho})^2}\left(\frac{\pi}{N} + \frac{1}{\sqrt{N}|U_N^l|}\frac{\overline{\sigma}(Q)}{\underline{\sigma}(Q)}\left(u^{\max}+\overline{u}\right)\tilde{\rho}^{N_r+1}(1-\tilde{\rho}^N)\right) + \frac{\overline{V}_N^l}{\underline{\sigma}(Q)|U_N^l|}\Bigg\}\end{aligned}$$

Proof.

$$\begin{aligned}&\overline{\sigma}\left(\mathbb{G}\left(e^{j\frac{2\pi(l+r)}{N}}\right)-\widehat{\mathbb{G}}\left(e^{j\frac{2\pi l}{N}}\right)\right)\\&\leq\overline{\sigma}\left(\mathbb{G}\left(e^{j\frac{2\pi(l+r)}{N}}\right)-\mathbb{G}\left(e^{j\frac{2\pi l}{N}}\right)\right)+\overline{\sigma}\left(\mathbb{G}\left(e^{j\frac{2\pi l}{N}}\right)-\widehat{\mathbb{G}}\left(e^{j\frac{2\pi l}{N}}\right)\right)\end{aligned}\tag{4.21}$$

The first term in the right hand side of (4.21) is given by (4.19) and the second term is given by (4.20). □

4.3 Error Bound on the Generalized Stability Margin Estimate

The generalized stability margin,

$$b_{P,C}=\|T(P,C)\|_{\infty}^{-1}.$$

As shown in Figure 3.1, $T(P,C)$ is a transfer function matrix from $\vec{u}(t)=\begin{bmatrix}u_1(t)\\u_2(t)\end{bmatrix}$ to $\vec{y}(t)=\begin{bmatrix}y_1(t)\\y_2(t)\end{bmatrix}$. Let us assume $\vec{y}(t)\in\mathbb{R}^{p\times 1}$, $\vec{u}(t)\in\mathbb{R}^{q\times 1}$, then conduct q distinct experiments to collect input output data set then we have,

$$\widehat{T}(P,C,\frac{2\pi l}{N})=\mathbb{Y}_N^l(\mathbb{U}_N^l)^{-1},$$

where $\mathbb{Y}_N^l\in\mathbb{C}^{p\times q}$, $\mathbb{U}_N^l\in\mathbb{C}^{q\times q}$.

Theorem 4.3.1. *Consider the estimate,*

$$\widehat{T}(P,C,\frac{2\pi k}{N})=\mathbb{Y}_N^k(\mathbb{U}_N^k)^{-1}.$$

Then, using Corollary 4.2.1, the estimate of $b_{P,C}$ is given by,

$$b_{P,C}\geq\frac{1}{\max_k\left[\overline{\sigma}\left(\widehat{T}(P,C,\frac{2\pi k}{N})\right)+\Delta T_k\right]},$$

where

$$\Delta T_k=\frac{\tilde{M}\tilde{\rho}}{(1-\tilde{\rho})^2}\left(\frac{\pi}{N}+\frac{1}{\sqrt{N}|U_N^k|}\frac{\overline{\sigma}(Q)}{\underline{\sigma}(Q)}\left(u^{\max}+\overline{u}\right)\tilde{\rho}^{N_r+1}(1-\tilde{\rho}^N)\right)+\frac{\overline{V}_N^k}{\underline{\sigma}(Q)|U_N^k|}.$$

4.4 Excitation Signal Design for Margin Estimation

In this section, we will design specific input vectors for experiments to estimate $\|\widehat{T}(P,C)\|_\infty$ from recorded data set.

4.4.1 Existence of ${\mathbb{U}_N^l}^{-1}$

We defined the MIMO ETFE in the form of (4.18) assuming that the inverse of the matrix DFT, ${\mathbb{U}_N^l}^{-1}$, exists. In our analysis, we form the vector input by multiplying a scalar input signal, $u(t)$, with a vector, $\vec{q}_i$. Therefore, the input design falls into designing of

1) the standard test signal introduced in Definition 4.2.1, $u(t)$, and

2) as many vectors, $\vec{q}_i$, as the number of inputs of the transfer function $\widehat{T}(P,C)$ so that Q has an appropriate condition number.

To have a wide band frequency components, the periodic swept-sine would be an appropriate choice for an input signal. Now the choice of $Q = [\vec{q}_1, \vec{q}_2, \cdots, \vec{q}_q]$ is fairly straightforward. A full rank matrix Q will make the matrix DFT, ${\mathbb{U}_N^l}^{-1}$, invertible. The Hadamard matrix or an identity matrix would be a good choice for Q but any matrix with good condition number would be chosen.

4.4.2 Scaling for Margin Estimation

In Chapter 3, we showed that input and output scaling matrices can reduce conservatism in the generalized stability margin computation. In the estimation of the generalized stability margin, the maximum singular value computations of the MIMO ETFE,

$$\mathbb{Y}_N^l(\mathbb{U}_N^l)^{-1},$$

is also involved at each frequency point $\omega = \frac{2\pi l}{N}$. Constant diagonal scaling matrices will be used in the estimation of the generalized stability margin in the following numerical example.

4.5 Numerical Example

In this numerical example, we estimate the generalized stability margin of a linearized the Modular Aero-Propulsion System Simulation (MAPSS) (Parker & Guo 2003) turbofan jet engine model and controller using input design developed in this chapter.

4.5.1 MAPSS Model

Figure 4.2 shows MAPSS and we will use its linearized version as the target system to be estimated. MAPSS is a Simulink-based turbofan engine simulation of a modern high-pressure ratio, dual-spool, low bypass, variable cycle, military type engine with a digital controller. In Figure 4.2, the two boxes represent the controller and engine components and each consists of a number of sub-modules, e.g., sensors, fan, compressor, combustor, bypass duct, afterburner, and nozzle. The sub-modules include various non-linearities. We extracted a linearized engine model and controller from MAPSS with power lever angle (PLA) of 21 degree, at static sea level operation.

4.5.2 $b_{P,C}$ Estimation for the Linearized MAPSS Model

Consider the following multi input multi output (MIMO) transfer function matrix $T(P,C)$,

$$\vec{y}(t) = T(P,C)\vec{u}(t). \tag{4.22}$$

$T(P,C)$ is 6×6 and each linearized P and C is a 3×3 system, which is extracted from MAPSS. We will use the standard test signal $u(t)$ that has frequency components from DC to 5 Hz. To make $\mathbb{U}_N^l$ invertible, we use the Hadamard matrix,

$$Q = \begin{bmatrix} 1 & 1 & 1 & 1 & 1 & 1 \\ 1 & -1 & 1 & 1 & 1 & 1 \\ 1 & 1 & -1 & 1 & 1 & 1 \\ 1 & 1 & 1 & -1 & 1 & 1 \\ 1 & 1 & 1 & 1 & -1 & 1 \\ 1 & 1 & 1 & 1 & 1 & -1 \end{bmatrix}.$$

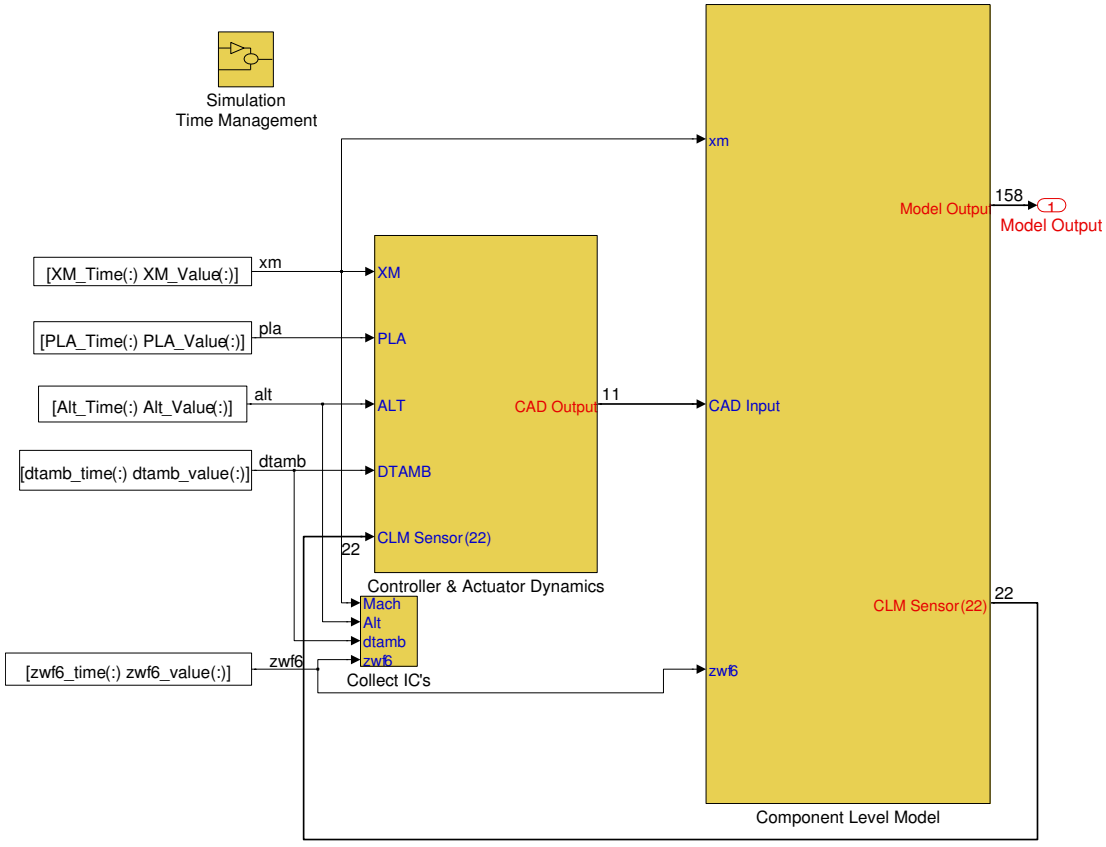

Figure 4.2: Simulink Model of MAPSS.

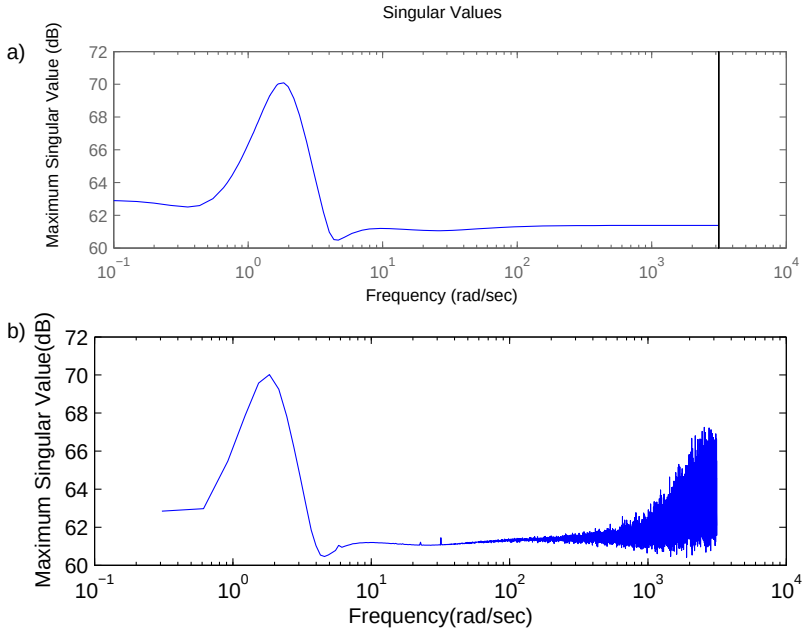

Figure 4.3: The Maximum singular value plot of a) $T(P,C)$ and b) $\widehat{T}(P,C)$.

In this example, since we have 6 inputs, we will perform 6 experiments to collect 6 vector outputs so that we have

$$\begin{aligned}
&[\vec{y}_1(t),\ \vec{y}_2(t),\ \vec{y}_3(t),\ \vec{y}_4(t),\ \vec{y}_5(t),\ \vec{y}_6(t)] \\
&= T(P,C)\ [\vec{u}_1(t),\ \vec{u}_2(t),\ \vec{u}_3(t),\ \vec{u}_4(t),\ \vec{u}_5(t),\ \vec{u}_6(t)] \\
&= T(P,C)\ Qu(t).
\end{aligned}$$

Then the matrix DFT, $\mathbb{Y}_N^l$ and the invertible matrix DFT $\mathbb{U}_N^l$, can be constructed. Here we will perform six consecutive experiments and before each experiment, we will exercise the pre-experiments. In this example, measurement noise is added at each channel and at each experiment. Figure 4.3 a shows the maximum singular value plot at each frequency point of $T(P,C)$ with $\|T(P,C)\|_\infty = 70.0884$ dB at $\omega = 1.8406$ rad/sec. We obtain an estimate of $\|\widehat{T}(P,C)\|_\infty$ from the following relationship,

$$\widehat{T}\left(e^{j\frac{2\pi l}{N}}\right) = \mathbb{Y}_N^l(\mathbb{U}_N^l)^{-1},$$

and Figure 4.3 b shows $\|\widehat{T}(P,C)\|_\infty = 70.0195$ dB at $\omega = 1.8408$ rad/sec.

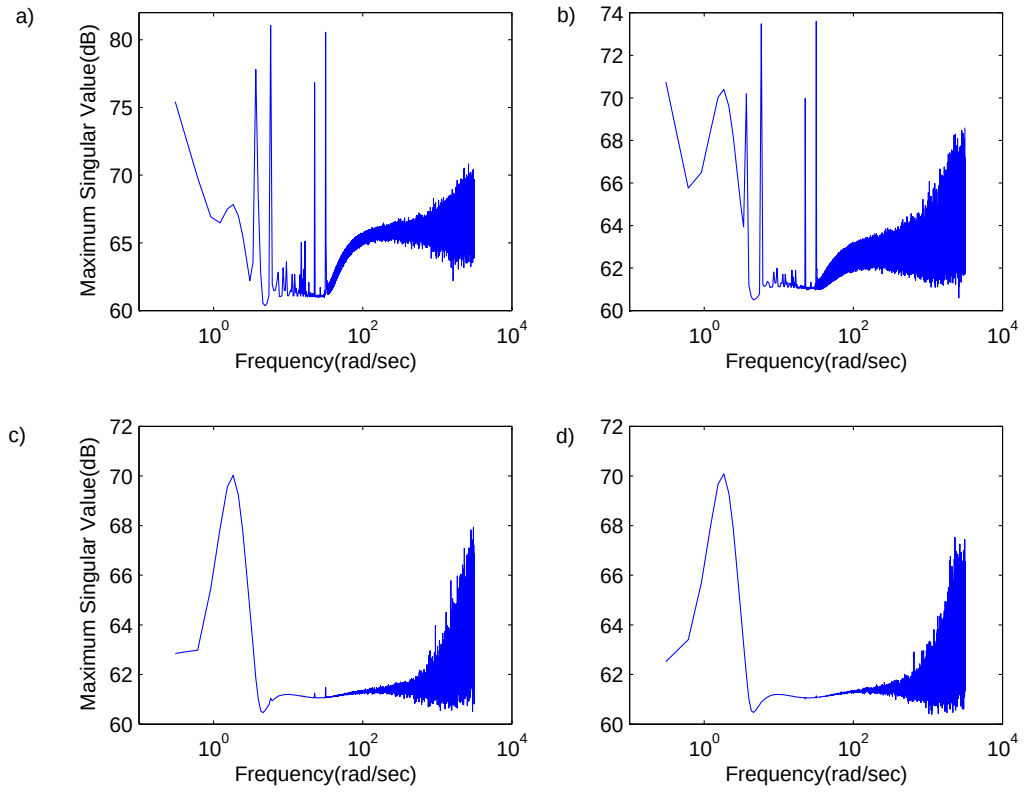

Figure 4.4: Effects of length of pre-experiments: a) No pre-experiments b) $\frac{1}{32}$ of input c) $\frac{1}{10}$ of input d) $\frac{1}{2}$ of input.

4.5.3 Pre-experiments

We will observe the effects of pre-experiments on the estimated $\|\widehat{T}(P,C)\|_\infty$. Figure 4.4 a to d show $\overline{\sigma}(\widehat{T}(P,C)(j\omega))$ with different lengths of pre-experiment. In Figure 4.4 a, we injected six consecutive vector inputs into $T(P,C)$ without pre-experiments and we see the estimation is greatly affected by the initial conditions from the previous experiment. Then we performed the pre-experiment before recording each output vector. We increased the length of pre-experiments by $\frac{1}{32}$, $\frac{1}{10}$, and $\frac{1}{2}$ the length of the input signal at Figure 4.4 b, c, and d, respectively. The estimation results are as follows.

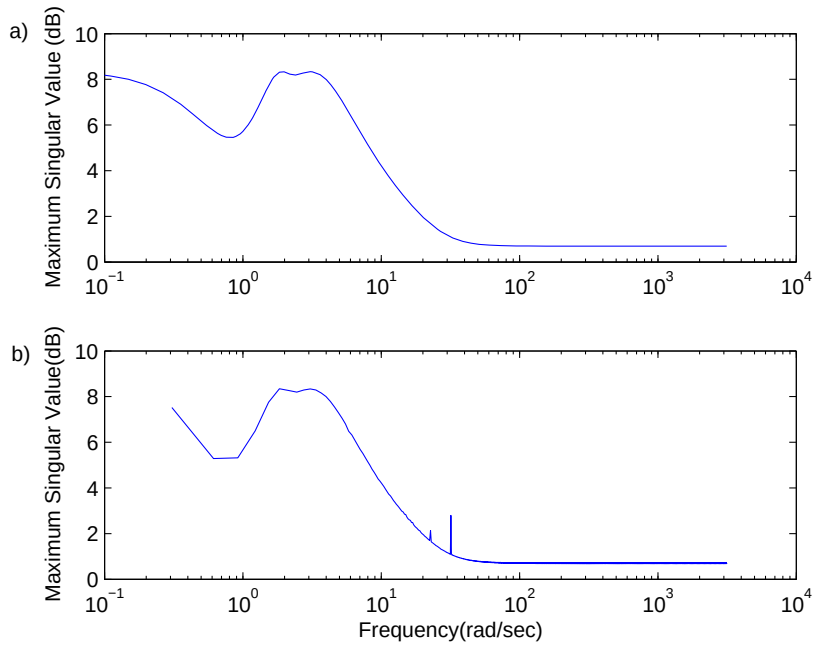

Figure 4.5: The Maximum singular value plot of a) $T(W_oPW_i, W_i^{-1}CW_o^{-1})$ and b) $\widehat{T}(W_oPW_i, W_i^{-1}CW_o^{-1})$.

Length of the Pre-experiments	$\|\widehat{T}(P,C)\|_\infty$	$\left\|\|T(P,C)\|_\infty - \|\widehat{T}(P,C)\|_\infty\right\|$
$0 \times u(t)$	81.0507 dB	10.9623 dB
$1/32 \times u(t)$	73.5809 dB	3.4925 dB
$1/10 \times u(t)$	70.0196 dB	0.0688 dB
$1/2 \times u(t)$	70.0881 dB	0.0003 dB

4.5.4 Scalings

In Figure 4.5, we used the constant diagonal scalings introduced in Chapter 3 to estimate the less conservative margin yielding $\|\widehat{T}(W_oPW_i, W_i^{-1}CW_o^{-1})\|_\infty = 8.523$ dB at $\omega = 3.068$ rad/sec.

4.6 Conclusion

In this chapter, we investigated estimation of the generalized stability margin with an error bound using the MIMO empirical transfer function estimate (ETFE). We used the standard test input to run the system for a specific amount of time before recording of the output signals to manage the error caused by the initial conditions.

For MIMO estimation, we perform as many experiments as the number of inputs. Each vector input was generated from multiplying the scalar input by each column vector of a full rank matrix so that invertibility of the input DFT matrix was assured. The magnitude of estimation error can depend on several factors, such as the number of samples in the DFT computation, energy in the input DFT at a specific frequency, the number of samples for pre-experimental running, and downsampling.

4.7 Appendices

4.7.1 Proof of Theorem 4.2.1

Define the elementary function

$$e_k(t) = \frac{1}{\sqrt{N}} e^{j\frac{2\pi k}{N}t}, \ k = 0, \cdots, N-1 \tag{4.23}$$

This set of functions defines a orthonormal basis for sequences on $[0, \cdots, N-1]$. Define

$$\hat{u}_k(t) = U_N^k e_k(t) \text{ and } \hat{y}_k(t) = Y_N^k e_k(t)$$

for $t = 0, 1, \cdots, N-1$. The infinite summation in the output $y(t)$ from (4.1) can be divided into two parts,

$$\sum_{n=0}^{t} g(n)u(t-n), \tag{4.24}$$

and

$$\sum_{n=t+1}^{\infty} g(n)u(t-n). \tag{4.25}$$

The finite summation (4.24) is computed from known input, $u(t)$ $(t \geq 0)$, while the infinite summation (4.25) depends on known input $u(t)$ $(-N_r \leq t < 0)$ and unknown input $u(t)$ $(t < -N_r)$. Now we define $\hat{u}_k^e(t)$, infinite extension of $\hat{u}_k(t)$,

$$\hat{u}_k^e(t - cN) \triangleq \hat{u}_k(t), \quad c \in \mathbb{Z} \ \text{ and } \ k = 0, 1, \cdots, N-1, \tag{4.26}$$

then note that the corresponding infinite extension of $u(t)$ for $t = 0, 1, \cdots, N-1$ is given by,

$$u^e(t) = \sum_{k=0}^{N-1} \hat{u}_k^e(t).$$

Since $u(t) = \sum_{k=0}^{N-1} U_N^k e_k(t)$ for $t = 0, 1, \cdots, N-1$, using the elementary functions, (4.23), we can write (4.24) as,

$$\sum_{n=0}^{t} g(n) \sum_{k=0}^{N-1} \hat{u}_k(t-n).$$

Next, swap the order of summation to yield,

$$\begin{aligned}
&\sum_{k=0}^{N-1} \sum_{n=0}^{t} g(n)\hat{u}_k(t-n) \\
&= \sum_{k=0}^{N-1} \left(\sum_{n=0}^{t} g(n)\hat{u}_k(t-n) + \sum_{n=t+1}^{\infty} g(n)\hat{u}_k^e(t-n) - \sum_{n=t+1}^{\infty} g(n)\hat{u}_k^e(t-n) \right).
\end{aligned}$$

Now using (4.26), we have

$$\begin{aligned}
&\sum_{k=0}^{N-1} \left(\sum_{n=0}^{\infty} g(n)\hat{u}_k(t-n) - \sum_{n=t+1}^{\infty} g(n)\hat{u}_k^e(t-n) \right) \\
&= \sum_{k=0}^{N-1} \left(\sum_{n=0}^{\infty} g(n) e^{-j\frac{2\pi k}{N}n} \frac{1}{\sqrt{N}} U\left(\frac{2\pi k}{N}\right) e^{j\frac{2\pi k}{N}t} - \sum_{n=t+1}^{\infty} g(n)\hat{u}_k^e(t-n) \right) \\
&= \sum_{k=0}^{N-1} G(e^{j\frac{2\pi k}{N}})\hat{u}_k(t) - \sum_{n=t+1}^{\infty} g(n) u^e(t-n).
\end{aligned}$$

Then $y(t)$ can be written as,

$$y(t) = \sum_{k=0}^{N-1} G(e^{j\frac{2\pi k}{N}})\hat{u}_k(t) + \sum_{n=t+1}^{\infty} g(n) \left(u(t-n) - u^e(t-n)\right) + v(t) \tag{4.27}$$

Define the error term $s(t)$,

$$s(t) \triangleq \sum_{n=t+1}^{\infty} g(n) \left(u(t-n) - u^e(t-n)\right) \tag{4.28}$$

Through the condition (4.10) with input, $u(t) = u^e(t)$ for $t \in [-N_r, -1]$, we eliminate error in $t \in [-N_r, -1]$,

$$\begin{aligned}
s(t) &= \sum_{n=t+1}^{t+N_r} g(n) \left(u(t-n) - u^e(t-n)\right) + \sum_{n=t+N_r+1}^{\infty} g(n) \left(u(t-n) - u^e(t-n)\right) \\
&= 0 + \sum_{n=t+N_r+1}^{\infty} g(n) \left(u(t-n) - u^e(t-n)\right).
\end{aligned} \tag{4.29}$$

Using (4.36) and (4.38) stack all signals for $t = 0, 1 \cdots, N-1$,

$$\sum_{k=0}^{N-1} \begin{bmatrix} \hat{y}_k(0) \\ \hat{y}_k(1) \\ \vdots \\ \hat{y}_k(N-1) \end{bmatrix} = \sum_{k=0}^{N-1} G(e^{j\frac{2\pi k}{N}}) \begin{bmatrix} \hat{u}_k(0) \\ \hat{u}_k(1) \\ \vdots \\ \hat{u}_k(N-1) \end{bmatrix} + \begin{bmatrix} s(0) \\ s(1) \\ \vdots \\ s(N-1) \end{bmatrix} + \begin{bmatrix} v(0) \\ v(1) \\ \vdots \\ v(N-1) \end{bmatrix} \tag{4.30}$$

By pre-multiplying the following row vector at (4.30)

$$\frac{1}{\sqrt{N}} \begin{bmatrix} 1 & e^{-j\frac{2\pi l}{N}} & \cdots & e^{-j\frac{2\pi l}{N}(N-1)} \end{bmatrix}$$

We have,

$$Y_N^l = G\left(\frac{2\pi l}{N}\right) U_N^l + S_N^l + V_N^l. \tag{4.31}$$

The bound on $\left|S_N^l\right|$ can be derived,

$$\begin{aligned} \left|S_N^l\right| &= \left| \frac{1}{\sqrt{N}} \sum_{t=1}^{N} e^{-j\frac{2\pi l}{N}t} \sum_{n=t+N_r+1}^{\infty} g(n) \left(u(t-n) - u^e(t-n)\right) \right| \\ &\leq \frac{1}{\sqrt{N}} \left(u^{\max} + \overline{u}\right) \sum_{t=1}^{N} \sum_{n=t+N_r+1}^{\infty} |g(n)| \\ &\leq \frac{1}{\sqrt{N}} \left(u^{\max} + \overline{u}\right) \frac{M\rho^2}{(1-\rho)^2} \rho^{N_r} (1-\rho^N) \end{aligned} \tag{4.32}$$

4.7.2 Proof of Theorem 4.2.2

$$e_k(t) = \frac{1}{\sqrt{N}} e^{j\frac{2\pi k}{N}t}, \ k = 0, \cdots, N-1$$

This set of functions defines a orthonormal basis for sequences on $[0, \cdots, N-1]$. Define

$$\hat{u}_k(t) = U_N^k e_k(t) \text{ and } \hat{\mathbf{y}}_{ik(t)} = \vec{Y}_{iN}^k e_k(t)$$

for $t = 0, 1, \cdots, N-1$. The infinite summation in the output vector $\vec{y}_i(t)$ from (4.14) can be divided into two parts,

$$\sum_{n=0}^{t} H(n)\vec{u}_i(t-n) = \sum_{n=0}^{t} H(n)\vec{q}_i u(t-n), \tag{4.33}$$

and

$$\sum_{n=t+1}^{\infty} H(n)\vec{u}_i(t-n) = \sum_{n=t+1}^{\infty} H(n)\vec{q}_i u(t-n). \tag{4.34}$$

The finite summation (4.33) is computed from known input, $u(t)$ $(t \geq 0)$, while the infinite summation (4.34) depends on unknown inputs $u(t)$ $(t < 0)$. Now we define $\hat{u}_k^e(t)$, infinite extension of $\hat{u}_k(t)$,

$$\hat{u}_k^e(t - cN) \triangleq \hat{u}_k(t), \quad c \in \mathbb{Z} \text{ and } k = 0, 1, \cdots, N-1, \tag{4.35}$$

then note that the corresponding infinite extension of $u(t)$ is given by,

$$u^e(t) = \sum_{k=0}^{N-1} \hat{u}_k^e(t).$$

Using the elementary function, (4.23), we can write (4.33) as,

$$\sum_{n=0}^{t} H(n)\vec{q}_i \sum_{k=0}^{N-1} \hat{u}_k(t-n).$$

Next, swap the order of summation to yield,

$$\begin{aligned}
&\sum_{k=0}^{N-1}\sum_{n=0}^{t} H(n)\vec{q}_i\hat{u}_k(t-n) \\
&= \sum_{k=0}^{N-1}\left(\sum_{n=0}^{t} H(n)\vec{q}\hat{u}_k(t-n) + \sum_{n=t+1}^{\infty} H(n)\vec{q}_i\hat{u}_k^e(t-n) - \sum_{n=t+1}^{\infty} H(n)\vec{q}_i\hat{u}_k^e(t-n)\right).
\end{aligned}$$

Now using (4.35), we have

$$\begin{aligned}
&\sum_{k=0}^{N-1}\left(\sum_{n=0}^{\infty} H(n)\vec{q}_i\hat{u}_k(t-n) - \sum_{n=t+1}^{\infty} H(n)\vec{q}_i\hat{u}_k^e(t-n)\right) \\
&= \sum_{k=0}^{N-1}\left(\sum_{n=0}^{\infty} H(n)e^{-j\frac{2\pi k}{N}n}\vec{q}_i\frac{1}{\sqrt{N}}U\left(\frac{2\pi k}{N}\right)e^{j\frac{2\pi k}{N}t} - \sum_{n=t+1}^{\infty} H(n)\vec{q}_i\hat{u}_k^e(t-n)\right) \\
&= \sum_{k=0}^{N-1} G(e^{j\frac{2\pi k}{N}})\vec{q}_i\hat{u}_k(t) - \sum_{n=t+1}^{\infty} H(n)\vec{q}_i u^e(t-n).
\end{aligned}$$

Then $\vec{y}_i(t)$ can be written as,

$$\vec{y}_i(t) = \sum_{k=0}^{N-1} \mathbb{G}(e^{j\frac{2\pi k}{N}})\vec{q}_i\hat{u}_k(t) + \sum_{n=t+1}^{\infty} H(n)\vec{q}_i\left(u(t-n) - u^e(t-n)\right) + \vec{v}_i(t) \tag{4.36}$$

Define the error vector $\vec{s}(t)$,

$$\vec{s}_i(t) \triangleq \sum_{n=t+1}^{\infty} H(n)\vec{q}_i \left(u(t-n) - u^e(t-n)\right) \tag{4.37}$$

Through the condition (4.10) with input, $u(t) = u^e(t)$ for $t \in [-N_r, -1]$, we eliminate error in $t \in [-N_r, -1]$,

$$\begin{aligned}\vec{s}_i(t) &= \sum_{n=t+1}^{t+N_r} H(n)\vec{q}_i \left(u(t-n) - u^e(t-n)\right) + \sum_{n=t+N_r+1}^{\infty} H(n)\vec{q}_i \left(u(t-n) - u^e(t-n)\right) \\ &= 0 + \sum_{n=t+N_r+1}^{\infty} H(n)\vec{q}_i \left(u(t-n) - u^e(t-n)\right).\end{aligned} \tag{4.38}$$

Using (4.36) and (4.38) stack all signals for $t = 0, 1 \cdots, N-1$,

$$\begin{aligned}&\sum_{k=0}^{N-1} \begin{bmatrix} \hat{y}_{1,ik}(0) & \hat{y}_{1,ik}(1) & \cdots & \hat{y}_{1,ik}(N-1) \\ \hat{y}_{2,ik}(0) & \hat{y}_{2,ik}(1) & \cdots & \hat{y}_{2,ik}(N-1) \\ \vdots & \vdots & \vdots & \vdots \\ \hat{y}_{p,ik}(0) & \hat{y}_{p,ik}(1) & \cdots & \hat{y}_{p,ik}(N-1) \end{bmatrix} \\ &= \sum_{k=0}^{N-1} \mathbb{G}(e^{j\frac{2\pi k}{N}}) \begin{bmatrix} \hat{u}_{1,ik}(0) & \hat{u}_{1,ik}(1) & \cdots & \hat{u}_{1,ik}(N-1) \\ \hat{u}_{2,ik}(0) & \hat{u}_{2,ik}(1) & \cdots & \hat{u}_{2,ik}(N-1) \\ \vdots & \vdots & \vdots & \vdots \\ \hat{u}_{q,ik}(0) & \hat{u}_{q,ik}(1) & \cdots & \hat{u}_{q,ik}(N-1) \end{bmatrix} \\ &+ \begin{bmatrix} s_{1,i}(0) & s_{1,i}(1) & \cdots & s_{1,i}(N-1) \\ s_{2,i}(0) & s_{2,i}(1) & \cdots & s_{2,i}(N-1) \\ \vdots & \vdots & \vdots & \vdots \\ s_{p,i}(0) & s_{p,i}(1) & \cdots & s_{p,i}(N-1) \end{bmatrix} + \begin{bmatrix} v_{1,i}(0) & v_{1,i}(1) & \cdots & v_{1,i}(N-1) \\ v_{2,i}(0) & v_{2,i}(1) & \cdots & v_{2,i}(N-1) \\ \vdots & \vdots & \vdots & \vdots \\ v_{p,i}(0) & v_{p,i}(1) & \cdots & v_{p,i}(N-1) \end{bmatrix}\end{aligned} \tag{4.39}$$

By post-multiplying the following column vector to (4.39)

$$\frac{1}{\sqrt{N}} \begin{bmatrix} 1 \\ e^{-j\frac{2\pi l}{N}} \\ \vdots \\ e^{-j\frac{2\pi l}{N}(N-1)} \end{bmatrix}$$

We have,

$$\vec{Y}_{Ni}^{l} = \mathbb{G}(e^{j\frac{2\pi l}{N}})\vec{U}_{Ni}^{l} + \vec{S}_{Ni}^{l} + \vec{V}_{Ni}^{l}. \tag{4.40}$$

By additional $(q-1)$ DFT vector relationships of (4.40), we have

$$\mathbb{Y}_{N}^{l} = \mathbb{G}(e^{j\omega})\mathbb{U}_{N}^{l} + \mathbb{S}_{N}^{l} + \mathbb{V}_{N}^{l}. \tag{4.41}$$

The bound on $\overline{\sigma}\left(S_{N}^{l}\right)$ can be derived,

$$\begin{aligned}
\overline{\sigma}\left(\mathbb{S}_{N}^{l}\right) &= \overline{\sigma}\left(\frac{1}{\sqrt{N}}\sum_{t=1}^{N} e^{-j\frac{2\pi l}{N}t} \sum_{n=t+N_r+1}^{\infty} H(n)Q\left(u(t-n) - u^{e}(t-n)\right)\right) \\
&\leq \frac{\overline{\sigma}(Q)}{\sqrt{N}}\left(u^{\max} + \overline{u}\right)\sum_{t=1}^{N}\sum_{n=t+N_r+1}^{\infty}\overline{\sigma}(H(n)) \\
&\leq \frac{\overline{\sigma}(Q)}{\sqrt{N}}\left(u^{\max} + \overline{u}\right)\frac{\tilde{M}\tilde{\rho}^{2}}{(1-\tilde{\rho})^{2}}\tilde{\rho}^{N_r}(1-\tilde{\rho}^{N})
\end{aligned} \tag{4.42}$$

Therefore we have the error bound, (4.19).

4.7.3 Downsampling and Averaging of DFT

Theorem 4.7.1. *Consider integers P, M, and N with $N = M \times P$ and DFT of an experimental data record, $\{u(0), u(1), \cdots, u(N-1)\}$,*

$$\begin{aligned}
U_{N}^{k} &= \frac{1}{\sqrt{N}}\sum_{t=0}^{N-1} u(t)e^{j\frac{2\pi k}{N}t} \\
&\text{for } k = 0, 1, \cdots, N-1.
\end{aligned} \tag{4.43}$$

Using P nonoverlapping segments of the original data record, define P of DFTs for $h = 0, 1, \cdots, (P-1)$,

$$\begin{aligned}
\left(U_{M}^{l}\right)_{h} &= \frac{1}{\sqrt{M}}\sum_{t=0}^{M-1} u(t + M\cdot h)e^{j\frac{2\pi l}{M}t}, \\
&\text{for } l = 0, 1, \cdots, (M-1).
\end{aligned}$$

Let us consider U_{N}^{k} only at

$$k = l \times P,$$

so that a downsampled DFT of (4.43) is given by,

$$\frac{1}{\sqrt{M \times P}}\sum_{t=0}^{N-1} u(t)e^{j\frac{2\pi l \times P}{M \times P}t}. \tag{4.44}$$

Then the downsampled DFT (4.44) is equal to an averaged DFT of the P blocks of data record,

$$\frac{1}{\sqrt{P}}\sum_{h=0}^{P-1}\left(U_M^l\right)_h. \tag{4.45}$$

Proof. From (4.44),

$$\begin{aligned}
&\frac{1}{\sqrt{M}}\frac{1}{\sqrt{P}}\sum_{t=0}^{N-1}u(t)e^{j\frac{2\pi l}{M}t}\\
=&\frac{1}{\sqrt{P}}\sum_{h=0}^{P-1}\frac{1}{\sqrt{M}}\sum_{t=M\cdot h}^{M(h+1)-1}u(t)e^{j\frac{2\pi l}{M}t}\\
=&\frac{1}{\sqrt{P}}\sum_{h=0}^{P-1}\frac{1}{\sqrt{M}}\sum_{t=0}^{M-1}u(t+M\cdot h)e^{j\frac{2\pi l}{M}t}\\
=&\frac{1}{\sqrt{P}}\sum_{h=0}^{P-1}\left(U_M^l\right)_h.
\end{aligned} \tag{4.46}$$

□

5

Conclusions and Future Work

5.1 Conclusions

The main theme of the dissertation is the generalized stability margin guarantee by pre-established stability of a ν-gap-wise adjacent controller. The thesis can be roughly divided in three parts although they are closely related to each other; a decision supporting tool for inference of the stability margin, computation of the maximal stability margin with the minimal ν-gap metric, and experiment for estimating the generalized stability margin.

The search algorithm for a subset of designed controllers to reduce the number of experiments required in controller certification has been developed in Chapter 2. By doing experiments only on a small subset of controllers, we can solve the certification problem for a large or, in the SISO case at least, an infinite set of candidate controllers in an efficient fashion. Precomputed design quantities such as $b_{\hat{P},C}$ and $\delta_\nu(C_i, C_j)$ are used to guide the search for controllers to be tested experimentally with the actual plant to yield certification of the complete set $\mathcal{C}$. A required margin for the controller certification can be maintained. For the SISO case when the candidate controller set has an infinite number of controllers, we have shown that only a finite number of experiments are required to solve the certification problem. We provided a theorem restricting a radius of a ball in the Euclidean space and we gave an example that the controller will guarantee a prescribed level of stability and performance if parameters of a scalar controller are contained in that ball.

In Chapter 3, we investigated the effects of scaling on the stability margin computation in controller certification. The input/output scaling on $b_{\hat{P},C_i}$ computation may reduce the conservatism in the $b_{\hat{P},C}$. However the use of scaling matrices without carefully considering how W_o and W_i will alter the ν-gap metric unfavorably to the controller certification. We proposed simultaneous scaling on $b_{\hat{P},C_i}$ and the ν-gap so that we can achieve an efficient controller certification. The scaling matrices for maximizing the generalized stability margin can be found by a convex optimization. Whereas, the minimization of the ν-gap metric cannot be formulated in a convex problem. We tackled this issue modifying the XY-centering algorithm. The scaling on the stability margin does not change the gain margin and phase margin in SISO case. Thus the purpose of scalings can be understood as a stability analysis and the scalings reveal how the generalized stability margin should be represented.

In Chapter 4, we investigated estimation of the generalized stability margin with an error bound using MIMO empirical transfer function estimate (ETFE) error analysis. We suggested running the system for a specific amount of time before recording of the output signals to manage the error caused by the initial conditions. The input signal for experiments also designed. The swept-sine signal is suggested as a scalar input signal. For MIMO experiments, we simply multiply this scalar input by a full rank matrix so that we can assure invertibility of the input DFT matrix. The magnitude of estimation error can depend on several factors, such as the number of samples in the DFT computation, energy in the input DFT at a specific frequency, the number of samples for pre-experimental running, and downsampling so on.

5.2 Future Research

- fleet-wide certification
- direct certification of non-linear engine model
- use of experimental data on updating the plant model, $\hat{P}$

Further work required in this area is apparent to explore joint approaches to incorporating controller certification and fleet variability. There remain many open questions

about extension to nonlinear systems and about the inclusion of significant time-variation among either or both the plants and controllers. Clearly, extension of the SISO results for continuously parametrized sets of MIMO controllers will require significant technical work. Although, from a practical perspective, this might be subsumed by the enumerated solution. Of particular interest is the extension of these results dealing with stability and stability margins to cover issues of guaranteed closed-loop performance. Already, weighting functions are used in the computation of MIMO margins and it is clear that weighting functions also play a central role in loop-shaping control designs. It would indeed be worthwhile to extend these stability metrics to include a performance metric.

Bibliography

Anderson, B. D. O., Brinsmead, T. S., De Bruyne, F., Hespanha, J., Liberzon, D. & Morse, A. S. (2000), 'Multiple model adaptive control. part 1: Finite contoller coverings', *International Journal of Robust and Nonlinear Control* **10**, 909–929.

Anderson, B. & Gevers, M. (1998), Fundamental problems in adaptive control, *in* D. Normad-Cyrot, ed., 'Perspectives in Control: Theory and Applications', Springer-Verlag, Berlin.

Blondel, V., Gevers, M. & Bitmead, R. (1997), 'When is a model good for control design?', *Proc. 36th IEEE Conference on Decision and Control, San Diego CA* pp. 1283–1288.

Boyd, S., Ghaoui, L. E., Feron, E. & Balakrishnan, V. (1994), *Linear Matrix Inequalities in Sytem and Control Theory*, SIAM, Philadelphia.

Boyd, S. & Vandenberghe, L. (2004), *Convex Optimization*, Cambridge University Press.

Brockett, R. W. (1976), 'Some geometric questions in the theory of linear systems.', *IEEE Transactions on Automatic Control* **21**(4), 449–455.

Broersen, P. (2004), 'Mean square error of the empirical transfer function estimator for stochastic input signals.', *Automatica* **40**, 95–100.

Chen, J. & Gu, G. (2000), *Control-Oriented System Identification: An $\mathcal{H}_\infty$ Approach*, Wiley, New York.

Davies, C., Holt, J. E. & Griffin, I. A. (2006), 'Benefits of inverse model control of rolls-royce civil gas turbines.', *International Control Conference* **44**, 952–955.

de Vries, D. (1994), Identification of Model Unceratinty for Control Design, PhD thesis, Delft University of Technology.

Fielding, C., Varga, A., Bennani, S. & Selier, M. (2002), *Advanced Techniques for Clearance of Flight Control Laws*, Springer, Berlin Heidelberg.

Glover, K., Vinnicombe, G. & Papageorgiou, G. (2000), 'Guaranteed multi-loop stability margins and the gap metric', *Proc. 39th IEEE Conference on Decision and Control, Sydney, Austraila* pp. 4084–4085.

Gu, G. & Khargonekar, P. P. (1992), 'A class of algorithm for identification in h_∞.', *Automatica* **28**(2), 299–312.

Hannan, E. J. & Deistler, M. (1998), *The Statistical Theory of Linear Systems*, John Wiley & Sons, Inc., New York.

Helmicki, A. J., Jacobson, C. A. & Nett, C. N. (1993), 'Least squares methods for h_∞ control-oriented identification.', *IEEE Transactions on Automatic Control* **38**(5), 819–826.

Holt, J. E. (2006), 'The challenges of civil aircraft engine control system development at rolls-royce.', *International Control Conference* **44**, 952–955.

Horowitz, I. M. & Sidi, M. (1972), 'Synthesis of feedback systems with large plant ignorance for prescribed time-domain tolerances.', *International Journal of Contol* **16**(2), 287–309.

Iwasaki, T. & Skelton, R. E. (1995), 'The xy-centering algorithm for the dual lmi problem: A new approach to fixed order control design.', *International Journal of Contol* **62**(6), 1257–1272.

Kay, S. M. (1988), *Modern Spectral Estimation: Theory and Application*, Prentice Hall, Upper Saddle River, NJ.

Ljung, L. (1985), 'On the estimation of transfer functions.', *Automatica* **21**, 677–696.

Ljung, L. (1999), *System Identification*, Prentice Hall Inc., Upper Saddle River, NJ.

McFarlane, D. C. & Glover, K. (1989), *Robust Controller Design Using Normalized Coprime Factor Plant Descriptions*, Springer-Verlag, Berlin Heidelberg.

Merrill, W. C., Beattie, E. C., LaPrad, R. F., Rock, S. M. & Akhter, M. M. (1984), Hytess - a hypothetical turbofan engine simplified simulation., *in* 'TM-83561', NASA Report.

Ninness, B. & Goodwin, G. C. (1995), 'Estimation of model quality.', *Automatica* **31**(12).

Papachristodoulou, A. & Prajna, S. (2002), 'On the construction of lyapunov functions using the sum of squares decomposition', *Proceedings of the 41st IEEE Conference on Decision and Control, Las Vegas USA* pp. 3482–3487.

Park, J. & Bitmead, R. R. (2008), 'Controller certification.', *Automatica* **44**(1), 167–176.

Parker, K. I. & Guo, T.-H. (2003), Development of a turbofan engine simulation in a graphical simulation environment, Reports NASA/TM-2003-212543, NASA.

Parker, P. J. & Bitmead, R. R. (1987), 'Adaptive frequency response identification', *Proceedings of the 26th IEEE Conference on Decision and Control, Los Angeles USA* pp. 348–353.

Pintelon, R. & Schoukens, J. (2001), 'Measurement of frequency response functions using periodic excitations, corrupted by correlated input/outpus errors.', *IEEE Trans. on Instrumentation and Measurement* **50**, 1753–1760.

Rantzer, A. (1996), 'On the kalman-yakubovich-popov lemma.', *System & Control Letters* **28**, 7–10.

Safonov, M. G. & Tsao, T. C. (1997), 'The unfalsified control concept and learning', *IEEE Transactions on Automatic Control* **42**(6), 843–847.

Steele, J. (2001), Approximation and Validation of Models with Uncertainty: A closed-loop perspective, PhD thesis, University of Cambridge.

Vinnicombe, G. (1993), 'Frequency domain uncertainty and the graph topology.', *IEEE Transactions on Automatic Control* **38**(9), 1371–1383.

Vinnicombe, G. (2001), *Uncertainty and Feedback: $\mathcal{H}_\infty$ loop-shaping and the ν-gap mectric*, Imperial College Press, London.

Zhou, K. & Doyle, J. (1998), *Essentials of Robust Control*, Prentice-Hall, Upper Saddle River NJ.